SYNTHESIS AND CHARACTERIZATION OF HIGHLY EFFICIENT CdSe/CdS CORE/SHELL NANOCRYSTALS WITH SILAR TECHNIQUE

A THESIS

SUBMITTED TO MATERIALS SCIENCE AND

NANOTECHNOLOGY PROGRAM OF

GRADUATE SCHOOL OF ENGINEERING AND SCIENCE

OF BILKENT UNIVERSITY

IN PARTIAL FULLFILMENT OF THE REQUIREMENTS

FOR THE DEGREE OF

MASTER OF SCIENCE

By

Yusuf Keleştemur

July 2012

I certify that I have read this thesis and that in my opinion it is fully adequate, in scope and in quality, as a thesis for the degree of Master of Science.

Assoc. Prof. Dr. Hilmi Volkan Demir

I certify that I have read this thesis and that in my opinion it is fully adequate, in scope and in quality, as a thesis for the degree of Master of Science.

Prof. Dr. Oğuz Gülseren

I certify that I have read this thesis and that in my opinion it is fully adequate, in scope and in quality, as a thesis for the degree of Master of Science.

Assoc. Prof. Dr. Dönüş Tuncel

Approved for the Graduate School of Engineering and Sciences:

Prof. Dr. Levent Onural
Director of Graduate School of Engineering and Sciences

ABSTRACT

SYNTHESIS AND CHARACTERIZATION OF HIGHLY EFFICIENT CdSe/CdS CORE/SHELL NANOCRYSTALS WITH SILAR TECHNIQUE

Yusuf Keleştemur
M.S. in Material Science and Nanotechnology
Supervisor: Assoc. Prof. Hilmi Volkan Demir
July 2012

Owing to their size tunable electronic structure and optical properties, semiconductor nanocrystal quantum dots (NQDs) have become attractive for a wide range of device applications ranging from life sciences to electronics in the last two decades. However, highly efficient and stable NQDs are essential to reaching high performance with these devices utilizing NQDs. In this thesis, to meet these requirements, a new class of CdSe/CdS core/shell NQDs are studied including their colloidal synthesis and nanocharacterization. In this work, CdSe/CdS core/shell NQDs were synthesized with successive ion layer adsorption and reaction (SILAR) technique, which enabled highly precise shell thickness control and uniform coating of the shell material.

When compared to the most commonly used CdSe/ZnS core/shell NQDs, CdSe/CdS core/shell NQDs were found to provide important advantages. First, the lattice mismatch within CdSe and CdS (3.9%) is lower than that within CdSe and ZnS (12%), which was very critical for obtaining highly efficient NQDs. Second, as a result of having lower bandgap in CdS, great enhancement in absorption cross section was achieved with more red-shifted emission, which is not possible with CdSe/ZnS core/shell NQDs. Moreover, suppression of Auger recombination was successfully observed with the partial separation of electron and hole wavefunctions in the synthesized CdSe/CdS core/shell NQDs. With all

these attractive properties that were experimentally measured, CdSe/CdS core/shell NQDs were found to make better alternatives to CdSe/ZnS core/shell for numerous applications.

Keywords: semiconductor nanocrystals, nanocrystal quantum dots, colloidal synthesis.

ÖZET

SILAR TEKNİĞİ İLE ÇOK VERİMLİ CdSe/CdS ÇEKİRDEK/KABUK NANOKRİSTAL KUVANTUM NOKTACIKLARININ SENTEZİ VE KARAKTERİZASYONU

Yusuf Keleştemur
Malzeme Bilimi ve Nanoteknoloji Yüksek Lisans
Tez Yöneticisi: Doç. Dr. Hilmi Volkan Demir
Temmuz 2012

Boyutları ile ayarlanabilen elektronik yapısı ve optik özellikleri sayesinde, yarı iletken nanokristal kuvantum noktacıkları son yirmi yıl içerisinde yaşam bilimlerinden elektroniğe kadar çok farklı alanlarda cihaz uygulamaları için cazip hale gelmiştir. Ancak, nanokristal kuvantum noktacıklarının kullanıldığı bu cihazlardan daha yüksek performans elde etmek için çok verimli ve kararlı nanokristal kuvantum noktacıklarına gerek duyulmaktadır. Bu tezde, bu gereksinimlere ulaşmak için, yeni bir çeşit CdSe/CdS çekirdek/kabuk nanokristallerinin sentezlenmesi ve nanokarakterizasyonu çalışılmıştır. Bu çalışmada, CdSe/CdS çekirdek/kabuk nanokristal kuvantum noktacıkları, hassas derecede kabuk kalınlığı kontrolü ve eşit kalınlıkta kaplama sağlayan SILAR tekniği ile sentezlenmiştir.

En sık kullanılan CdSe/ZnS çekirdek/kabuk nanokristal kuvantum noktacıkları ile karşılaştırıldıklarında, CdSe/CdS çekirdek/kabuk nanokristal kuvantum noktacıkları önemli avantajlar sağlamaktadır. Birincisi, yüksek verimlikli nanokristal kuvantum noktacıkları elde etmek için kafes uyuşmazlığı çok önemlidir ve CdSe ile CdS arasındaki kafes uyuşmazlığı (3.9%) CdSe ile ZnS arasındakine (12%) göre daha düşüktür. İkinci olarak, CdS'nın daha düşük bir bant aralığına sahip olmasından dolayı, CdSe/ZnS çekirdek/kabuk nanokristal kuvantum noktacıkları ile elde edilmesi mümkün olmayan, soğurma kesitinde

büyük bir artış ve daha kırmızıya kaydırılabilen ışımalar elde edilmiştir. Ayrıca, sentezlenen CdSe/CdS çekirdek/kabuk nanokristal kuvantum noktacıklarında, elektron ve hol dalga fonksiyonlarının kısmen ayrılması sayesinde, Auger rekombinasyonlarının baskılandığı gözlenmiştir. Deneylerle ölçülen ve gösterilen bütün bu çekici özellikleri ile, CdSe/CdS çekirdek/kabuk nanokristal kuvantum noktacıkları çok geniş bir uygulama alanında CdSe/ZnS çekirdek/kabuk nanokristal kuvantum noktacıklarına göre daha iyi bir alternatif olabilecekleri bulunmuştur.

Anahtar Sözcükler: Yarı iletken nanokristaller, nanokristal kuvantum noktacıkları, kolloidal sentez.

Acknowledgements

First of all, I would like to thank my supervisor Prof. Hilmi Volkan Demir. Two years ago, I joined the Demir Group. Through these years he provided me with invaluable guidance, helpful suggestions and motivation in both scientific study and life.

I would also like to thank Prof. Dönüş Tuncel and Prof. Oğuz Gülseren for being on my thesis committee and their valuable comments on my thesis work.

This thesis would not be possible without good friends and colleagues. First, I would also thank all the past and present members of the Demir Group for being helpful and friendly. Especially, I would like to thank Dr. Evren Mutlugün from whom I have learned my basic skills. He always shares his knowledge and experience with me related to both research and life. I would also like to thank Özgün Akyüz, Emre Ünal, Dr. Nihan Koşku Perkgöz, Dr. Urartu Şeker, Dr. Pedro L. Hernandez, Dr. Vijay Kumar Sharma, Emre Sarı, Can Uran, Aydan Yeltik, Cüneyt Eroğlu, Talha Erdem, Burak Güzeltürk, Sayim Gökyar, Akbar Alipour, Mustafa Akın Sefünç, Kıvanç Güngör, Ahmet Fatih Cihan, Shahab Akhavan, Togay Amirahmadov, Ozan Yerli, Erdal Gönendik, İbrahim Akcalı, Halil Akcalı for their friendship.

I would also like to acknowledge the professors, instructors, engineers and graduate students at UNAM.

Finally, I would like to thank my parents, Bedrettin and Fatma Keleştemur for their love, support and encouragement without any expectation. I would like to especially thank my elder sister and brother who have always been with me whenever I need them.

Table Of Contents

ABSTRACT……...iii

ÖZET…….....….....v

ACKNOWLEDGEMENT.....vii

1. INTRODUCTION…….……..……...1

1.1. Nanocrystal Quantum Dots…….1

1.2. Synthesis of Nanocrystal Quantum Dots……3

1.3. Motivation of This Study……5

2. CHARACTERIZATION OF NANOCRYSTAL QUANTUM DOTS…….....7

2.1. Optical Characterization……7

2.1.1. UV-Vis Spectroscopy……..8

2.1.2. Fluorescence Spectroscopy……10

2.1.3. Determination of Photoluminescence Quantum Yield……..12

2.2. Structural Characterization……...16

2.2.1. X-Ray Diffraction……..16

2.2.2. X-Ray Photoelectron Spectroscopy……...19

2.2.3. Transmission Electron Microscopy……22

2.2.4. Scanning Electron Microscopy……..26

3. SYNTHESIS AND CHARACTERIZATION OF HIGHLY EFFICIENT CdSe/CdS CORE/SHELL NANOCRYSTALS FOR OPTICAL GAIN WITH TWO PHOTON INFRARED PUMPING……...27

3.1. Introduction……...27

3.2. Experimental Design…….……30

3.2.1. Chemicals……...30

3.2.2. Synthesis of CdSe Core Nanocrystals……30

3.2.3. Synthesis of CdSe/CdS Core/Shell Nanocrystals with SILAR Technique……33

3.2.4. Preparation of Precursor Solution for SILAR Technique……..33

3.2.5. Calculation of Injection Amounts for Precursor Solutions……34

3.2.6. Preparation of CdSe/CdS Core/Shell NQDs with SILAR Technique……35

3.3. Results and Discussion……36

3.3.1. Optical Characterization……36

3.3.2 Structural Characterization……..……..…….48

3.4. Application……...60

4. CONCLUSION……...65

BIBLIOGRAPHY……...67

List of Figures

Figure 1.1.1 Schematic representation of quantum confinement effect in NQDs having different size……..……**2**

Figure 1.2.1 a) La Mer's model for the nucleation and growth stage of colloidal NQD synthesis and b) schematic representation of NQD synthesis apparatus [26]…….... **5**

Figure 2.1.1.1 Absorption spectra of different size CdSe NQDs…….**....8**

Figure 2.1.1.2 Different sizing curves for CdSe NQDs [35]……..……..**9**

Figure 2.1.2.1 Schematic representation of photoluminescence process [42]**....11**

Figure 2.1.2.2 Photoluminescence spectra of different size CdSe NQDs…..…**11**

Figure 2.1.3.1 Absorption and photoluminescence spectra of R6G dissolved in methanol…….……**13**

Figure 2.1.3.2 Absorption and photoluminescence spectra of 3 ML CdSe/CdS NQDs**.....14**

Figure 2.1.3.3 Absorption spectra of R6G and 3ML CdSe/CdS NQD……..**15**

Figure 2.1.3.4 Photoluminescence spectra of R6G and 3ML CdSe/CdS core shell NQD with the same excitation wavelength of 475 nm ……..……...**15**

Figure 2.2.1.1 Bragg's Law and schematic representation of constructive interference between X-Rays [74]…..……..…….……**16**

Figure 2.2.1.2 Unit cell of zinc blende crystal structure and wurtzite crystal structure [75]……..…….**17**

Figure 2.2.1.3 Absorption and photoluminescence spectra of CdSe having zinc blende crystal structure and wurtzite crystal structure [48]……**18**

Figure 2.2.1.4 Schematic representation of different growth kinetics for CdSe seeds having wurtzite crystal structure and zinc blende crystal structure [47]**...18**

Figure 2.2.2.1 Schematic representation of core/shell NQDs……**20**

Figure 2.2.3.1 Schematic representation of typical TEM system [76]…..……..**22**

Figure 2.2.3.2 a) Low resolution TEM image of 8 ML CdSe/CdS core/shell NQDs and b) high resolution TEM image of 3 ML CdSe/CdS core/shell NQDs……...**24**

Figure 2.2.3.3 a) High resolution TEM images of 4 ML CdSe/CdS core/shell NQDs and b) reciprocal lattice image of the same 4 ML CdSe/CdS core/shell NQDs after the application of FFT…….**25**

Figure 2.2.4.1 SEM images of 10 ML giant CdSe/CdS core/shell NQDs…….**26**

Figure 3.1.1 Conduction and valence band position of semiconductor materials with their lattice mismatch values [32]……...**28**

Figure 3.2.2.1 Photograph of glove box at our lab…….**31**

Figure 3.2.2.2 Photograph of our synthesis setup……...…**32**

Figure 3.3.1.1 Photoluminescence and absorption spectra of different size CdSe NQDs……..……**36**

Figure 3.3.1.2 Emission and absorption peaks fore different size of CdSe NQDs……...**37**

Figure 3.3.1.3 a) Absorption and emission spectra of CdSe NQDs having trap state emission and b) surface dependent emission behavior of CdSe NQDs [66]……..**38**

Figure 3.3.1.4 Absorption spectrum of CdSe NQDs (black line) and fitted absorption spectrum of CdSe NQDs (red line)…….……...**40**

Figure 3.3.1.5 Energy difference between the first and second excitonic peaks (E2-E1) vs energy of the first excitonic peak curve of different size CdSe NQDs…….....……**40**

Figure 3.3.1.6 Absorption spectrum of CdSe NQDs with magic size CdSe clusters (black line) and without magic size CdSe clusters (red line)…….....…**41**

Figure 3.3.1.7 Absorption spectra of CdSe/CdS core/shell NQDs having a small CdSe core with different monolayers (1 ML increments)…….**43**

Figure 3.3.1.8 Emission spectra of CdSe/CdS core/shell NQDs having a small core with different monolayers (1 ML increments)……...**43**

Figure 3.3.1.9 Absorption spectra of CdSe/CdS core/shell NQDs having a large CdSe core with different monolayers (1 ML increments)……**44**

Figure 3.3.1.10 Emission spectra of CdSe/CdS core/shell NQDs having a large core with different monolayers (1ML increments)……..……...**45**

Figure 3.3.1.11 Photoluminescence spectra of CdSe/CdS core/shell NQDs with CdS NQDs (black line) and without CdS NQDs (red line)……**46**

Figure 3.3.1.12 Absorption spectra of CdSe/CdS core/shell NQDs having a small CdSe core with different monolayers (0.8 ML increments)……..……**47**

Figure 3.3.1.13 Photoluminescence spectra of CdSe/CdS core/shell NQDs having a small CdSe core with different monolayers (0.8 ML increments)…...**47**

Figure 3.3.2.1 EDAX analysis of CdSe NQDs with quantitative results……..**48**

Figure 3.3.2.2 Comparison of experimental and theoretical S/Se ratios…..…..**49**

Figure 3.3.2.3 TEM images of CdSe core NQDs with a) 20 nm and b) 10 nm scale bars…….**50**

Figure 3.3.2.4 High resolution TEM image of 3.2 ML CdSe core/shell structure with a size distribution in the inset…..……...……**51**

Figure 3.3.2.4 TEM images of 3.2 ML CdSe/CdS core/shell NQDs with a) 20 nm and b) 10 nm scale bars……**52**

Figure 3.3.2.6 X-ray diffraction patterns of CdSe core NQDs having wurtzite crystal structure……...……**53**

Figure 3.3.2.7 Comparison X-ray diffraction pattern of CdSe core and 4 ML CdSe/CdS core/shell NQDs……...……...…..**54**

Figure 3.3.2.8 a) High resolution TEM images of 4 ML CdSe/CdS core/shell NQDs and b) selected area diffraction pattern (SAED) images of the same 4 ML CdSe/CdS……...….**55**

Figure 3.3.2.9 XPS spectra of Cd, Se and S peaks for CdSe core NQDs and 3 ML CdSe/CdS core/shell NQDs …...…….……..**57**

Figure 3.3.2.10 XPS spectra of Se and S peaks for CdSe core NQDs and CdSe/CdS core/shell NQDs having different number of monolayers……...….**59**

Figure 3.4.1 Experimental setup for optical gain study with NQDs……..**62**

Figure 3.4.2 Photoluminescence spectra of CdSe/CdS core/shell NQDs showing both spontaneous and amplified spontaneous emission (ASE)……..…….**63**

Figure 3.4.3 Change in the photoluminescence intensity with the change in the excitation pulse fluence**...**……..…..**64**

Figure 3.4.4 Normalized photoluminescence spectra of CdSe/CdS core/shell having spontaneous emission (black line) and amplified spontaneous emission (ASE) (red line)……...**64**

List of Tables

Table 3.3.2.1 Interplanar spacing values of different planes for bulk wurtzite CdSe crystal, 4 ML CdSe/CdS core/shell NQDs and bulk wurtzite CdS crystal……...……...……**56**

Table 3.3.2.2 Expected radii of NQDs and measured radii of NQDs using XPS and TEM…….……**58**

Chapter 1

Introduction

1.1. Nanocrystal Quantum Dots

Semiconductor nanocrystal quantum dots (NQDs) are tiny particles consisting of a few hundreds to thousands of atoms. Generally, their sizes are within the range of molecular and bulk forms of the matter and typically smaller than exciton Bohr radius, which results in confinement of electron-hole pairs in all three dimensions. As a result, discrete energy levels are observed in NQDs while continuous band levels are observed for their bulk counterparts. By changing the size of NQDs, energy gap between the valence and the conduction band changes (Figure 1.1.1). This is known as quantum confinement effect [1,2] and enables novel size dependent optical properties for NQDs. Therefore, by changing the size of NQDs, their emission and absorption spectrum can be tuned easily. For example, while larger size CdSe NQDs emit in the red region, by decreasing the size of CdSe NQDs, the emission can be shifted to shorter wavelengths [3].

Moreover, when compared to their organic counterparts, they offer superior properties [4]. They have very narrow emission spectrum covering a wide spectral range from ultraviolet to infrared region depending on the size and composition of NQDs. In addition, they have very broad absorption spectrum, which also allows formation of multiexcitons with single photon excitation. Their photoluminescence quantum yields are also very high. Furthermore, although they have very small size, they yield higher molar extinction coefficient [5,6]. Moreover, their stability against photo bleaching and chemical

degradation is better than their organic counterparts. They also feature longer lifetime. These attractive properties make NQDs the most promising candidates for many applications from biology including imaging [4], tagging [4] and sensing [7] to optoelectronic devices such as light emitting diodes [8], solar cells [9], lower threshold lasers [10] and photodetectors [11,12].

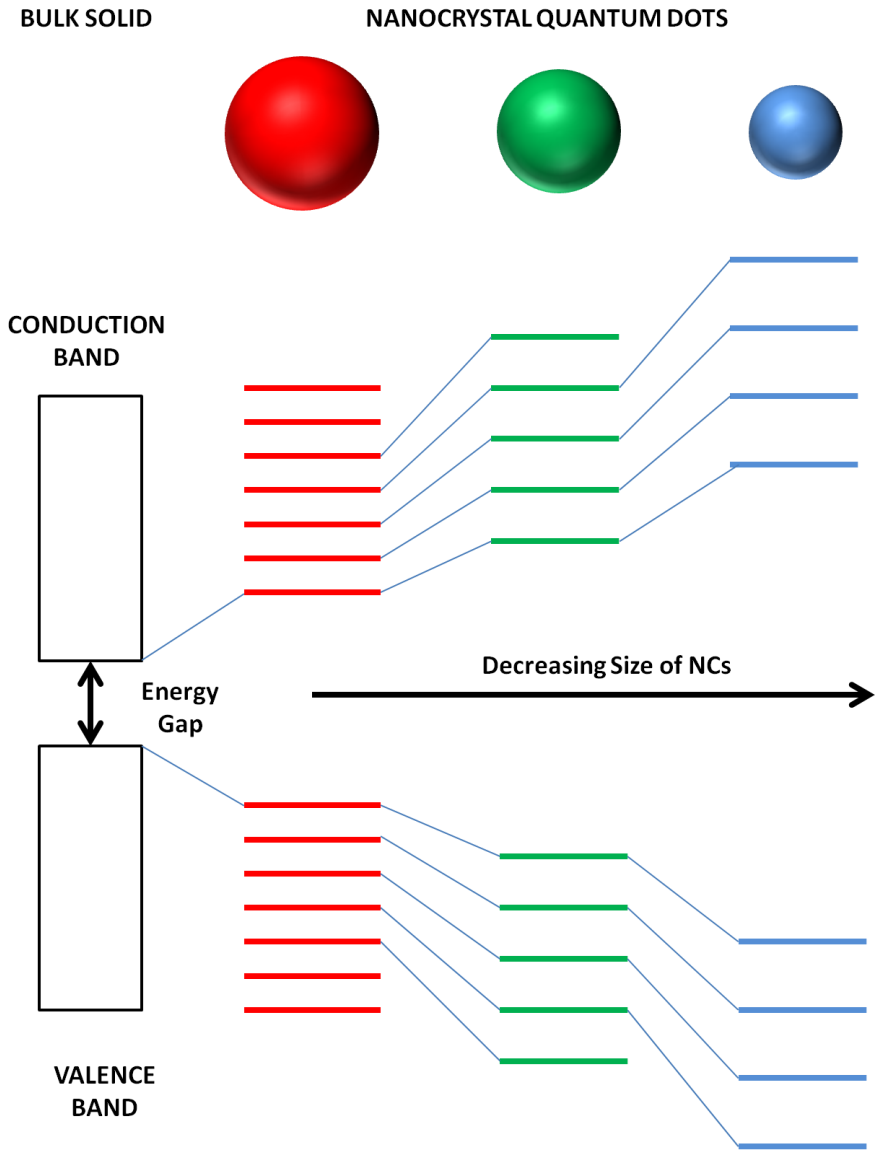

Figure 1.1.1 Schematic representation of quantum confinement effect in NQDs having different size.

Furthermore, the bandgap of NQDs can be engineered using different ways to develop new exciting properties and applications. First of all, the easiest way to tune their optical properties is by changing the size of NQDs [3]. Secondly, there is strong correlation between the optical properties and the shape of NQDs. With synthesis of different shapes of NQDs such as nanorods [13], tetrapods [14] and nanobarbells [15], the emission spectrum, absorption spectrum and lifetime behavior of NQDs can be modified. Thirdly, with the creation of strain in the NQDs, it is also possible to tune electronic and optical properties of NQDs [16]. Finally, with alloying, the emission spectrum of NQDs can be altered. For example, while it is not possible to achieve highly efficient and stable CdSe NQDs having emission in the short wavelength range of the visible region, after alloying with ZnSe, highly stable and luminescent NQDs can be obtained for this spectral range [17].

1.2. Synthesis of Nanocrystal Quantum Dots

NQDs were first synthesized inside glass matrix by adding required precursors [18]. Then, NQDs nucleated and grew inside the glass matrix by heating the samples to high temperatures. However, since these NQDs are embedded in the glass matrix, further processes and characterizations are limited. Molecular beam epitaxy (MBE) [19] and metalorganic-chemical-vapor deposition (MOCVD) [20] were also used for the epitaxial growth of NQDs. However, these methods also have some disadvantages. For the epitaxial growth of NQDs, special substrates are required and they suffer from morphology and size control during the growth of NQDs. Following these approaches, the colloidal synthesis of NQDs was shown by Bawendi and coworkers [3] to obtain high quality NQDs. They have shown that highly monodisperse and highly crystalline NQDs can be achieved with colloidal synthesis. In addition, different size and shape of NQDs can be synthesized and easily incorporated into optoelectronic device by using inexpensive processes such as drop casting, spin casting, layer by layer assembly [21], spray coating, contact printing [22] and inject printing [23].

Colloidal synthesis of NQDs involves decomposition of molecular precursor at higher temperatures. After the injection of precursors into hot coordinating solvent, discrete nucleation takes place and it is followed by the growth of NQDs (Figure 1.2.1). Nucleation is achieved with obtaining supersaturation condition with the injection of precursor solution. Then, the concentration is decreased below the critical value for nucleation and the growth of NQDs takes place with the addition of monomers to existing nuclei from the solution. Since, discrete nucleation step is observed during the synthesis of NQDs, highly monodisperse NQDs are obtained with colloidal synthesis.

Growth stage of NQDs can also be divided into two parts. In the first part, as a result of higher monomer concentration, smaller NQDs grow faster than larger NQDs and size distribution of NQDs is decreased. In the second part, with decreased monomer concentration over time, diffusion of atoms between NQDs takes place. Since, smaller NQDs have higher surface to volume ratio, which decrease the stability, they start to dissolve while larger particles start to grow. Therefore, size distribution of NQDs is increased and this stage is called as Ostwald ripening [24]. In order to obtain highly monodisperse NQDs optimization of growth time for the synthesis of NQDs is required.

In addition, surfactants are used during the synthesis of NQDs and they play an important role in the final properties of NQDs. With the passivation of surface atoms of NQDs, they both enhance the photoluminescence quantum yield and prevent aggregation of NQDs. The nucleation and growth rate of NQDs are also strongly affected with the concentration of surfactants and the strength of interaction between NQDs and surfactant [25]. Moreover, the final size and shape of NQDs depends on the ligands. For example, while weakly binding surfactants support growing of larger NQDs, smaller NQDs can be synthesized by using tightly binding surfactants.

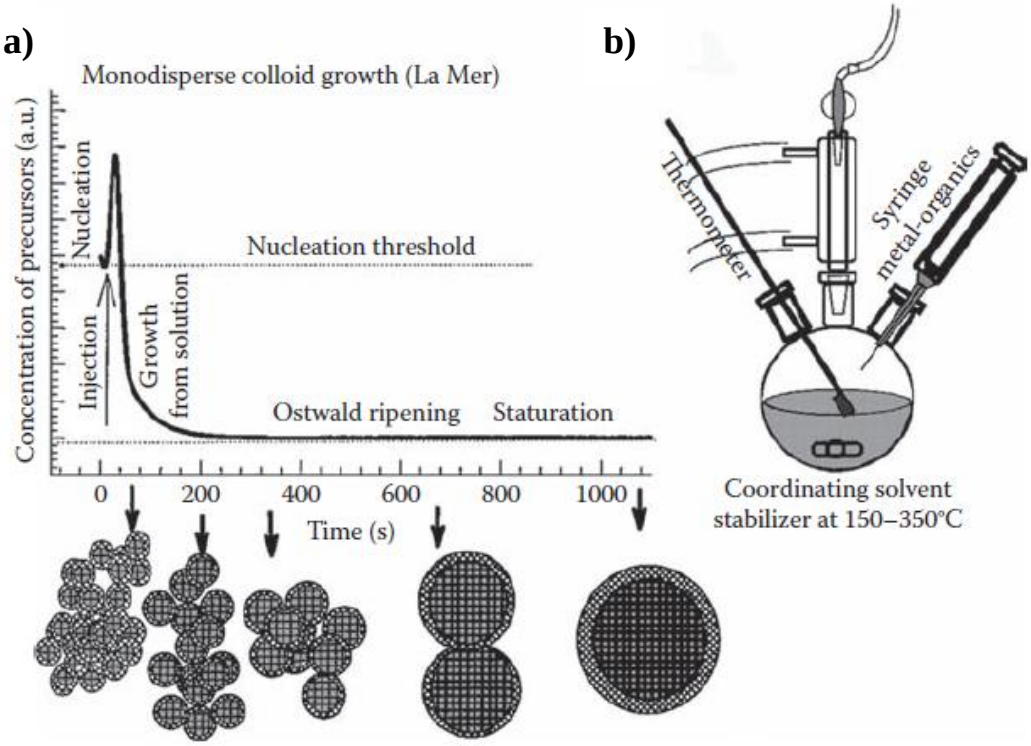

Figure 1.2.1 a) La Mer's model for the nucleation and growth stage of colloidal NQD synthesis and b) schematic representation of NQD synthesis apparatus [26].

After the firstly highly monodisperse and successful colloidal synthesis of Cd-based NQDs (CdSe, CdTe and CdS) was shown by Bawendi and coworkers in 1993 [3], researchers have extended and modified this synthesis to obtain highly monodisperse, highly stable, highly crystalline and highly efficient NQDs from II-VI [27,28], IV-VI [29] and III-V [30] groups. In addition, by time, pyrophoric, hazardous and expensive precursors have been replaced with more stable and safer chemicals. For example, dimethylcadmium and diethylzinc were replaced with cadmium oxide and zinc oxide, respectively.

1.3. Motivation of This Study

Until now, most of the efforts have been made for the increasing the photoluminescence quantum yield and the stability of the NQDs. Since, both of them play a critical role for the performance of single NQD particle and NQD-incorporated devices [31]. In other words, increasing the efficiency and the

stability of NQD leads to high device performance. Therefore, to obtain better performance, CdSe/ZnS core/shell NQDs [32,33,34] have been widely used where ZnS shell allows for both electrical and chemical passivation for the CdSe core. However, although ZnS has a higher bang gap material and supply better confinement of electron and holes inside the core, as a result of higher lattice mismatch (12%) between ZnS and CdSe, it is not easy to obtain NQDs having near-unity quantum yield with ZnS shell. Therefore, instead of ZnS shell, we used CdS for uniform coating of CdSe core with successive ion layer adsorption and reaction (SILAR) technique. Since CdS has a lower lattice mismatch (3.9%) with CdSe, the probability of formation of crystal defects is decreased. Moreover, owing to having a lower bandgap of CdS, optical absorption cross-section of CdSe/CdS core/shell NQDs shows great enhancement with respect to CdSe/ZnS core/shell NQDs [35]. In addition, as a result of the band alignment between CdSe and CdS, electrons are localized through whole crystal structure while holes are confined in the core. Therefore, with the decreased overlap of electron and hole wavefunctions, suppression of Auger recombination is observed for CdSe/CdS core/shell NQDs [36]. All of these attractive properties of CdSe/CdS core/shell NQDs provide us with motivation for the synthesis and characterization of these core/shell NQDs in this thesis.

In this thesis, we present systematic synthesis and complete characterization of CdSe/CdS core/shell NQDs having near-unity quantum yield. Moreover, by taking into advantages of suppression of Auger recombination, we also showed that they can be used as an optical gain medium for lasing application.

Chapter 2

Characterization of Nanocrystal Quantum Dots

Characterization of nanocrystal quantum dots (NQDs) is very important for the understanding of optical, physical and chemical properties of these materials, which can be divided into two main groups: optical characterization and structural characterization. There is a strong correlation between optical properties and crystal structure of NQDs. For example, to obtain highly efficient core/shell NQDs in terms of quantum yield, uniform shell coverage and highly crystalline NQDs are required [37].

2.1. Optical Characterization

For NQDs, optical characterization generally includes UV-Vis spectroscopy and fluorescence spectroscopy. By using these characterization tools, size, concentration, and photoluminescence quantum yield of NQDs can be determined.

2.1.1. UV-Vis Spectroscopy

UV-Vis spectroscopy is one of the most widely used tools to determine absorption of NQDs. Absorption is a physical process where an incoming photon having a higher energy than the bandgap of material is absorbed, creating electron–hole pairs. Because of the quantum confinement effect, the absorption of NQDs can be tuned by changing the size of nanocrystals. Therefore, absorption spectrum gives valuable information about the size of NQDs. For example, Figure 2.1.1.1 shows absorption spectra of CdSe NQDs with different sizes. As it can be seen from Figure 2.1.1.1, by increasing the size of CdSe cores, the first excitonic peaks shift to longer wavelengths.

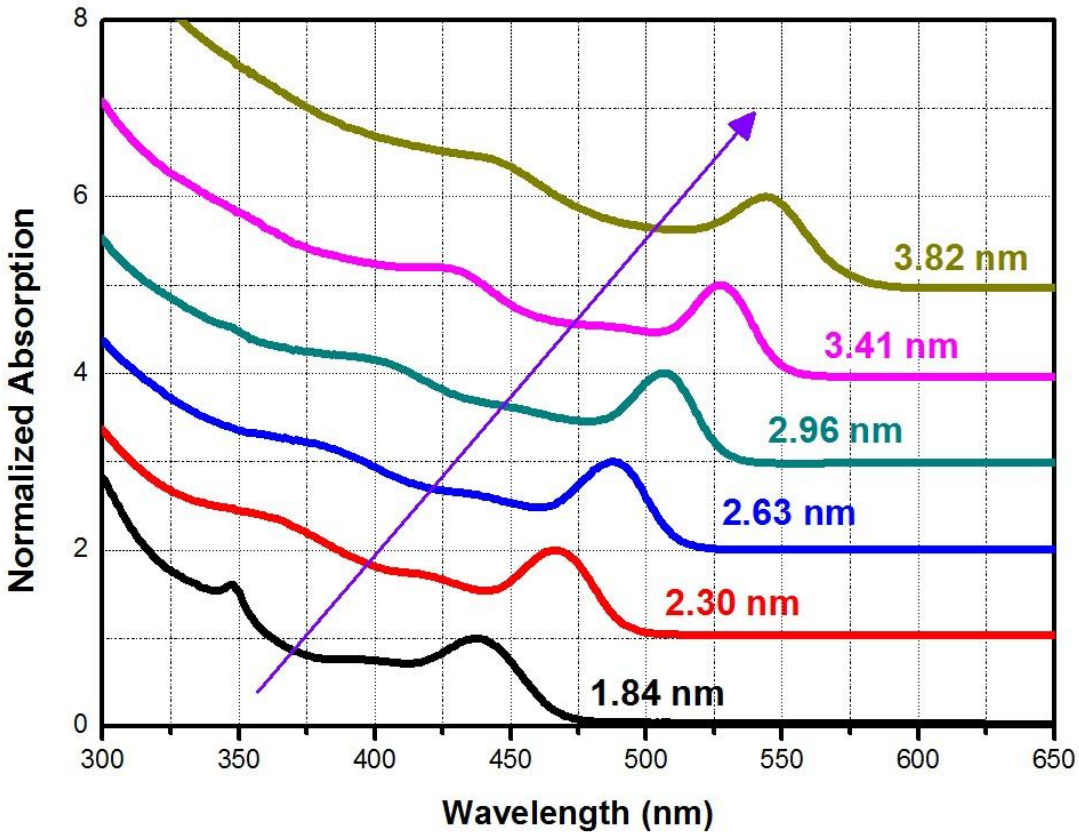

Figure 2.1.1.1 Absorption spectra of different size CdSe NQDs.

In addition, in literature, by making a correlated study with transmission electron microscopy (TEM), small angle X-ray scattering (SAXS) and UV-Vis spectroscopy, sizing curves for CdSe [6,5] NQDs were obtained. Therefore, from the first excitonic peak or lowest exciton peak energy extracted from the absorption spectrum, the radius of CdSe NQDs can be determined easily by using the sizing curves (Figure 2.1.1.2).

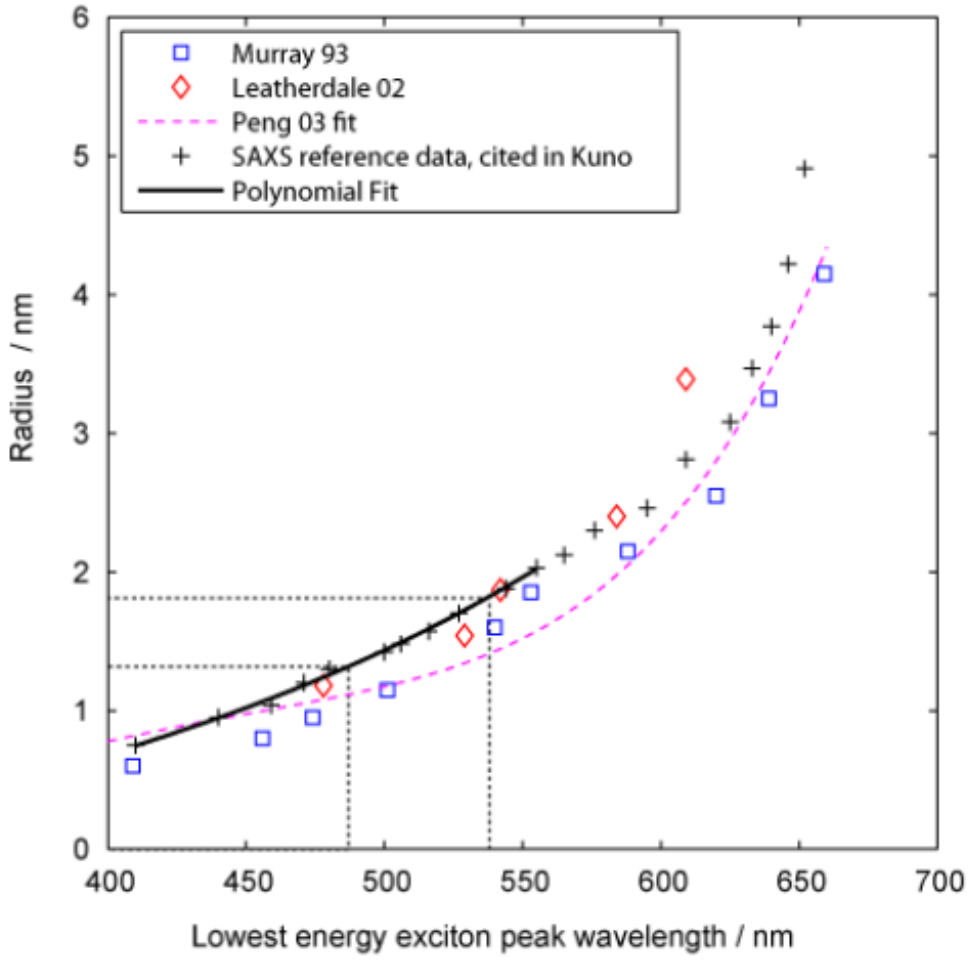

Figure 2.1.1.2 Different sizing curves for CdSe NQDs [35].

Moreover, molar extinction coefficients were calculated in literature for the most commonly synthesized NQDs such as CdSe [6,38,39,5], CdTe [6,40], and CdS [6]. Therefore, with a known molar extinction coefficient, concentration of

NQDs in solution can be determined from Beer-Lambert Law by using absorption spectrum

$$A = \varepsilon CL \tag{1}$$

where A is the absorbance and ε is the molar extinction coefficient (L/mol-cm). C gives the concentration of NQD solution (mol/L), while L is the length of cuvette (cm). Finally, with a known cuvette length (generally 1 cm) and molar extinction coefficient, concentration of NQDs solution can be easily calculated from Equation 1.

Furthermore, the lowest energy part of the absorption spectrum can be used to determine to crystal structure of NQDs by fitting with three Gaussian functions [41] to extract excitonic peaks. The reason for using Gaussian function is that although NQDs have atomic-like discrete band diagram, because of the size distribution, these excitonic peaks have Gaussian distribution. Then, energy difference between the first and second excitonic peak is calculated for different size of CdSe NQDs by fitting. After that, energy difference between the first and second excitonic peak (E2-E1) versus the first excitonic peak energy (E1) curve is plotted. Finally, after analyzing the curve, the crystal structures are determined according to value of E1 at E2-E1=0 which is shown in Chapter 3.

2.1.2. Fluorescence Spectroscopy

Fluorescence spectroscopy is used for analyzing photoluminescence of NQDs and it is one of the major tools for optical characterization. Photoluminescence can be described as a two-step physical process. First, an incoming photons having higher energy than the bandgap of material are absorbed and they create electron-hole pairs or excitons. After that, relaxation processes take place via phonons and electron-hole pairs recombine radiatively and emit a photon having energy of bandgap of material (Figure 2.1.2.1).

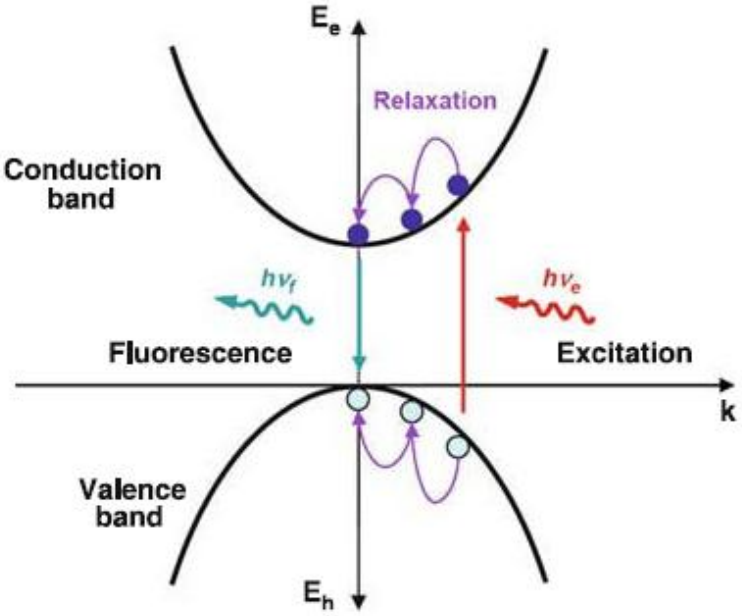

Figure 2.1.2.1 Schematic representation of photoluminescence process [42].

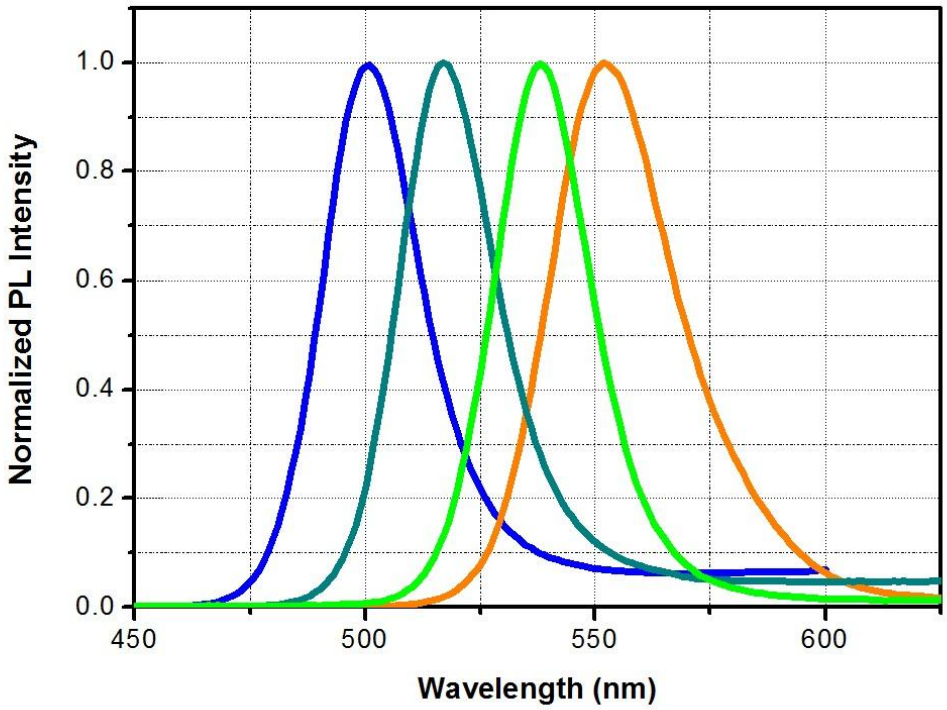

Figure 2.1.2.2 Photoluminescence spectra of different size CdSe NQDs.

Moreover, because of the quantum confinement effect, the band structure of NQDs is discritized and also with decreasing size of NQDs the effective energy bandgap of the structure increases. Therefore, emission is shifted with size and size tunable emission properties of NQDs can be observed clearly with fluorescence spectrometer. For instance, photoluminescence of size series of CdSe NQDs are shown in Figure 2.1.2.2. In addition, the full-width-at-half-maximum (FWHM) of emission peak of NQDs also gives idea about the size distribution of NQDs. Thus, their emission strongly depends on their size, and increasing size distribution results in increased FWHM.

2.1.3. Determination of Photoluminescence Quantum Yield

Photoluminescence quantum yield (QY) can be defined as the number of emitted photons per number of absorbed photons [43]. The QY measurements are very important, since both performance of single NQD for biological application including bio-detection [44], biological fluorescence imaging [44] and their device applications such as NQD based light emitting diodes [45] depend on the QY of NQDs.

For the calculation of the QY of NQDs, first, absorption and emission spectrum of the NQDs are obtained. Then, according to their absorption and emission wavelength range, a reference dye is selected, which has absorption and emission levels approximately in the same range for a reliable comparison. After that, at the same excitation wavelength, where both sample and reference dye have the same absorbance, the emission spectrum measurement is taken under the same instrumental condition. Finally, after the data is evaluated, the Q.Y. is calculated by using Equation 2 [43]

$$Q.Y._{sample} = Q.Y._{reference-dye} \frac{F_{sample}}{F_{reference-dye}} \frac{f_{reference-dye}}{f_{sample}} \frac{n_{sample}^{2}}{n_{reference-dye}^{2}} \qquad (2)$$

where F corresponds to spectrally integrated number of photons. *f* is the absorption factor and n is the refractive index.

For a wavelength region between 500-600 nm, Rhodamine 6G (R6G) is the most widely used reference dye with a well-known QY of 0.95 in methanol [46] (Figure 2.1.3.1). In addition, in photoluminescence measurements, the optical densities of reference dye and NQD should be lower than 0.1-0.14 at the excitonic peak wavelength in order to guaranty that there is no re-absorption taking place and the light penetration depth is approximately equal in the cuvvettes. In this thesis, all the reported QY values are calculated with respect to R6G.

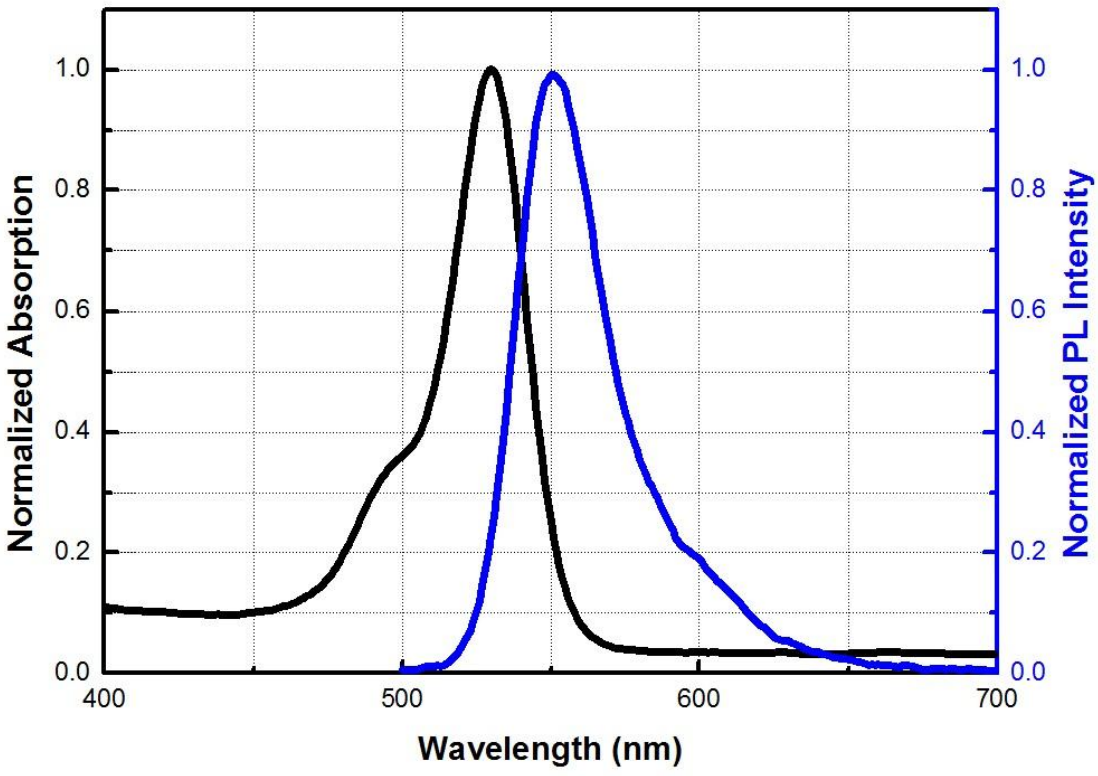

Figure 2.1.3.1 Absorption and photoluminescence spectra of R6G dissolved in methanol.

One example of the QY measurement was shown in Figures 2.1.3.2, 2.1.3.3 and 2.1.3.4. First, the absorption and emission spectra of 3 ML CdSe/CdS core/shell NQDs were taken (Figure 2.1.3.2). Then, as a reference dye R6G was selected, since both of them are in the same absorption and emission wavelength region. After that, with the excitation wavelength of 475 nm where both of them have the same absorbance value (Figure 2.1.3.3), their emission spectra were taken (Figure 2.1.3.4). Finally, by integrating the area under the photoluminescence curve over photon energy, QY is calculated by using Equation 2 and it was found to be 92% for 3 ML CdSe/CdS core/shell NQDs.

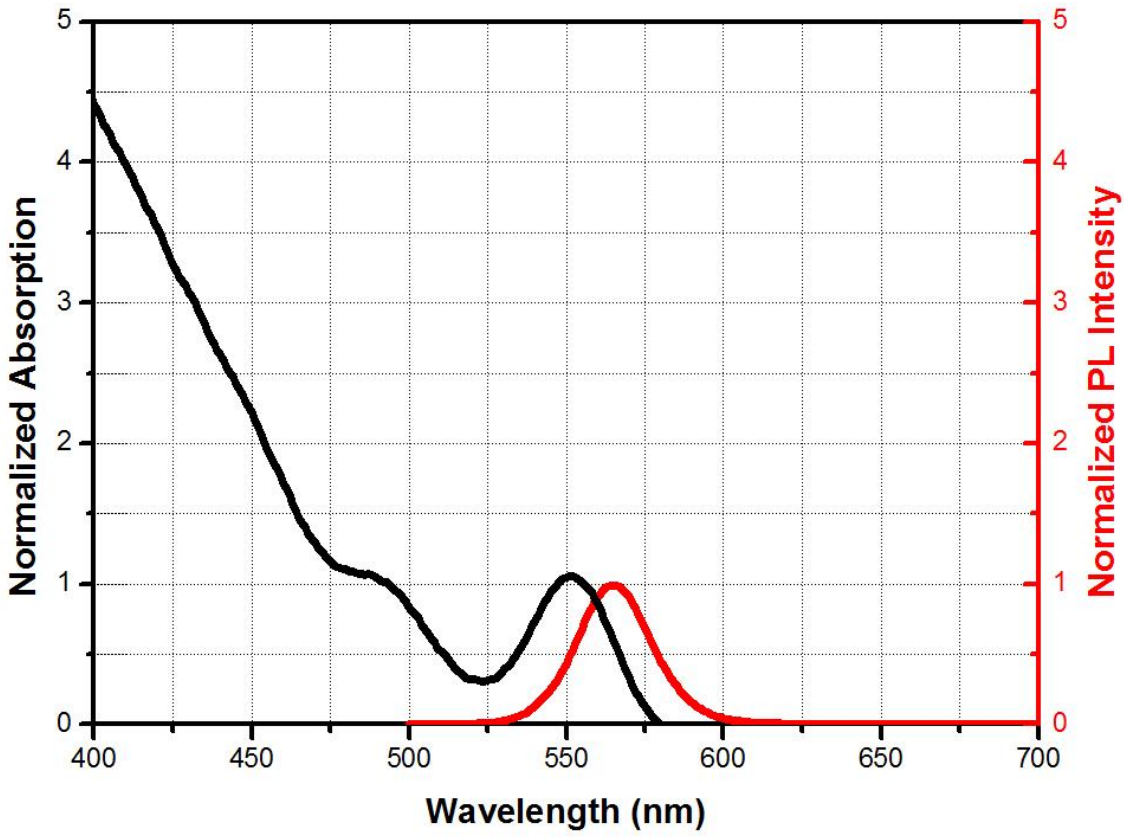

Figure 2.1.3.2 Absorption and photoluminescence spectra of 3 ML CdSe/CdS NQDs.

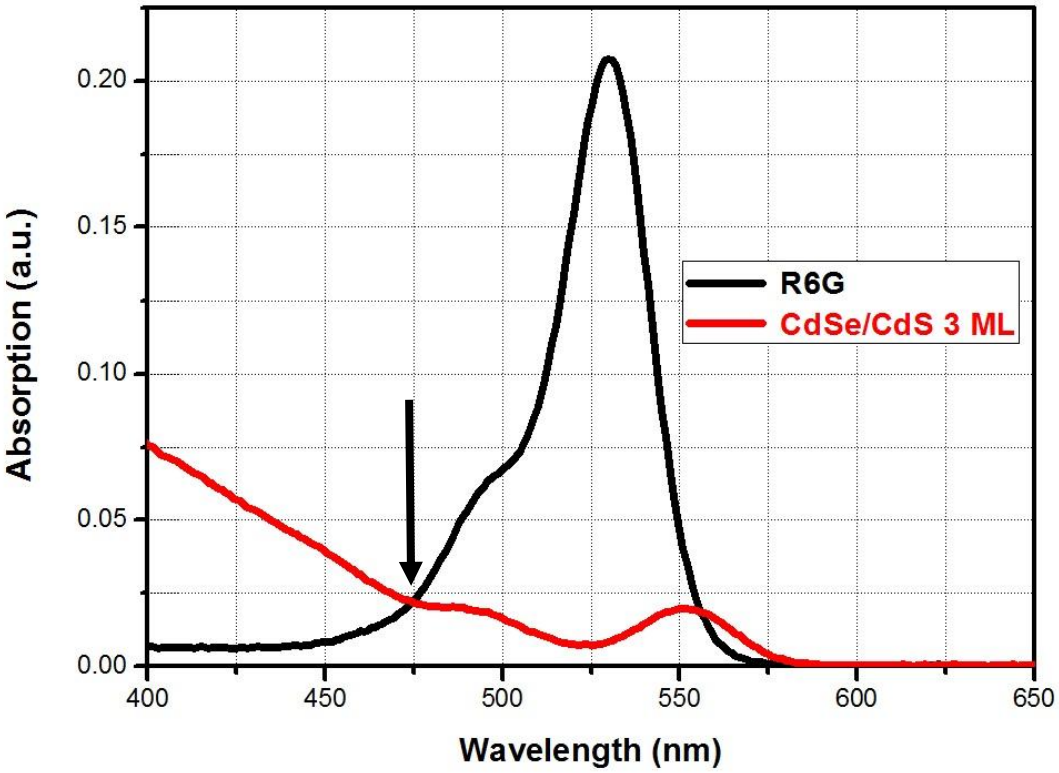

Figure 2.1.3.3 Absorption spectra of R6G and 3ML CdSe/CdS NQDs.

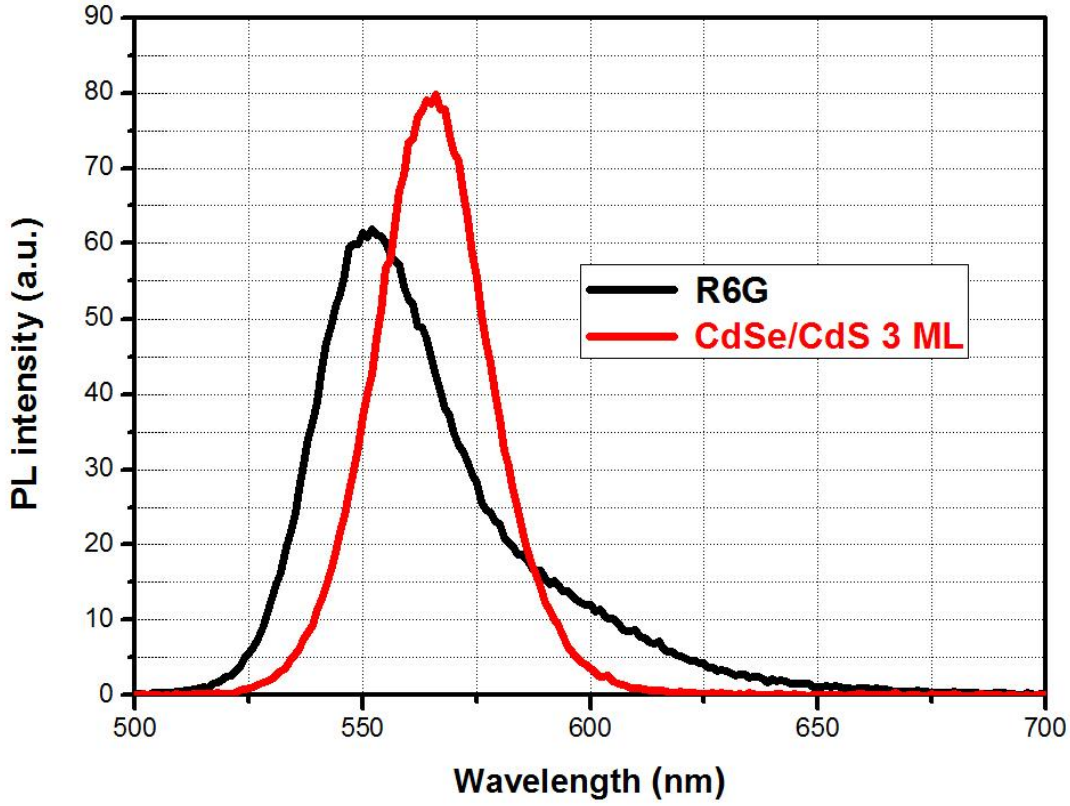

Figure 2.1.3.4 Photoluminescence spectra of R6G and 3ML CdSe/CdS core/shell NQDs with the same excitation wavelength of 475 nm.

2.2. Structural Characterization

Structural characterization of NQDs includes X-ray diffraction (XRD), X-ray photoelectron spectroscopy (XPS), transmission electron microscopy (TEM) and scanning electron microscopy (SEM). By using these characterization tools, very useful information related to the crystal structure, morphology, chemical composition and size of NQDs is obtained.

2.2.1. X-Ray Diffraction

XRD is a very common and important tool for the characterization of crystal structure properties of NQDs such as their phase, inter-planar spacing, and size by using X-rays having a wavelength between 0.1 Å (Angstrom) and 100 Å.

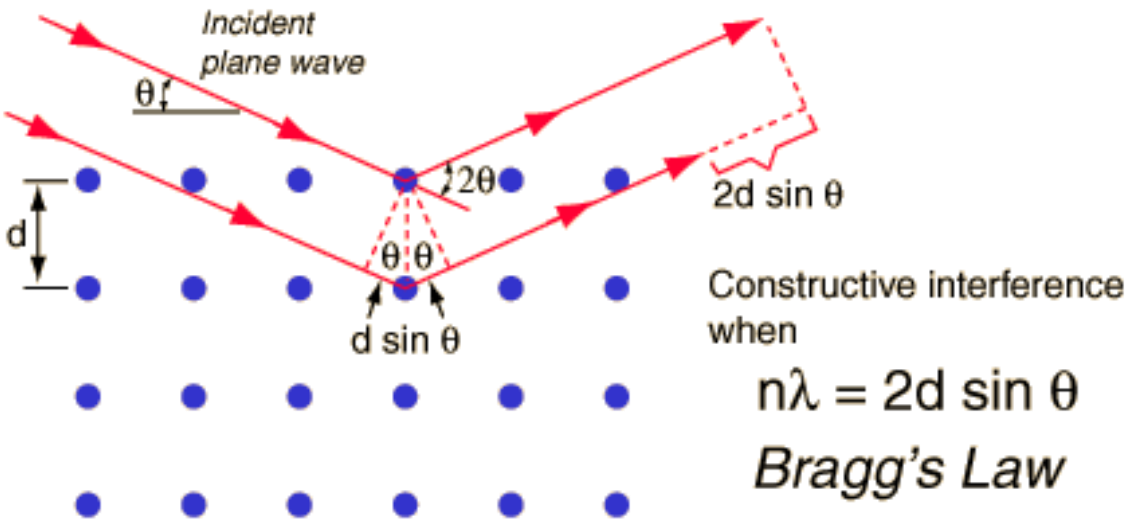

Figure 2.2.1.1 Bragg's Law and schematic representation of constructive interference between X-Rays [74].

In crystal structures, atoms are arranged in regular and repeating order. Therefore, X-rays incident on the sample form either constructive or destructive interferences according to inter-planar spacing or distance between planes. As it

can be seen from Figure 2.2.1.1, if the path difference between two scattered X-ray beams is equal to an integer number of wavelength, they will form a constructive interference and it is known as Bragg's condition

$$n\lambda = 2d_{hkl}\sin\theta \qquad (3)$$

where n is the integer number, λ is the wavelength of incident X-rays, d is the inter-planar spacing, and Θ is the half of the angle between the incident and scattered X-rays. Therefore, from Equation 3, the inter-planar spacing and lattice constants of crystal structures are calculated.

Zinc Blende Crystal Structure **Wurtzite Crystal Structure**

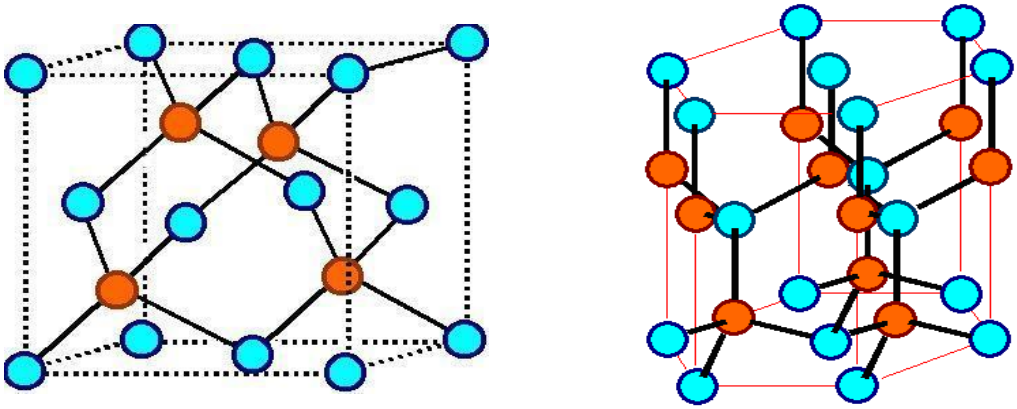

Figure 2.2.1.2 Unit cell of zinc blende crystal structure and wurtzite crystal structure [75].

For NQDs, crystal structures or phases are very important, and the easiest way to understand their crystal structure is by using XRD. For example, the most widely synthesized CdSe nanocrystal can be either in wurtzite crystal structure or zinc blende crystal structure depending on the synthesis parameter such as ligands used during synthesis [41,46,47] (Figure 2.2.1.2). According to the crystal structure, optical properties of NQDs are changed; they show different absorption and emission behavior [48] (Figure 2.2.1.3).

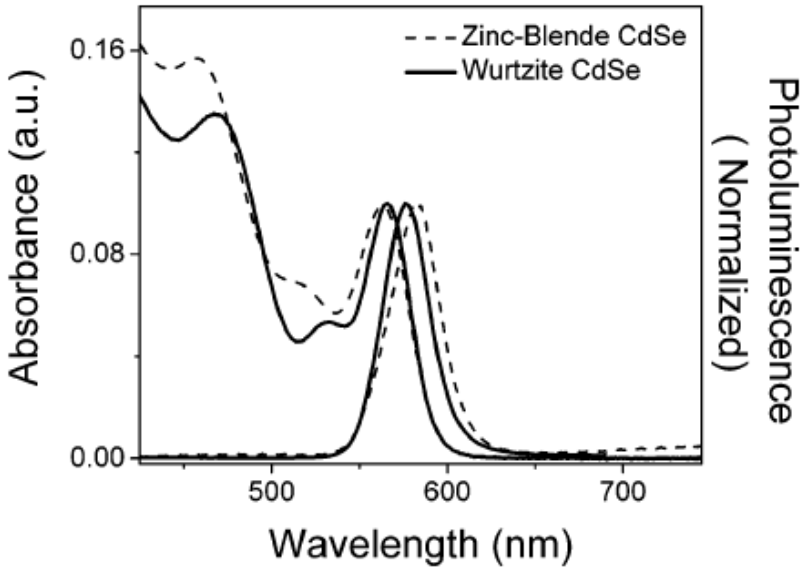

Figure 2.2.1.3 Absorption and photoluminescence spectra of CdSe having zinc blende crystal structure and wurtzite crystal structure [48].

Moreover, the crystal structure of NQDs affects the final shape of core/shell NQDs. For example, it is shown that coating of CdSe NQDs having wurtzite crystal with CdS results in more uniform shell deposition and spherical nanocrystals. On the other hand, for CdSe having zinc blende crystal structure, coating with CdS results in tetrahedral shape nanocrystals [41]. In addition, initial crystal structure of CdSe seeds plays an important role for the synthesis of heterostructure NQDs. For instance, CdSe seeds having wurtzite crystal structure shows formation of core/shell nanorod structure, whereas CdSe seeds having zinc blende structure shows tetrapod formation [47] (Figure 2.2.1.4).

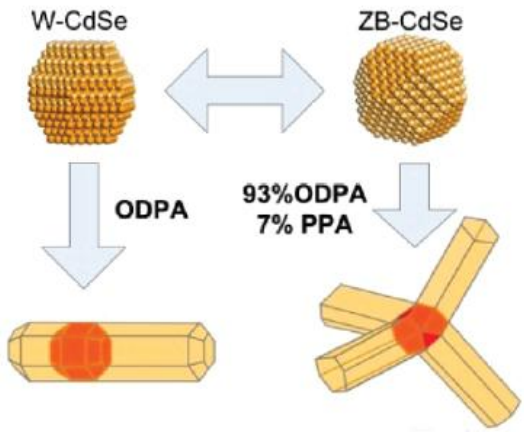

Figure 2.2.1.4 Schematic representation of different growth kinetics for CdSe seeds having wurtzite crystal structure and zinc blende crystal structure [47].

2.2.2. X-Ray Photoelectron Spectroscopy

XPS is a very useful and important tool for the characterization of surface chemical properties of NQDs. The reason why it gives information only about surfaces is related to the mean free path of electron. Since the mean free paths of electrons are generally less than 10 nm, surface related properties are obtained from XPS. XPS uses X-ray beams to bombard the material and determine the binding energy of the ejected electrons from their orbitals by using detector under ultra-high vacuum (UHV) condition by

$$E_{binding} = E_{X-Ray} - E_{kinetic} \quad (4)$$

where $E_{X\text{-}ray}$ is the energy of incoming X-ray, $E_{kinetic}$ is the energy of ejected electron from its orbital, and $E_{binding}$ is the binding energy of the electron.

By using Equation 4, XPS spectrum is obtained, which shows the intensity versus binding energy. Then, by analyzing the spectrum, very important information about chemical composition [49], surface ligand coverage [49], surface shell coverage [50] and surface oxidation [49] can be acquired for NQDs.

Moreover, by using XPS in conjunction with TEM, a shell thickness calculation can be undertaken. In literature, shell thickness calculation of the capping layer for CdS [51] and ZnS [52] core NQDs is shown by Sarma and co-workers. By extending their equation, we calculated the shell thickness in CdSe/CdS core/shell NQDs.

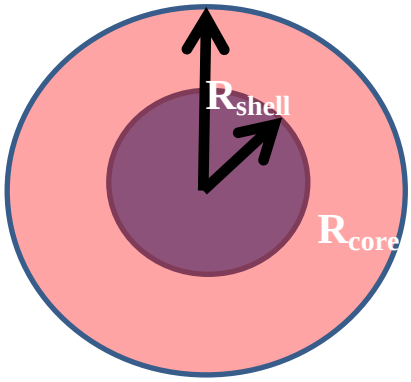

Figure 2.2.2.1 Schematic representation of core/shell NQDs.

First of all, in order to calculate the thickness of shell from the XPS, the shell thickness should be lower than the mean free path of electron. Otherwise, it will be a wrong assumption, since the decrease in the intensity of photoelectron peaks of the core material does not reflect the coating of shell material.

The intensity of photoelectron from any atom is given as Equation 5 in terms of escape depth,

$$dI = I_0 \exp(\frac{-z}{\lambda})dv \qquad (5)$$

In Equation 5, dI is the infinitesimal intensity contribution from volume dv, z is the distance between the surface and origin of photoelectron, λ is the mean free path of electron, I_0 is the constant which depends on the type of electronic level, properties of sample and instrumental factors such as geometry and angular acceptance of analyzer, transmission coefficient and photon flux. However, for both core and shell measurements, instrumental factors are the same, so the difference in the value of I_0 for the core and the shell comes from material properties. For example, in our case we have CdSe core and CdS shell where density of Se and S atoms are not the same. Therefore, this can be easily calculated from the physical properties of these materials,

$$\frac{I_0^{CdS}}{I_0^{CdSe}} = \frac{\rho^{CdS}}{M^{CdS}} \frac{M^{CdSe}}{\rho^{CdSe}} \tag{6}$$

where ρ represents the density of material and M represents the molecular weight of material. Then, the intensity of photoelectrons for both the core and shell can be calculated by taking integral of Equation 5 with suitable limits from Figure 2.2.2.1. In addition, it is expressed in terms of spherical coordinates. Then, Equation 5 becomes

$$I = I_0 \int_{R'}^{R''} \int_0^{\pi} \int_0^{2\pi} \exp(-\frac{f(r,\theta)}{\lambda}) r^2 dr \sin\theta d\theta d\phi \tag{7}$$

where $f(r,\theta) = (R^2 - r^2 \sin^2\theta)^{1/2} - r\cos\theta$. In addition, the integral of Equation 7 over θ always equals to 2π because of the spherical symmetry. Therefore, the ratios of the intensity of photoelectrons for both the core and shell can be calculated by the following equation

$$\frac{I_{Shell}}{I_{Core}} = \frac{I_0^{CdS} \int_{R_c}^{R_S} \int_0^{\pi} \exp(\frac{-f(r,\theta)}{\lambda}) r^2 dr \sin\theta d\theta}{I_0^{CdSe} \int_0^{R_c} \int_0^{\pi} \exp(\frac{-f(r,\theta)}{\lambda}) r^2 dr \sin\theta d\theta} \tag{8}$$

where R_s represents the radius of shell and R_c represents the radius of the core. Finally, these integrals can be solved for different values of R_s and R_c numerically. Initial values of R_c are determined by using TEM and subsequently shell thickness are calculated from Equation 8 by using the intensity of photoelectrons peaks. The measurements results of our synthesized NQDs are discussed and tabulated in Chapter 3.

2.2.3. Transmission Electron Microscopy

Transmission electron microscopy (TEM) is the most powerful and necessary tool for characterization of NQDs. TEM is used to obtain reliable information about the size and shape of the NQDs. In addition, it gives information about the crystal structure [32,46], chemical composition [52,14], strain formation [13], shell formation [54], and crystal defects [47] such as stacking faults.

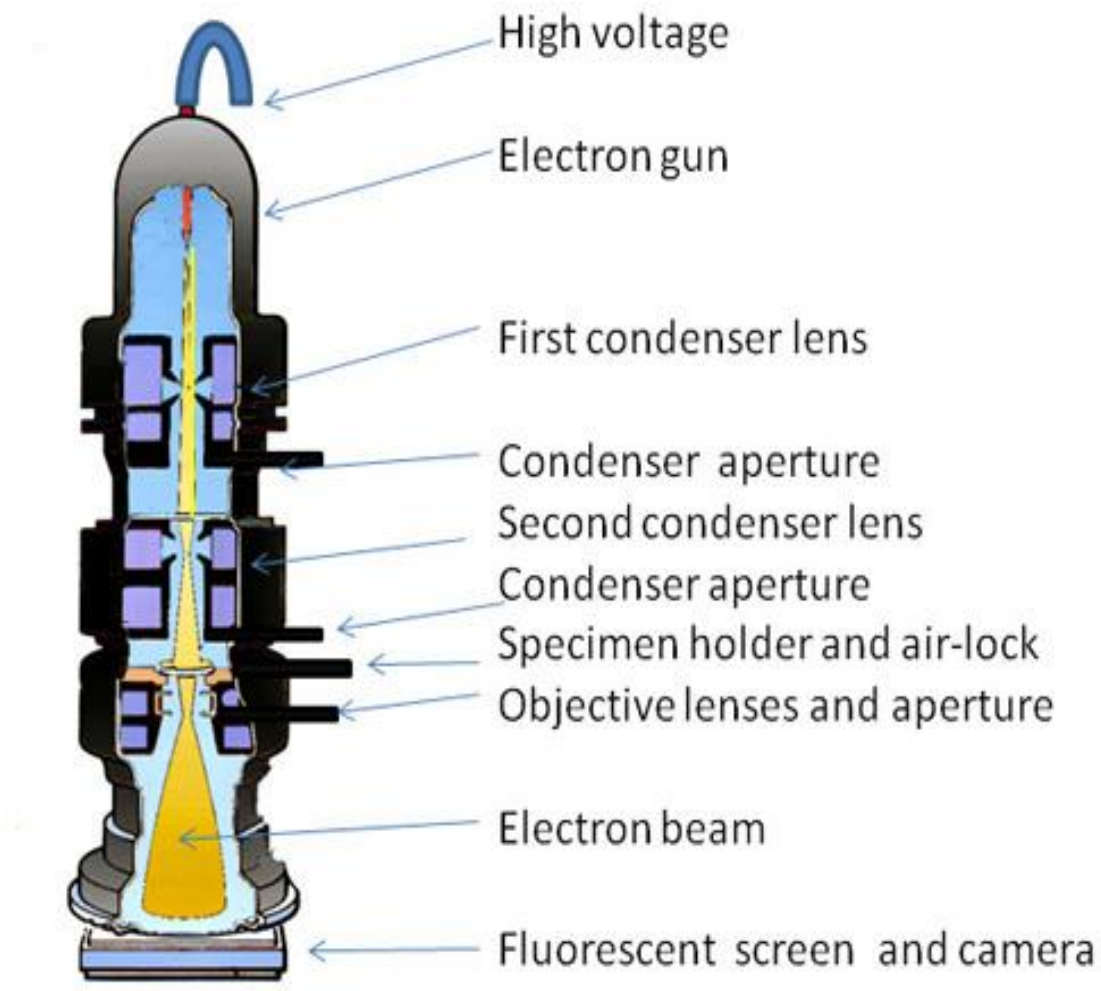

Figure 2.2.3.1 Schematic representation of typical TEM system [76].

In TEM, electrons are accelerated by the application of high voltage in the range of 100 kV and 400 kV. Then, by using a set of condenser lenses and apertures, electron beams are focused on the sample. After, the interaction of electron beams with the sample, electrons are scattered either elastically or inelastically. Finally, the scattered electrons are gathered and focused again for the formation of image (Figure 2.2.3.1).

Generally, according to resolution, TEMs can be divided into two groups: high resolution TEMs and low resolution TEMs. By using low resolution TEMs, size and shape of NQDs are determined. On the other hand, with high resolution TEM, in addition to the size and shape of NQDs, information about the internal structure can be determined. For example, Figures 2.2.3.2.a and 2.2.3.2.b show a low resolution TEM image of the 8 ML CdSe/CdS and a high resolution TEM image of 3 ML CdSe/CdS, respectively. As it can be seen from the figures, when compared with low resolution TEM, it is possible to achieve higher magnification with high resolution TEM. In addition, with high resolution TEM, lattice fringes become clear, which are important for the analysis of crystal structure, interplanar spacing, stacking faults, and dislocations.

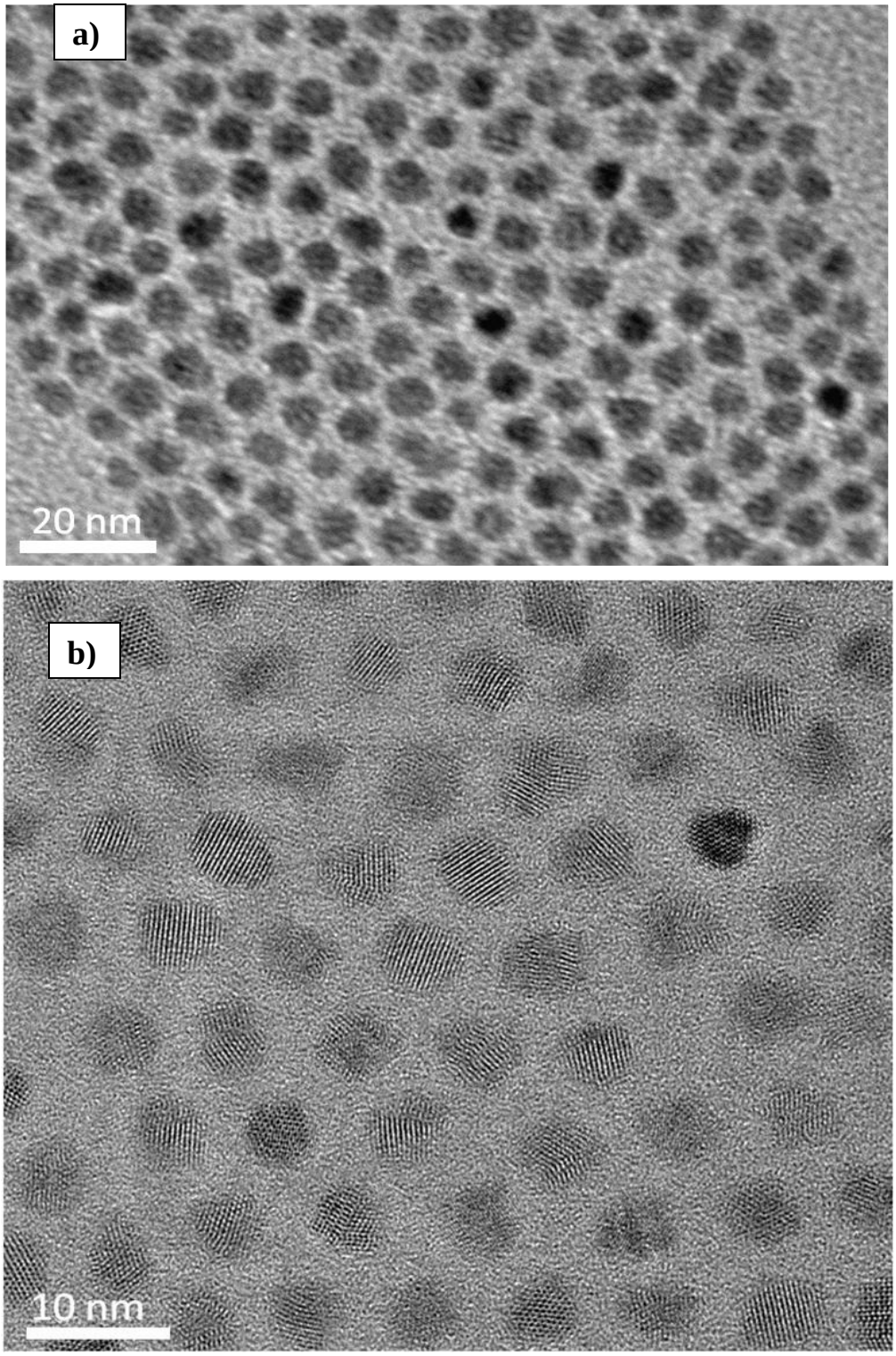

Figure 2.2.3.2 a) Low resolution TEM image of 8 ML CdSe/CdS core/shell NQDs and b) high resolution TEM image of 3 ML CdSe/CdS core/shell NQDs.

In addition, fast fourier transformation (FFT) of high resolution TEM images can be taken to determine the crystal structure [47]. When FFT is applied to the image representing the real space, a new image is obtained corresponding to the reciprocal space of material. Then, from the reciprocal space, the crystal structure of materials can be understood (Figure 2.2.3.3). For example, in Figure 2.2.3.3 a, a high resolution TEM image of 4 ML CdSe/CdS core/shell nanocrystal is shown. When FFT of this image is taken, it gives the reciprocal space of NQDs (Figure 2.2.3.3 b). From the reciprocal image, it can be determined that this sample has wurtzite crystal structure according to position of points corresponding to crystal planes. Moreover, selective area X-ray diffraction (SAED) can be taken from TEM. This gives idea about whether the material is single crystal or polycrystalline from the diffraction pattern. In addition, the interplanar spacing can also be determined from the SAED images for the crystal structures of interest.

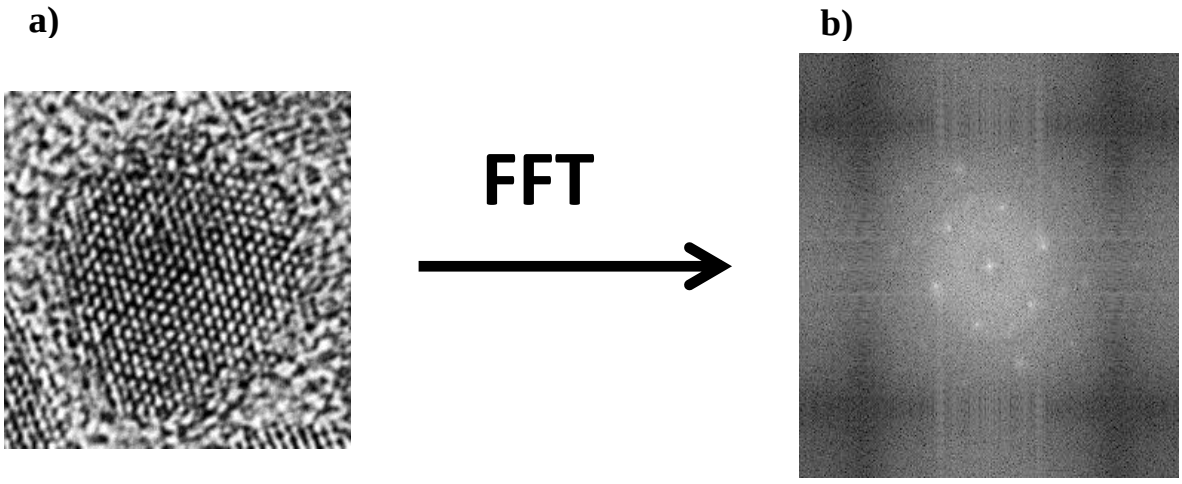

Figure 2.2.3.3 a) High resolution TEM image of 4 ML CdSe/CdS core/shell NQDs and b) reciprocal lattice image of the same 4 ML CdSe/CdS core/shell NQDs after the application of FFT.

2.2.4. Scanning Electron Microscopy

Generally, SEM can produce images with features down to length scales of 10 nm. Therefore, the resolution of SEM is not enough for the characterization of morphology and shape of smaller NQDs. However, with larger NQDs such as giant CdSe/CdS core/shell NQDs, it is possible to obtain images showing size, shape and distribution of NQDs (Figure 2.2.4.1). Therefore, for the NQDs, SEM is widely used for the energy dispersive X-ray spectroscopy (EDAX). EDAX gives information about chemical composition of samples depending on the characteristic X-ray radiation of materials. They are formed with heavy bombardment of sample with an electron beam and then characteristic X-Ray radiations are collected with a detector. After that, since each material has its own characteristic X-ray radiation, the chemical composition of samples is calculated from the intensity of peaks.

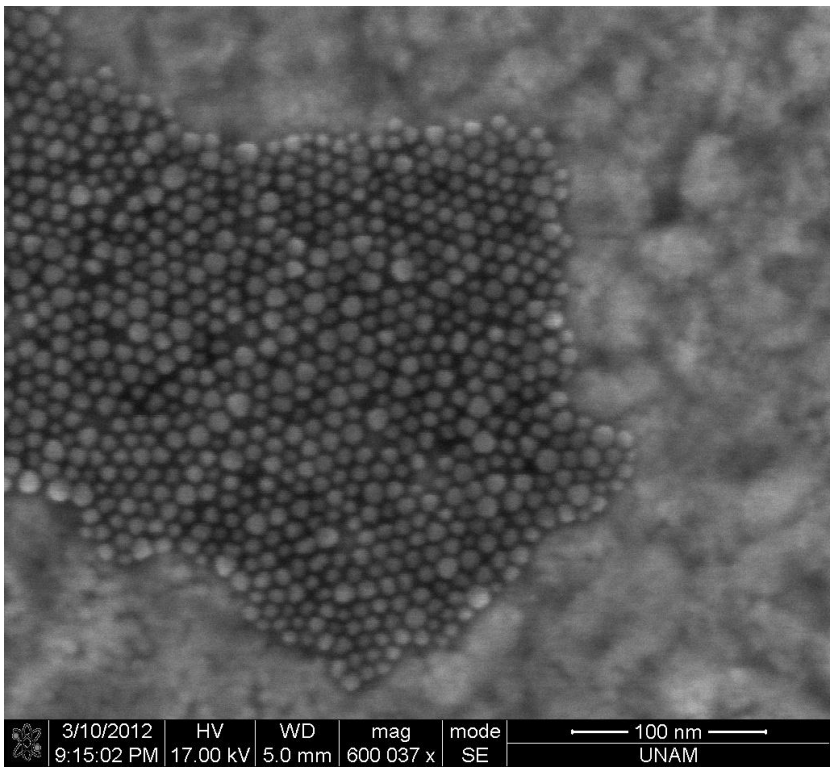

Figure 2.2.4.1 SEM images of 10 ML giant CdSe/CdS core/shell NQDs.

Chapter 3

Synthesis and Characterization of Highly Efficient CdSe/CdS Core/Shell Nanocrystals for Optical Gain with Two-Photon Infrared Pumping

3.1. Introduction

After the first successful highly monodisperse colloidal synthesis of nanocrystal quantum dot is shown by Bawendi and co-workers [3], they become very popular for researchers with their novel size tunable optical properties. When compared to their organic counterparts, they feature higher photoluminescence quantum yield, higher molar extinction coefficient [5], broad band absorption spectrum, lower full-width-at-half-maximum (FWHM) or narrow emission behavior spanning from UV to near-infrared region, and higher stability against photobleaching and chemical degradation [4,54]. All these properties make NQDs the most promising candidates for many applications from biology including imaging [56], labeling [4] and sensing [7] to optoelectronic devices such as light emitting diodes [8], photodetectors [11], solar cells [9] and lasers [10].

Having size tunable emission across whole visible spectrum and optimized synthesis conditions make CdSe one of the most extensively studied NQDs.

Until now, most of the efforts have been made especially for increasing the photoluminescence quantum yield and stability of these NQDs. Although the surface of NQDs are capped with organic ligands, it is not easy to passivate both anion and cation atoms by using the same ligand simultaneously. Therefore, only core NQDs generally have lower quantum efficiency and stability. To increase the efficiency and the stability of these NQDs, coating with another semiconductor material having a higher band gap is generally used. According to band alignment of the core and shell material after coating with higher band gap material, both electrons and holes are confined inside the core and they are taken away from the surface of NQDs. NQDs having this band alignment are called as Type I NQDs and by elimination of surface trap states and protection of surface core atoms against oxidation, coating with shell material improves the efficiency and stability in Type I NQDs.

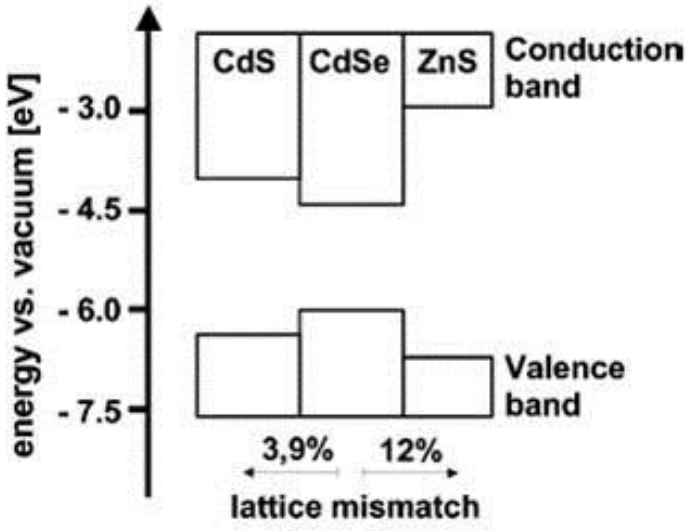

Figure 3.1.1 Conduction and valence band position of semiconductor materials with their lattice mismatch values [32].

For CdSe NQDs, the most widely used shell materials are CdS and ZnS, both of which have a higher band gap than CdSe (Figure 3.1.1). In literature, they were applied either in the form of pure CdS [56,49] and ZnS [33] shell, or in the form of heterostructure with alloyed [53] and/or composition gradient structure

$Cd_xZn_{1-x}S$ [58]. As it can be seen from Figure 3.1.1, ZnS has a higher bandgap than CdS, and therefore, it supplies better confinement for both electrons and holes in the core with respect to CdS. On the other hand, when compared to CdS, ZnS has a higher lattice mismatch with CdSe, so it increases the probability of formation crystal defects such as dislocations, which increase the nonradiative recombination of excitons or electron-hole pairs and limit the thickness of ZnS shell. Therefore, to obtain highly efficient and stable NQDs, combination of CdS and ZnS shells are studied excessively by combining the advantages of both of them [32].

Recently, synthesis of CdSe/CdS core/shell NQDs have shown that it is also possible to obtain high photoluminescence quantum yield without using ZnS as a shell material with some new optical properties [58,59]. First of all, as a result of smaller lattice mismatch (3.9%) and having the same wurtzite crystal structure, CdSe/CdS core/shell NQDs offer high quality crystal structure without formation of any defect [60]. Second, coating with CdS having a lower bandgap than ZnS increases the absorption cross-section above the band gap of shell material [61] and increases absorption. Third, in CdSe/CdS core/shell NQDs, because of the inefficient electronic barriers for electrons, electrons are localized through whole structure, while holes are confined in the core. Therefore, with the separation of electron and hole wavefunctions, Auger recombination [62] can be suppressed in CdSe/CdS NQDs, which otherwise lowers the device performance of NQDs [63] by increasing the rate of nonradiative combination. Moreover, as a result of weakly confining shell or localization of electrons through whole structure, more red-shift in the emission is observed with coating CdS shell instead of ZnS.

In this study, we report the synthesis and characterization of CdSe/CdS core/shell NQDs with successive ion layer adsorption and reaction (SILAR) technique for the optical gain studies with two-photon infrared pumping using all these advantages described above by following the recipe of Bawendi and co-workers [59].

3.2. Experimental

3.2.1. Chemicals

Cadmium oxide (99.99%), trioctylphosphine oxide (TOPO, technical grade 90%), trioctylphosphine (TOP, technical grade 90%), tributylphosphine (TBP, technical grade), octadecene (ODE, technical grade 90%), oleic acid (OA, ≥99%), selenium (Se pellets <4mm, 99.99%), hexamethyldisilathiane ($(TMS)_2S$, synthesis grade), oleylamine (technical grade, 70%) were purchased from Aldrich. Tetradecylphosphonic acid (TDPA, 98%) was purchased from Alfa.

3.2.2. Synthesis of CdSe Core Nanocrystals

CdSe core NQDs were synthesized by following standard recipes from literature [32,58]. For the synthesis of small size CdSe NQDs 96 mg of CdO, 450 mg of TDPA and 6 g of TOPO were loaded in a three-neck flask and evacuated at 150 ^{0}C for 1 hour to remove any organic residuals. Then, temperature was increased to 350 ^{0}C under argon flow to get optically clear solution. After all CdO was dissolved completely, the temperature was lowered to 273 ^{0}C for injection of 3.3 mL of TOP-Se (1.5 M) or 3.3 mL of TBP-Se (1.5 M) solution prepared inside the glove box (Figure 3.2.2.1). After the injection, the temperature was decreased to room temperature immediately. With this procedure, CdSe NQDs having the first absorption peak approximately between 480 – 490 nm were obtained.

Figure 3.2.2.1 Photograph of the glove box at our lab.

Generally, the ratio of CdO:TDPA:Se determines the final size of NQDs. Therefore, it is possible to obtain different size of CdSe NQDs by changing the ratios. For the synthesis of large size CdSe NQDs, 51.4 mg of CdO, 225 mg of TDPA and 4 g of TOPO were loaded into three-neck flask and connected to a schlenk line (Figure 3.2.2.2). Then, for removal of any organic residuals, it was evacuated at 150 ^{0}C for 1 hour. After that, the temperature was increased to 350 ^{0}C under argon flow for obtaining optically clear solution. After obtaining clear solution, the temperature was decreased to 270 ^{0}C for the injection of TBP-Se solution (2.0 g of TBP and 63.2 mg of Se). After the injection, the temperature was set to 250 ^{0}C for the growth of CdSe NQDs. Then, the reaction was stopped when the desired size of CdSe NQDs is reached. With this procedure, it was possible to obtain CdSe NQDs having the first absorption peak at 540 nm and longer wavelengths.

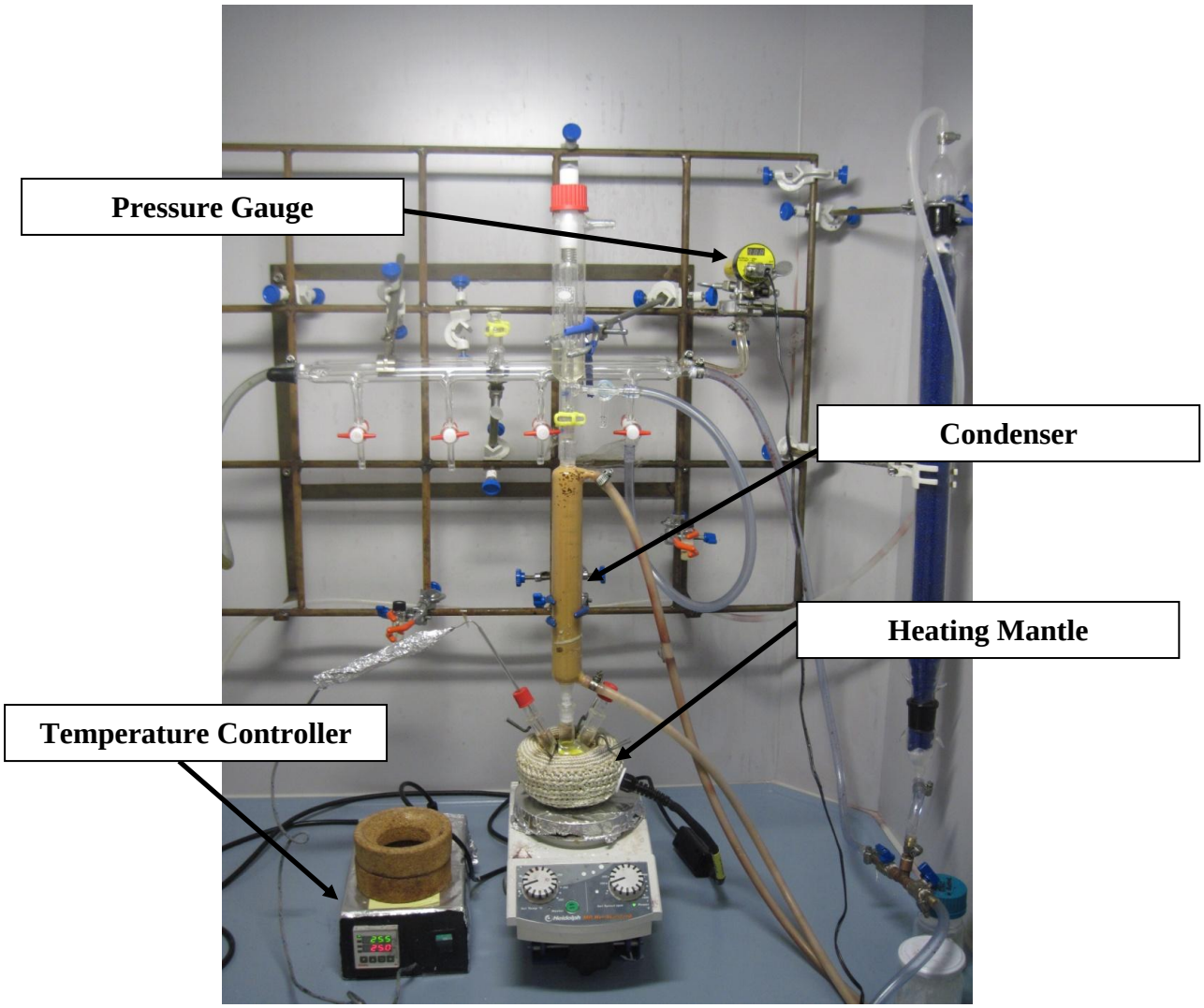

Figure 3.2.2.2 Photograph of our synthesis setup.

For the purification step, after the temperature of the solution was decreased, it was diluted with hexane and centrifuged to remove any unreacted or undissolved particles. Then, supernatant liquid was taken and fluctuated with acetone or methanol to precipitate CdSe NQDs. After removal of supernatant liquid, CdSe NQDs were dissolved in hexane and held at refrigerator or approximately at 4 ^{0}C for one day in order to remove colorless by-products and unstable magic size CdSe clusters [64]. After that, before addition of buthanol and methanol for the second precipitation, NQDs solution was centrifuged again

to remove precipitated materials. Finally, after the second precipitation, CdSe NQDs solution was dissolved in hexane for the next coating step.

3.2.3. Synthesis of CdSe/CdS Core/Shell Nanocrystals with SILAR Technique

CdSe/CdS core/shell NQDs were synthesized with SILAR technique which is firstly shown by Peng and co-workers [58,49]. It was originally developed for the deposition of high quality thin films by switching on and off molecular beams of anion and cation precursors in alternating manner for molecular beam epitaxy. Since anion and cation precursors are not present simultaneously in the reaction chamber, the risk of homogenous nucleation is eliminated. Therefore, this technique is better for the deposition of high quality thin films in a controllable way. Then, Peng and co-workers extended this technique for the synthesis of core/shell NQDs. In SILAR technique for synthesis of core/shell NQDs, first anion or cation precursor is injected to the reaction solution. Then, after waiting sufficiently for the complete deposition of one precursor, another precursor is injected and alternating injections of anion and cation precursors continue until the desired thickness is reached. When compared with other shell synthesis techniques, SILAR technique offers highly precise shell thickness control and homogenous growth of shell materials.

3.2.4. Preparation of Precursor Solution for SILAR Technique

For the shell growth with SILAR technique, precursor solutions containing CdO and $(TMS)_2S$ were used. The cadmium precursor (0.2 M) was prepared by loading CdO, OA and ODE in 50 mL three-neck flask and it was evacuated at 100^0C for 1 hour. Subsequently, temperature was increased to 240^0C under argon flow for complete dissolution CdO. After obtaining optically clear solution, temperature was decreased to room temperature. Then, it was taken

without being exposed to atmosphere and stored in the glove box. After that, it was diluted with TOP and oleylamine until the final Cd concentration became 0.1 M in the glove box. The sulfur precursor was prepared by mixing 105 μL of $(TMS)_2S$ with 4.9 mL of TOP to yield 0.1 M sulfur concentration in the glove box.

3.2.5. Calculation of Injection Amounts for Precursor Solutions

Calculation of injection amounts is the most important part for the synthesis of core/shell NQDs with SILAR technique. While excess amounts of injection results in formation of separated nuclei, nonhomogeneous coating of shell material is observed with the insufficient amount of injection. First of all, the size of CdSe NQDs need to be determined from the first excitonic absorption peak in the absorption spectrum by using the sizing curves [5,59]. Then, with a known molar extinction coefficient of CdSe NQDs, the concentration of NQD solution need to be determined again from the absorption spectrum [5]. After that, thickness of 1 monolayer ML (0.337nm) CdS is estimated on the basis of distance between the most closed packed planes (100) in wurtzite crystal structure. Then, with a known shell thickness, volume occupied by shell material is calculated by

$$V_{shell} = \frac{4}{3}\pi\left[\left(r_c + m \times d_{ML}\right)^3 - r_c^3\right] \quad (9)$$

where r_c is the radius of core, m is the number of monolayer and d_{ML} is the thickness of one monolayer of CdS shell. After that, by dividing the volume of shell to the unit cell volume of CdS, a number of Cd atoms required for one nanocrystal is calculated. Finally, the number of Cd atoms required for one nanocrystal is multiplied with total moles of NQDs in solution to determine the amount of injection solutions.

3.2.6 Preparation of CdSe/CdS Core/Shell NQDs with SILAR Technique

CdSe/CdS core/shell NQDs were prepared with the recipe of Bawendi and co-workers [58,35]. In a typical synthesis, 6 mL of ODE and 3 mL of oleylamine were loaded in 50 mL three-neck flask and evacuated at 100 ^{0}C for 30 min for removal any organic residuals. Then, temperature was decreased to room temperature. After that, certain amount of CdSe NQDs in hexane was injected into solution and the solution was evacuated again to remove hexane and any other impurities. Subsequently, temperature of the solution was increased to shell growth temperature 180 ^{0}C under argon flow. After that, by using syringe pump, cadmium precursor was injected within 3 minutes in a controllable way and it was waited for 12 minutes to complete the reaction of cadmium precursor before injection of sulfur precursor. Then, the sulfur precursor was injected again in 3 minutes, waiting for 12 minutes for the complete reaction. Similarly, alternating injections were carried out with the injection starting every 15 minutes. After the desired thickness of CdS was reached, the temperature was decreased to 80 ^{0}C for the annealing treatment. Then, the solution was diluted with hexane and centrifuged to remove unreacted materials before CdSe/CdS were precipitated by fluctuating with acetone or methanol. Finally, CdSe/CdS core/shell NQDs were dispersed in hexane and stored in a refrigerator.

3.3. Results and Discussion

3.3.1. Optical Characterization

Following the synthesis of CdSe/CdS core/shell NQDs, characterization of the CdSe cores is very important. By using two different recipes described above, different sizes of CdSe NQDs were obtained having the first absorption peak between 480 – 550 nm. As a result of incomplete passivation of surface atoms, they resulted in lower quantum efficiency and lower stability against oxidation. However, they exhibited narrow emission spectrum and their FWHM values are generally within 24-28 nm (Figure 3.3.1.1).

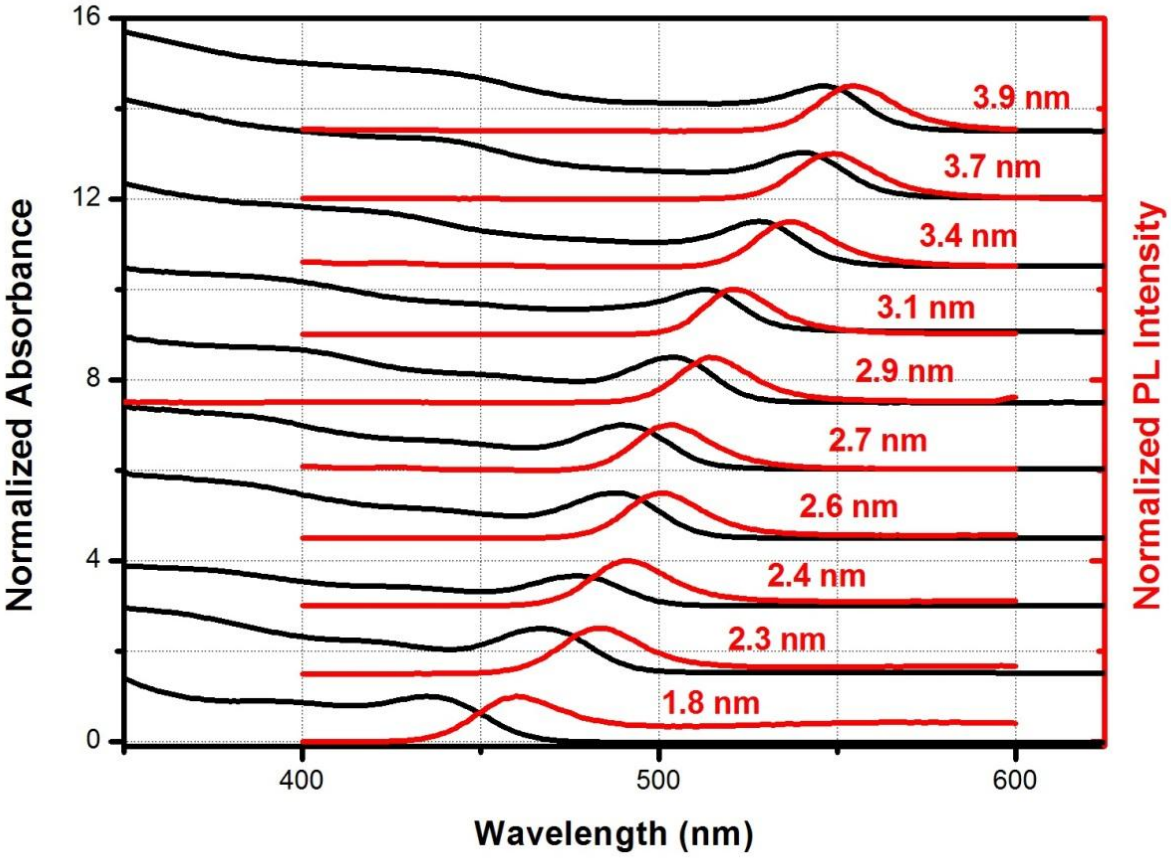

Figure 3.3.1.1 Photoluminescence and absorption spectra of different size CdSe NQDs.

As also clearly seen from Figure 3.3.1.1, there was a Stoke shift, which is known as the energy difference between the first absorption peak and emission peak. By increasing the size of CdSe NQDs, decreased in Stoke shift was observed. While approximately 25 nm Stokes shift was observed in the smaller CdSe core, it was decreased to 10 nm for the larger CdSe core (Figure 3.3.1.2).

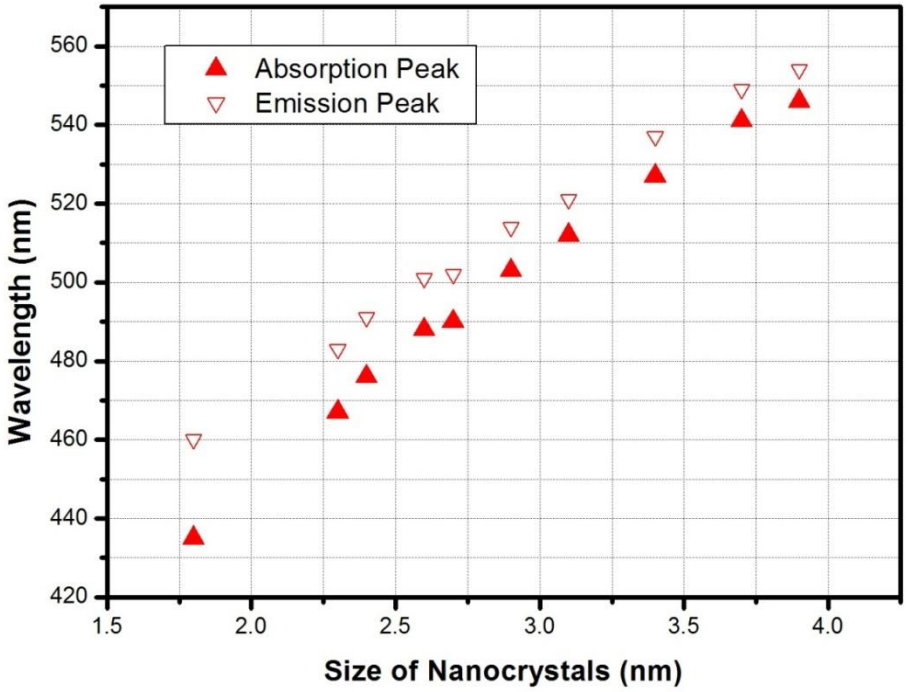

Figure 3.3.1.2 Emission and absorption peaks for different sizes of CdSe NQDs.

For CdSe core NQDs, it was also observed that in photoluminescence spectrum, there were two peaks: one of them belongs to the band edge emission and another one belongs to the trap emission at longer wavelengths (Figure 3.3.1.3a). Deep trap states are formed as a result of incomplete passivation of surface atoms especially for the anion rich (Se atoms) surfaces, because Se atoms have fewer tendencies to bind with organic ligand when compared to Cd atoms. As it can be seen from Figure 3.3.1.3 b, while the trap state emission is observed for NQDs having anion rich surfaces, with the addition of excess Cd atoms for passivation of Se atoms, surface trap emission is eliminated in NQDs having cation rich surfaces [65]. Therefore, for the CdSe NQDs having the Se anion rich surfaces, it is normal to observe two emission peaks. Moreover, it was

also an expected observation for our CdSe NQDs, because for the synthesis of CdSe NQDs, we used excess amount of Se with a ratio of 1.0:6.6 Cd:Se.

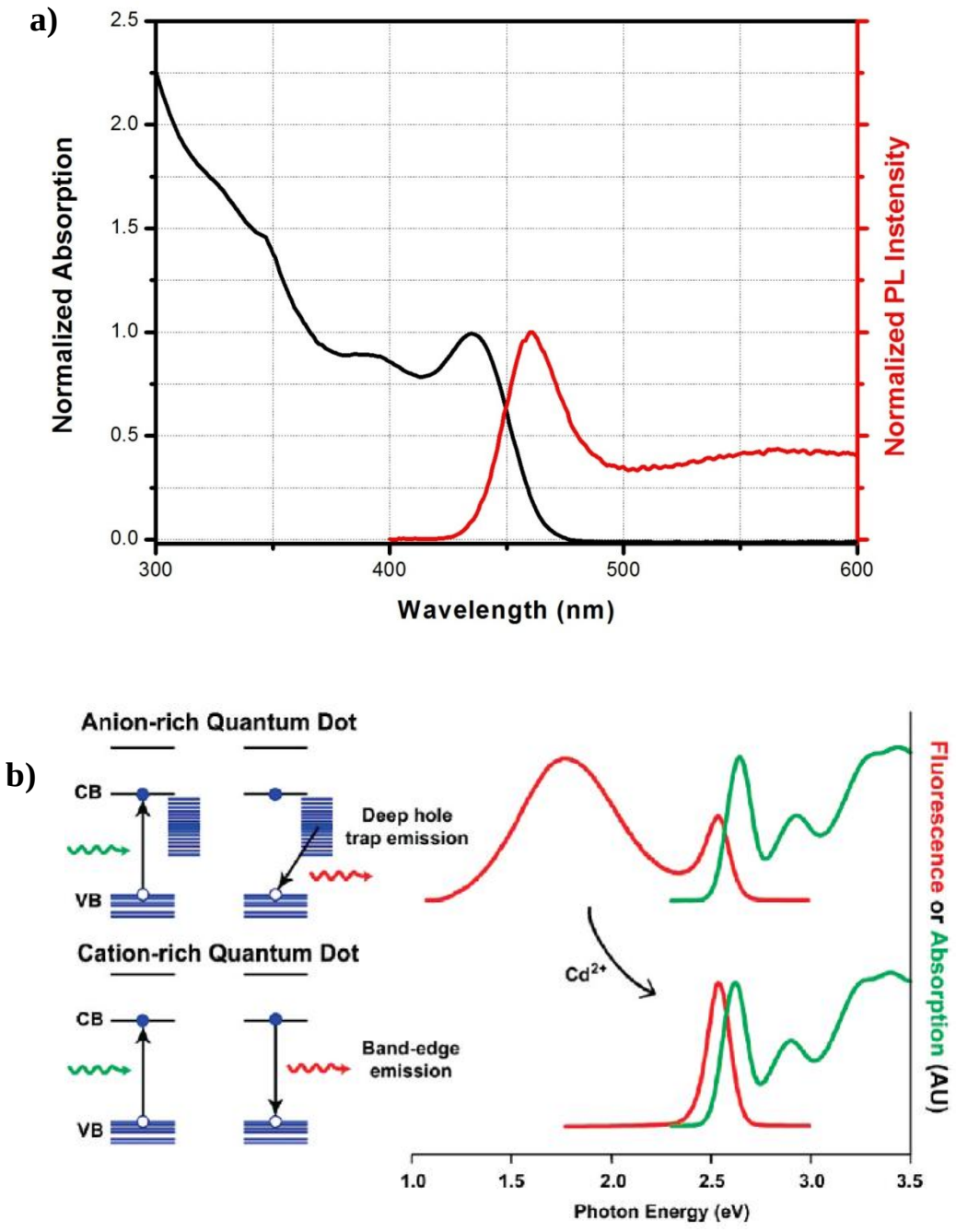

Figure 3.3.1.3 a) Absorption and emission spectra of CdSe NQDs having trap state emission and b) surface dependent emission behavior of CdSe NQDs [66].

CdSe NQDs can have either wurtzite crystal structure or zinc blende crystal structure depending on the synthesis parameters. Generally, their crystal structure can be determined from the XRD and HRTEM. However, because of the smaller size of CdSe NQDs, there is an increase in signal-to-noise ratio and broadness of the peaks, which make it difficult to use these characterization tools. Dubertret and co-workers [41] showed that the crystal structure of CdSe NQDs can be determined from the absorption spectrum owing to their different optical properties. For a different size of CdSe NQDs, energy difference between the first and second excitonic peaks is different for zinc blende and wurtzite crystal structures. The first and second excitonic peak energies can be calculated by fitting absorption spectrum with an equation composed of three Gaussians

$$y = P_1 \exp\left[\frac{-(x-P_2)^2}{2P_3^2}\right] + P_4 \exp\left[\frac{-(x-P_5)^2}{2P_6^2}\right] + P_7 \exp\left[\frac{-(x-P_8)^2}{2P_9^2}\right] \quad (10)$$

where P_1-P_9 are corresponding fitting parameters. Figure 3.3.1.4 shows an example of fitting of the absorption spectrum of CdSe NQDs having a wurtzite crystal structure with three Gaussians in order to accurately determine the position of the first and second excitonic peaks. Then, after fitting the absorption spectrum of different size of CdSe NQDs, we plot the graph of energy difference between the first and second excitonic peaks E_2-E_1 vs the first excitonic peak E_1 (Figure 3.3.1.5). After fitting these data points, the crossing of the linear fitting at E_2-E_1 = 0 gives the band gap of materials. We find the value of 1.76 eV, which is very close the band gap value of CdSe NQDs having wurtzite crystal structure. In addition, we confirmed this estimation with our XRD measurements.

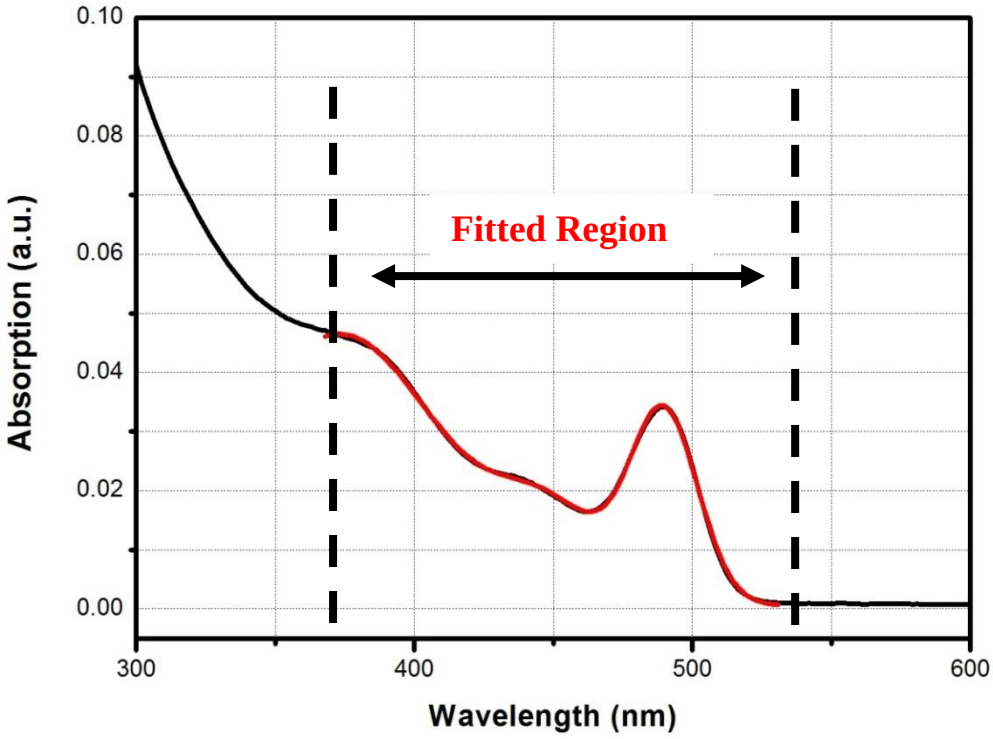

Figure 3.3.1.4 Absorption spectrum of CdSe NQDs (black line) and fitted absorption spectrum of CdSe NQDs (red line).

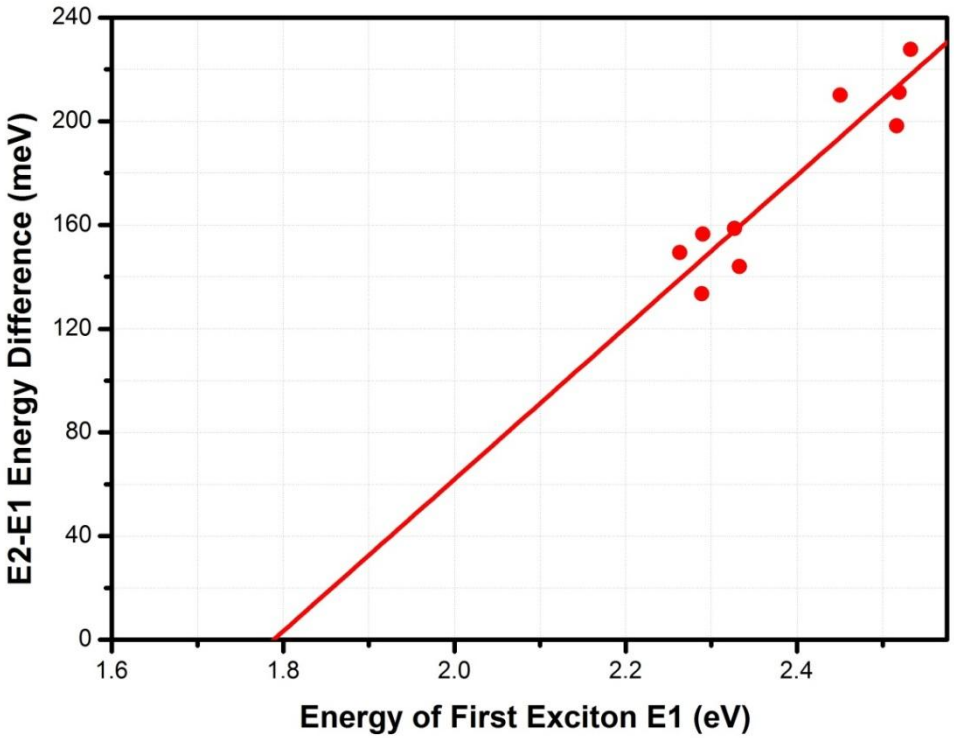

Figure 3.3.1.5 Energy difference between the first and second excitonic peaks (E2-E1) vs energy of the first excitonic peak curve of different size CdSe NQDs.

Before the synthesis of CdSe/CdS core/shell NQDs, purification of CdSe cores is very important, since formation of magic size CdSe clusters [64] were observed during the synthesis of small size CdSe NQDs. If the shell synthesis was carried out without removal of magic size CdSe clusters, it would result in inhomogeneous coating of shell and unexpected emission spectrum having two peaks. For example, in Figure 3.3.1.6, it is clearly seen that before purification of CdSe NQDs, there was a sharp peak appearing at 350 nm corresponding to magic size CdSe clusters. After keeping NQD solution at 4 ^{0}C for 24 hours and following with a purification step, magic size CdSe NQDs were removed and the peak at 350 nm disappeared.

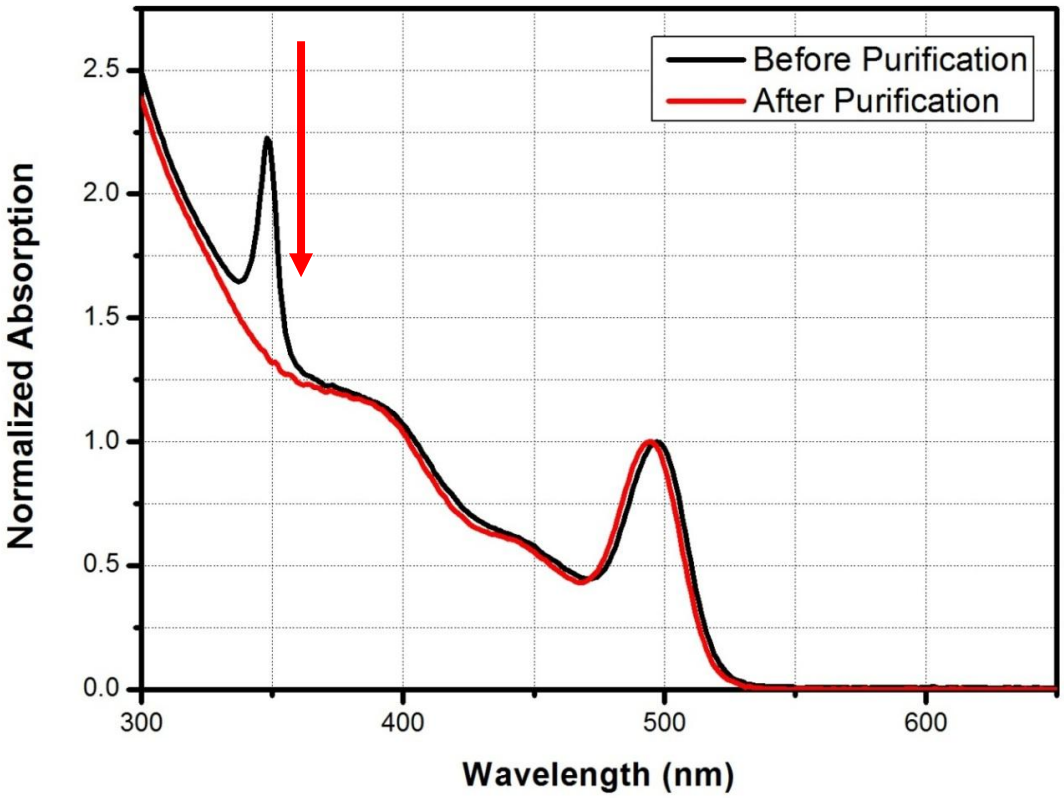

Figure 3.3.1.6 Absorption spectrum of CdSe NQDs with magic size CdSe clusters (black line) and that without magic size CdSe clusters (red line).

By using different size of CdSe cores, we performed CdSe/CdS core/shell NQDs synthesis with SILAR technique for tuning their emission and other optical properties with 1ML (0.337 nm) icrementals in shell thickness for each SILAR cycle. Here, we discuss two representative CdSe/CdS core/shell NQDs having different CdSe core size and the same shell thickness in terms of their absorption, emission behavior, and photoluminescence quantum yield.

As it can be seen from Figure 3.3.1.7, by increasing the thickness of CdS, we observed large amount of red shift in the absorption spectrum. For CdSe/CdS core/shell NQDs having a core size of 2.7 nm, approximately 65 nm red shift was observed as a result of 4 ML CdS coating. However, the amount of red-shifting is not directly related to just number of monolayers. In other words, we did not observe the same amount of shifting for each cycle of SILAR. The amount of shifting was decreased continuously with the increasing the shell thickness. While roughly 25 nm red shift was obtained for the first monolayer, the amount of shifting decreased to 10 nm for the fourth monolayer. In addition, with the increased shell thickness, we found that photoluminescence quantum yield of NQDs greatly enhanced with narrow emission behavior having FHWM value of 28 nm (Figure 3.3.1.8). For 2-3 ML CdSe/CdS core/shell NQDs, quantum yield of 85-95% was obtained as a result of elimination of surface trap states (Figure 3.3.1.8) and passivation of core atoms from environment without formation of any defect sites. However, further coating resulted in decreased quantum yield. As a result of increase in the shell thickness, the material cannot withstand high amount of strain and this starts to relax via formation of crystal defects such as dislocations. Therefore, after 3 ML shell thickness, decrease in quantum yield was observed. Moreover, the enhancement in the absorption at lower wavelengths was observed owing to lower band gap of CdS and it was also indicative of the formation of CdS shell for CdSe/CdS core/shell NQDs (Figure 3.3.1.7).

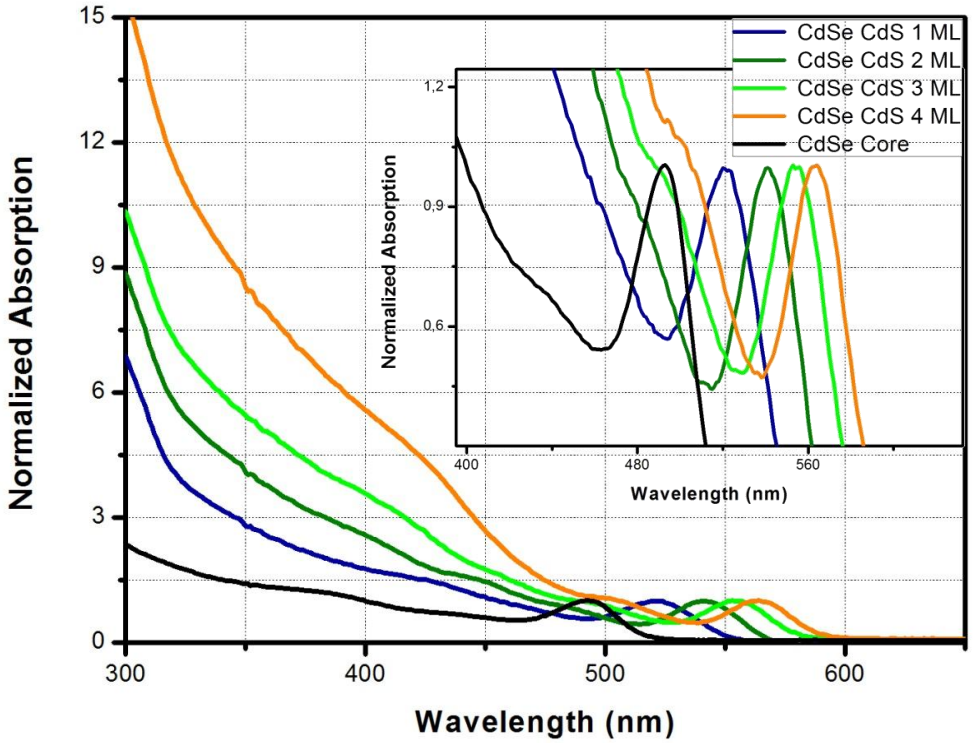

Figure 3.3.1.7 Absorption spectra of CdSe/CdS core/shell NQDs having a small CdSe core with different monolayers (1 ML increments).

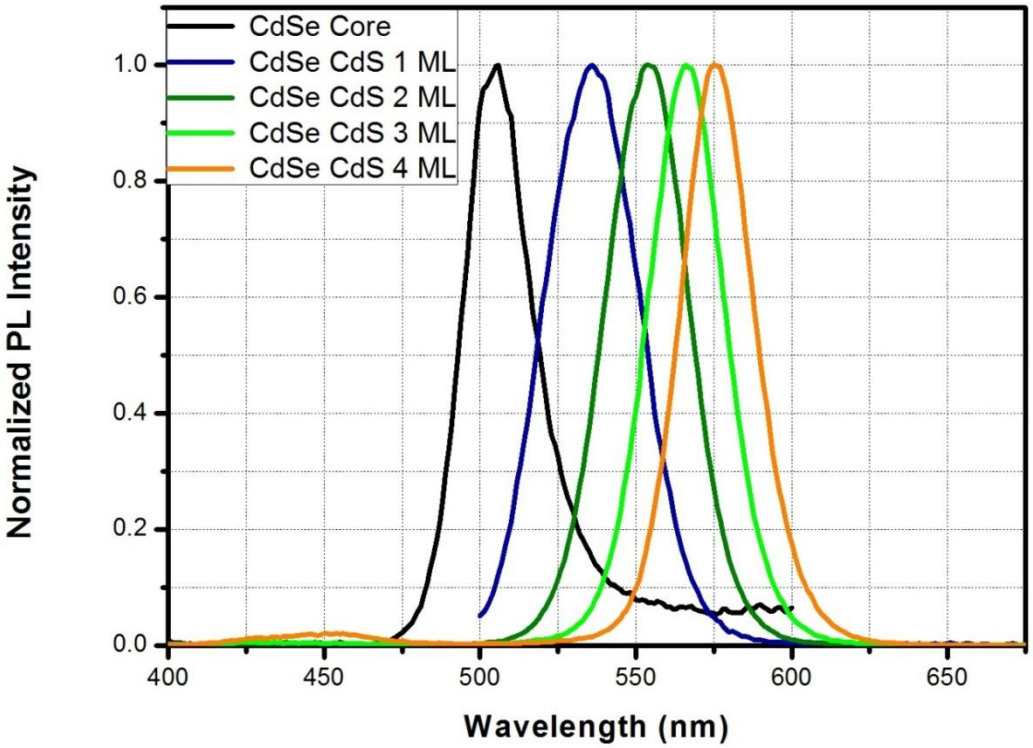

Figure 3.3.1.8 Emission spectra of CdSe/CdS core/shell NQDs having a small core with different monolayers (1 ML increments).

For 4 ML CdSe/CdS core/shell NQDs having a 3.5 nm of CdSe core, approximately 45 nm of red shift was observed in the first absorption peak (Figure 3.3.1.9). Since larger CdSe cores fall in the weak confinement region, we found weaker red shift in the absorption spectrum when compared to 4 ML CdSe/CdS core/shell NQDs having smaller CdSe core. Similarly, decrease in the amount of shifting was observed by increasing the shell thickness. In addition, with increasing shell thickness, increase in the quantum yield was accompanied with a narrow emission behavior (Figure 3.3.1.10). However, we could not observe near-unity quantum yield. For 2-3 ML CdSe/CdS core/shell NQDs, the quantum yield was measured in the range of 75-85%. We also increase the interface area between the shell and core materials by increasing the size of the core, which also increases strain build up with the coating of shell materials. Therefore, it is not possible to obtain near unity quantum yield with larger CdSe cores.

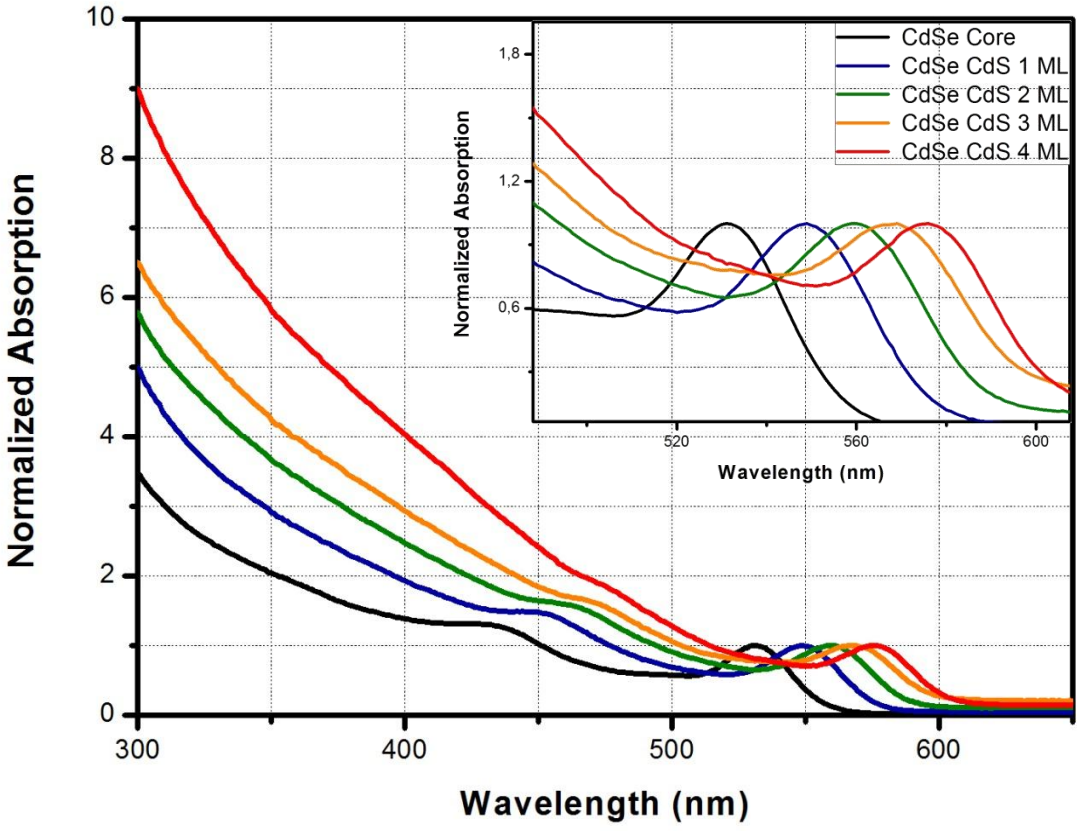

Figure 3.3.1.9 Absorption spectra of CdSe/CdS core/shell NQDs having a large CdSe core with different monolayers (1 ML increments).

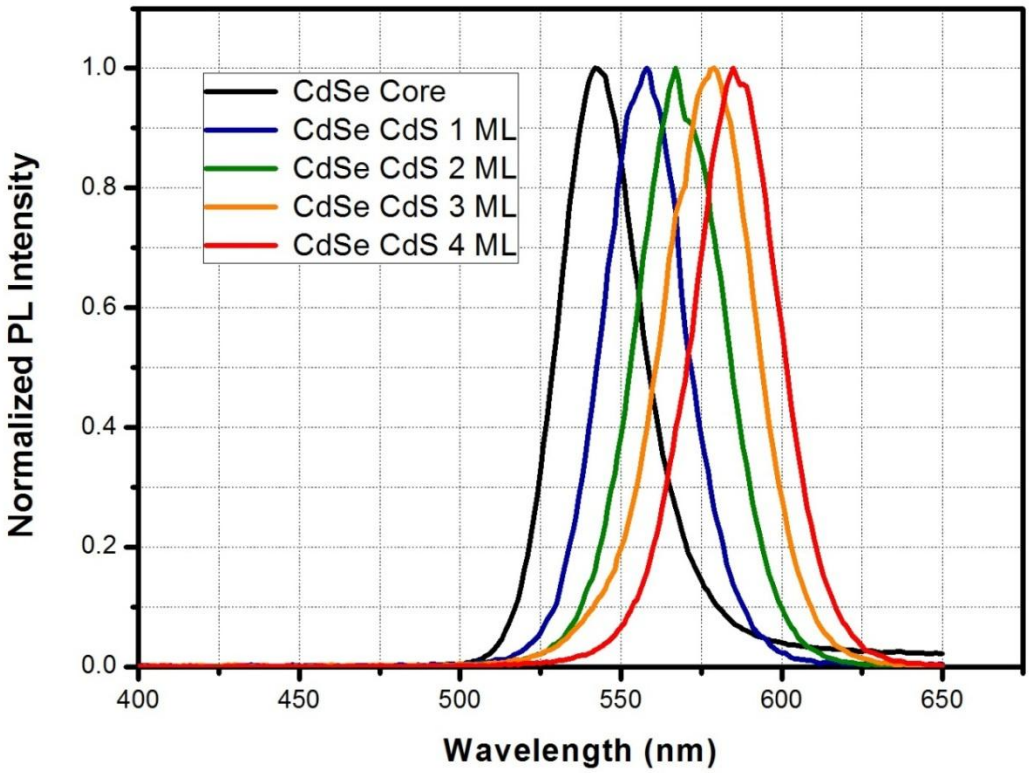

Figure 3.3.1.10 Emission spectra of CdSe/CdS core/shell NQDs having a large core with different monolayers (1ML increments).

However, sometimes we observed homogenous nucleation of CdS nanocrystals during the core/shell synthesis. When compared to the most common CdSe/CdS core/shell synthesis [49,32], we used hexamethyldisilathiane $(TMS)_2S$ as sulfur precursor instead of elemental sulfur. $(TMS)_2S$ has a higher reactivity and higher reaction yield compared to elemental sulfur [35]. Therefore, any excess precursor injection, due to experimental mistakes, will result in formation of separate CdS NQDs. Fortunately, we could manage to remove separate CdS NQDs from CdSe/CdS core/shell NQDs with size selective precipitation or extraction method [50]. As it can be seen from the emission spectrum in Figure 3.3.1.11, there were two peaks, one of which belongs to CdSe/CdS core/shell NQDs and the other of which belongs to CdS NQDs (at 440 nm) before purification. After size selective precipitation, we completely removed separate CdS NQDs, which is also clearly seen in Figure 3.3.1.11 with the emission around at 440 nm fully diminished.

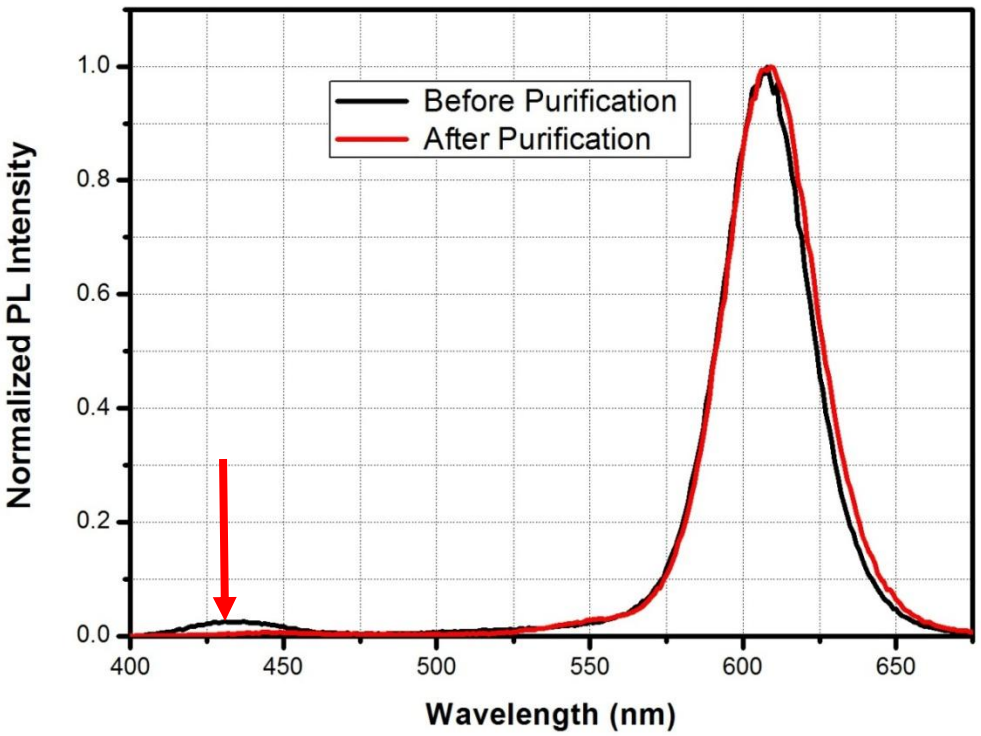

Figure 3.3.1.11 Photoluminescence spectra of CdSe/CdS core/shell NQDs with CdS NQDs (black line) and without CdS NQDs (red line).

Finally, in order to suppress any homogenous nucleation of CdS NQDs, we performed CdSe/CdS core/shell synthesis with submonolayer 0.8 ML (0.27 nm) increase in shell thickness for each SILAR cycle. By decreasing the amount of precursor for each injection step, we decreased the probability of formation of CdS NQDs due to experimental mistakes. As it can be seen from Figure 3.3.1.12, as a result of 3.2 ML CdS coating of CdSe core having a diameter of 2.2 nm, approximately 65 – 70 nm red shift was observed in the absorption spectrum. This higher amount of red-shifting was also an indicative of the homogenous coating of precursors without formation of any separate CdS NQDs. With the coating of the first monolayer, the trap emissions were eliminated as a result of surface passivation (Figure 3.3.1.13). In addition, by increasing the shell thickness, emission level of NQDs was increased and for 2.4 ML and 3.2 ML CdSe/CdS core/shell NQDs, 85-95% quantum efficiency was obtained.

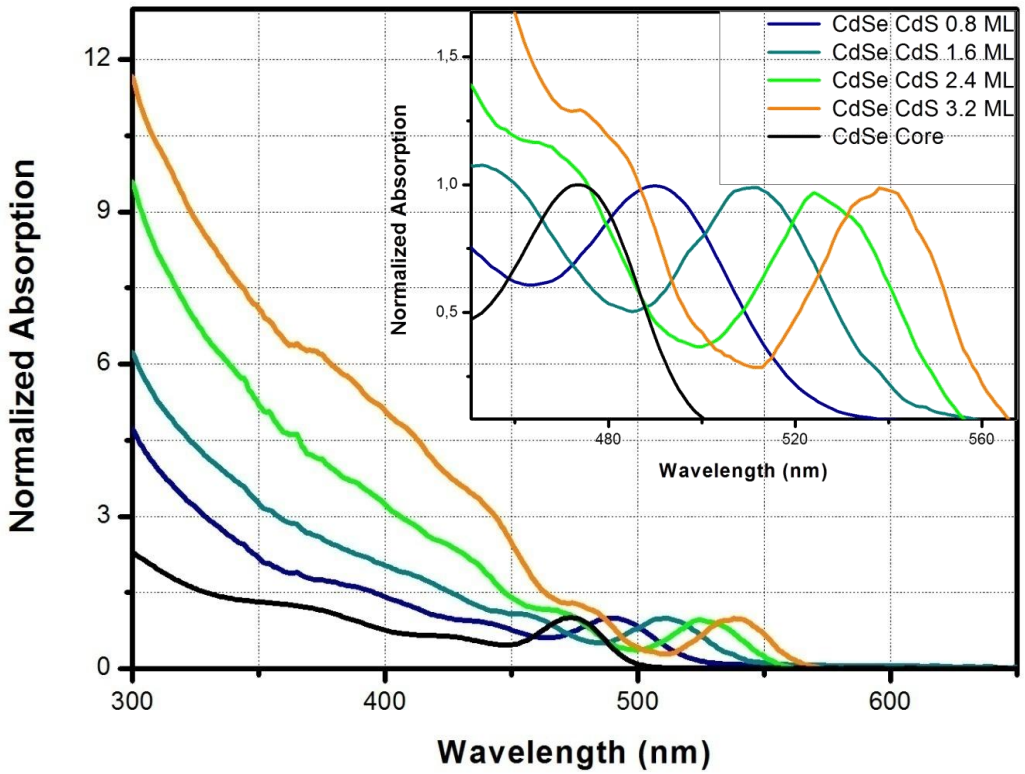

Figure 3.3.1.12 Absorption spectra of CdSe/CdS core/shell NQDs having a small CdSe core with different monolayers (0.8 ML increments).

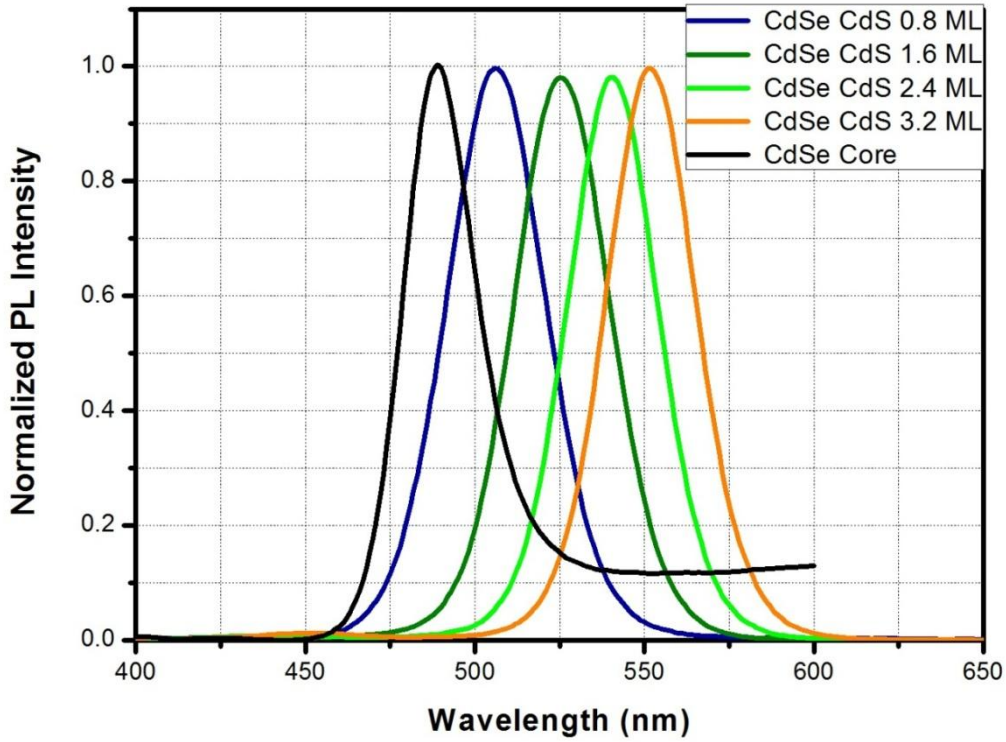

Figure 3.3.1.13 Photoluminescence spectra of CdSe/CdS core/shell NQDs having a small CdSe core with different monolayers (0.8 ML increments).

3.3.2. Structural Characterization

For the analysis of elemental composition of CdSe core and CdSe/CdS core/shell NQDs, we performed energy dispersive X-ray spectroscopy (EDAX) by drop-casting NQD solutions on Si wafer. First, we analyzed CdSe NQDs and Se/Cd ratio was found to be 1.2 (Figure 3.3.2.1). Generally, nanoparticles have higher surface-to-volume ratio, and the elemental ratio of compounds are therefore significantly affected by the number of surface atoms. Since we used excess amount of Se during the synthesis, surface of CdSe NQDs were terminated with Se atoms. Thus, we observed higher amount of Se atoms with respect to Cd atoms from the EDAX results. In addition, we observed some P coming from the ligands of CdSe NQDs.

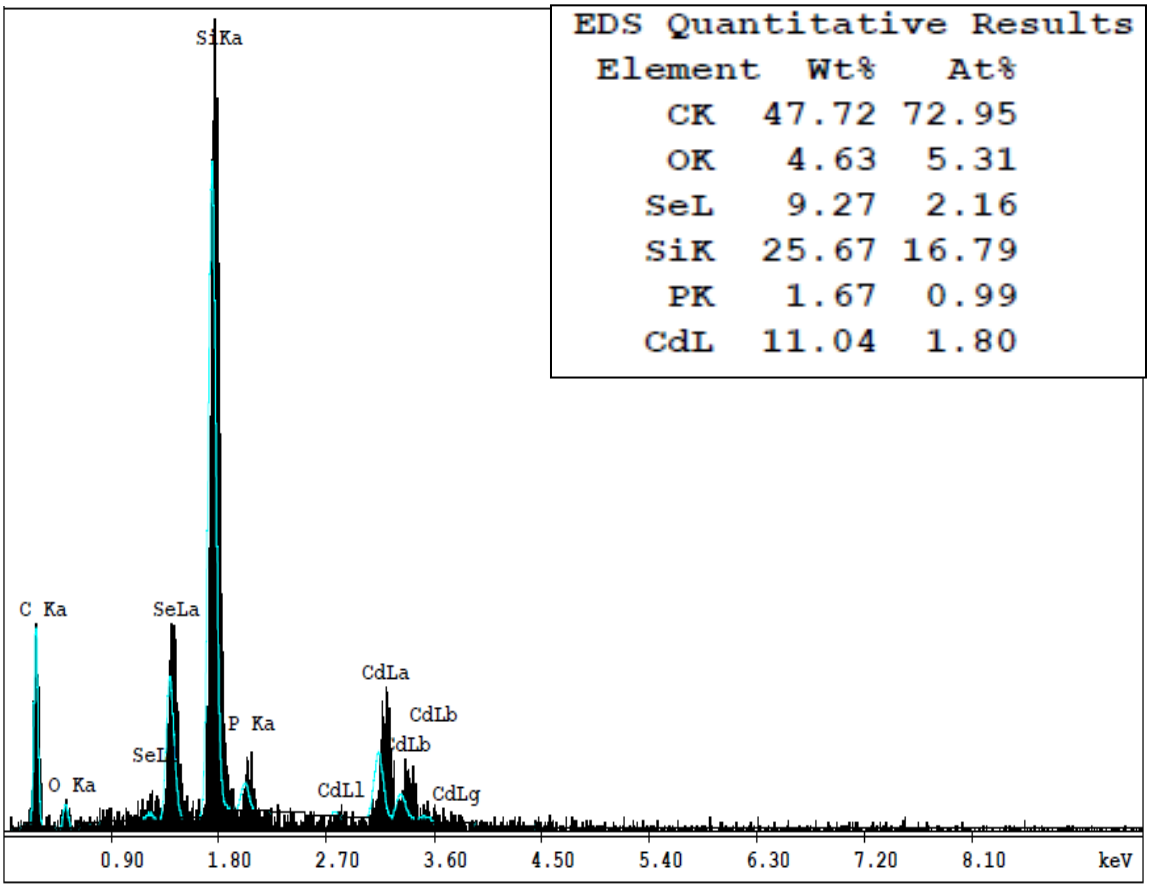

Figure 3.3.2.1 EDAX analysis of CdSe NQDs with quantitative results.

Moreover, we analyzed CdSe/CdS core/shell NQDs having different shell thicknesses in order to confirm uniform coating CdS. Therefore, the experimental S/Se ratio was compared with the theoretical calculated S/Se. To determine S/Se ratio theoretically, we used their occupied volume for the CdSe core having a radius of 1.2 nm and the thickness of one monolayer as 0.337 nm. By increasing the thickness of shell, increasing in S/Se ratio was observed (Figure 3.3.2.1). In addition, there was a good correlation with experimental results and theoretical results except 2.4 ML CdSe/CdS core/shell NQDs.

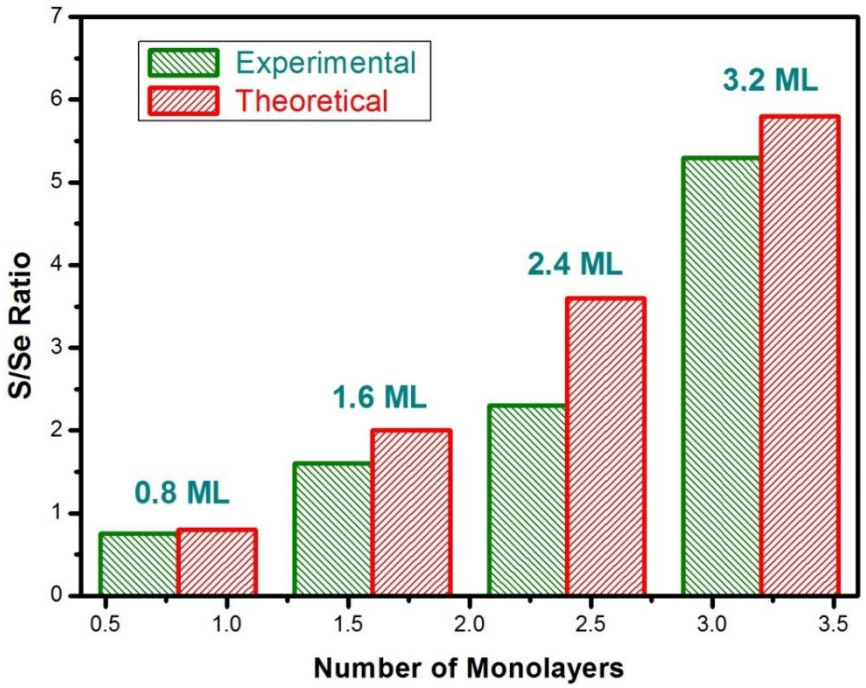

Figure 3.3.2.2 Comparison of experimental and theoretical S/Se ratios.

EDAX gives information only about the elemental composition of NQDs. Therefore, to obtain information about the size, shape and crystal structure of NQDs, we used high resolution TEM. Moreover, thickness and uniformity of shell can be accurately determined with TEM. TEM images of CdSe core NQDs are presented below (Figure 3.3.2.3). They have the radius of approximately 1.2-1.3 nm and they seem quite spherical. However, since their size is so small, we could not manage to get image showing their lattice fringes clearly.

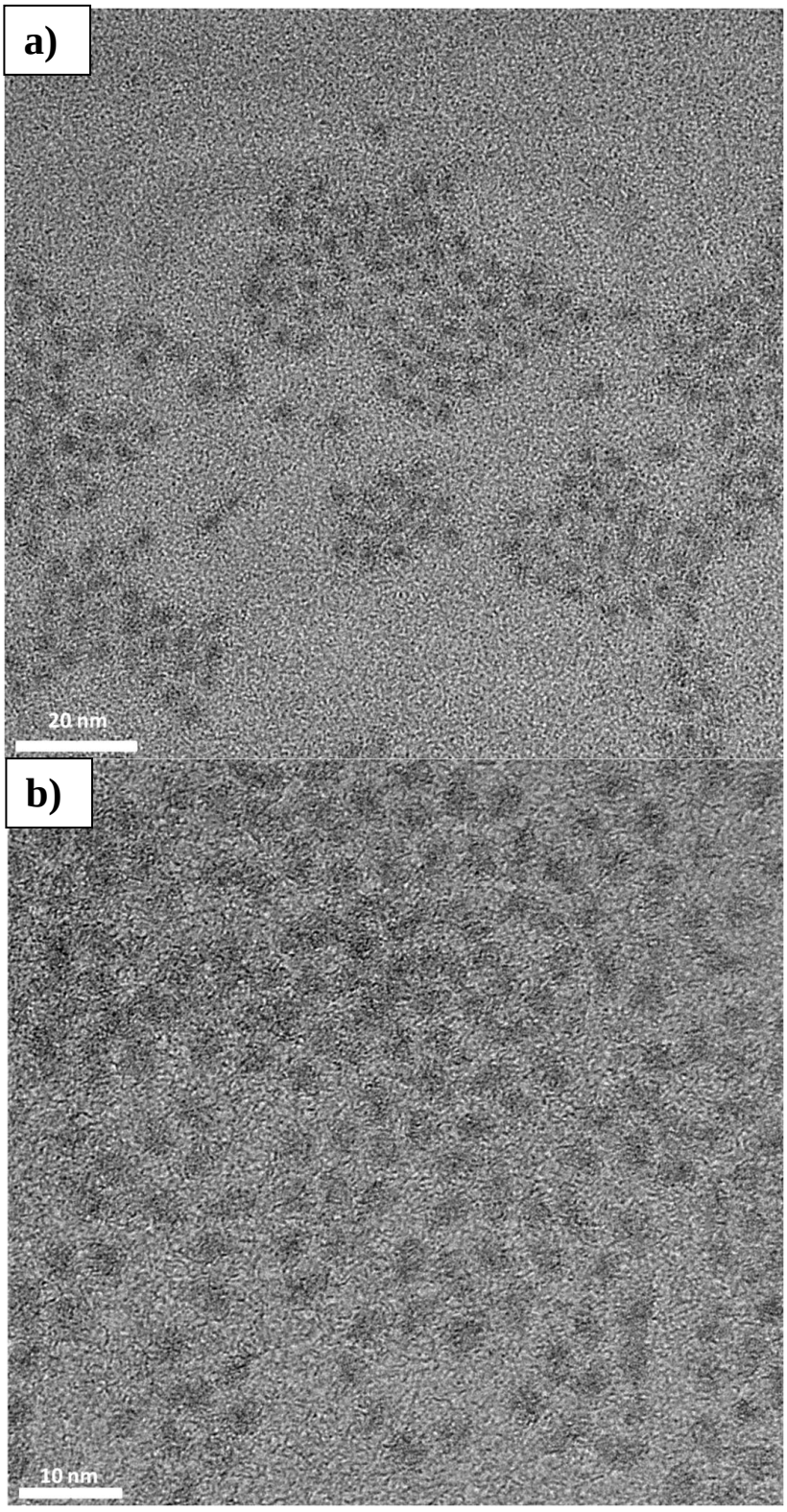

Figure 3.3.2.3 TEM images of CdSe core NQDs with a) 20 nm and b) 10 nm scale bars.

Then, we analyzed uniformity and thickness of shell for the 3.2 ML CdSe/CdS core/shell NQDs having a core radius of 1.2-1.3 nm. As it can be seen from the figures below, the coating of CdS is homogenous and highly monodisperse CdSe/CdS core/shell NQDs were obtained. Here, almost perfect arrangement of NQDs is also an indicative of having smaller size distribution and uniform shell thickness (Figure 3.3.2.5). Moreover, the size distribution of CdSe/CdS core/shell NQDs was obtained by measuring the size of more than 100 NQDs (Figure 3.3.2.4). The average diameter of CdSe/CdS core/shell NQDs was found to be 4.27 nm ± 0.3 nm, which is strongly consistent with the estimated thickness of shell.

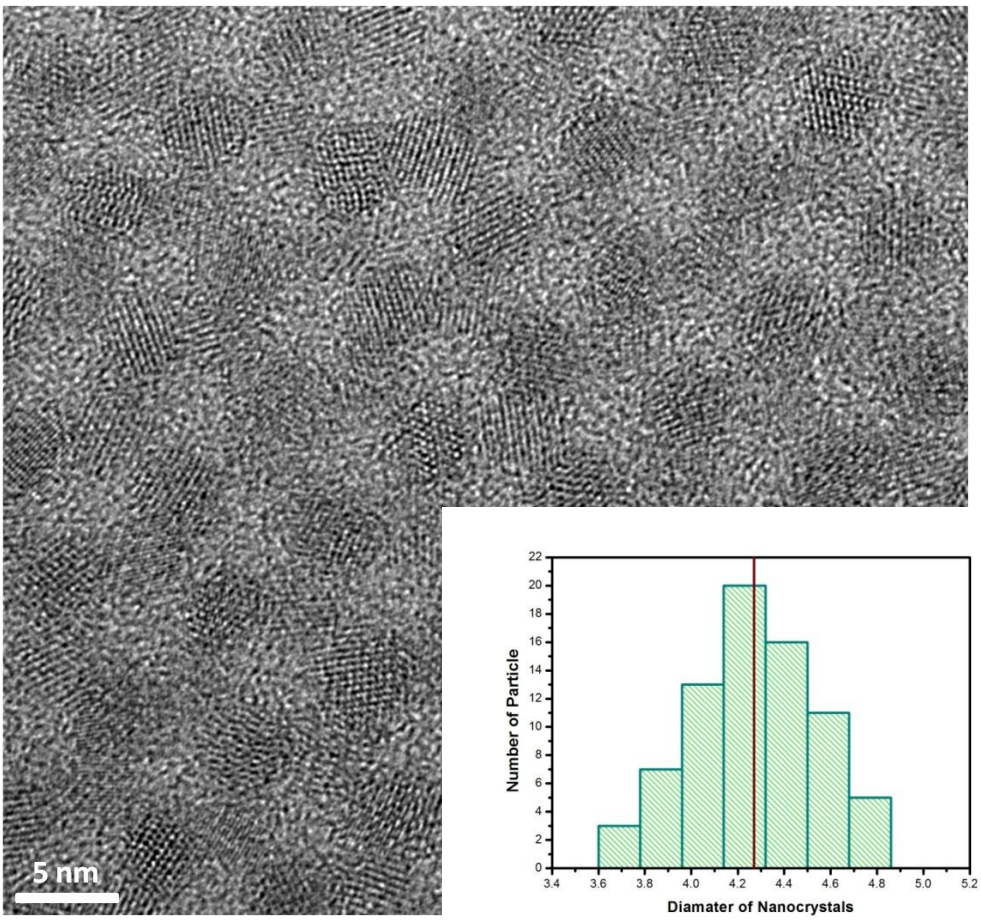

Figure 3.3.2.4 High resolution TEM image of 3.2 ML CdSe/CdS core/shell structure with a size distribution in the inset.

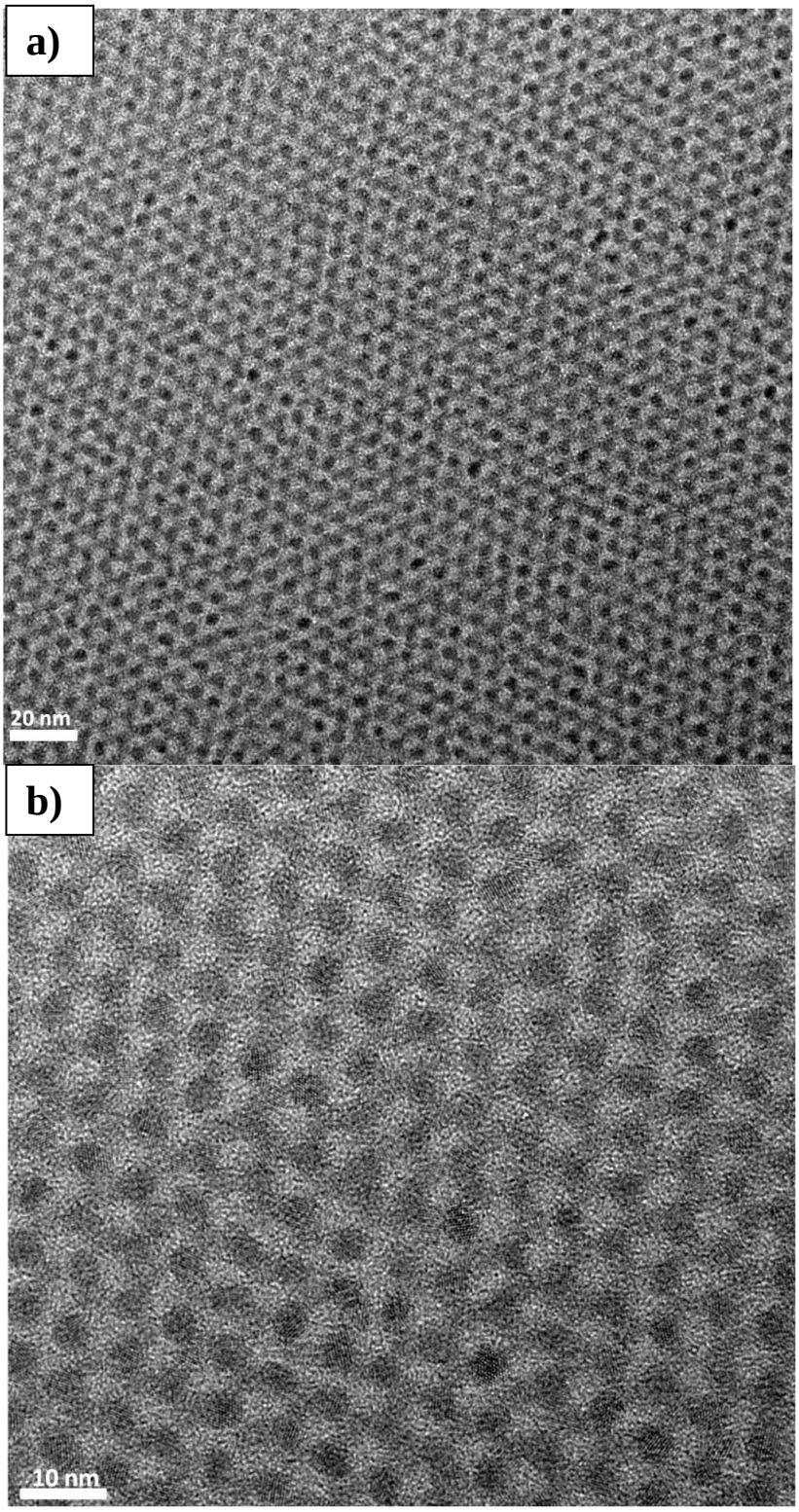

Figure 3.3.2.5 TEM images of 3.2 ML CdSe/CdS core/shell NQDs with a) 20 nm and b) 10 nm scale bars.

Furthermore, determination of the crystal structure for CdSe core and CdSe/CdS core/shell NQDs is very important, since CdSe NQDs having different crystal structures exhibit different electrical and optical properties. In addition, it is shown that coating of CdSe NQDs having wurtzite crystal structure resulted in more uniform and homogeneous shell when compared to CdSe NQDs having zinc blende crystal structure [41]. Therefore, we analyzed the crystal structure of CdSe NQDs having a diameter of 3.8 nm with X-ray diffraction by using powder sample of NQDs (Figure 3.3.2.6). As it can be seen from Figure 3.3.2.6 below, the peak positions for CdSe NQDs are consistent with the bulk wurtzite CdSe crystal. As a result of having smaller size of CdSe NQDs, we observed very broad peaks. However, diffraction from (102) plane proved that our CdSe NQDs have wurtzite crystal structure since, in zinc blende crystal structure, no diffraction is observed from (102) planes.

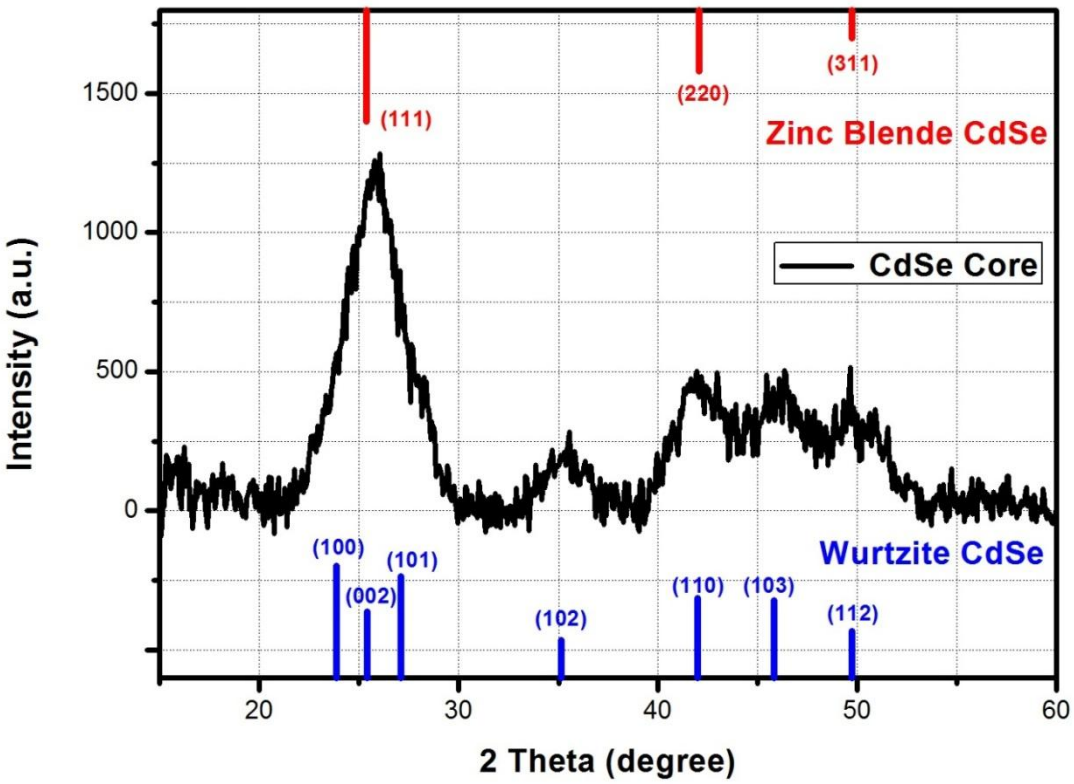

Figure 3.3.2.6 X-ray diffraction patterns of CdSe core NQDs having wurtzite crystal structure.

Moreover, we carried out X-ray diffraction for CdSe/CdS core/shell NQDs having a core diameter of 3.8 nm and 4 ML CdS (Figure 3.3.2.7). With the growth of shell material, the peaks are sharpened as a result of the increase in total size of NQDs and increase in the crystal quality. For example, while we observed only one peak around 24^0-26^0 for CdSe core NQDs, with the increase in shell thickness, the resolution was increased and diffraction from (100), (002) and (101) planes became clear for 4 ML CdSe/CdS core/shell NQDs. In addition, positions of the peaks were shifted to values for a bulk wurtzite CdS crystal with the formation of strain upon the growing CdS shell.

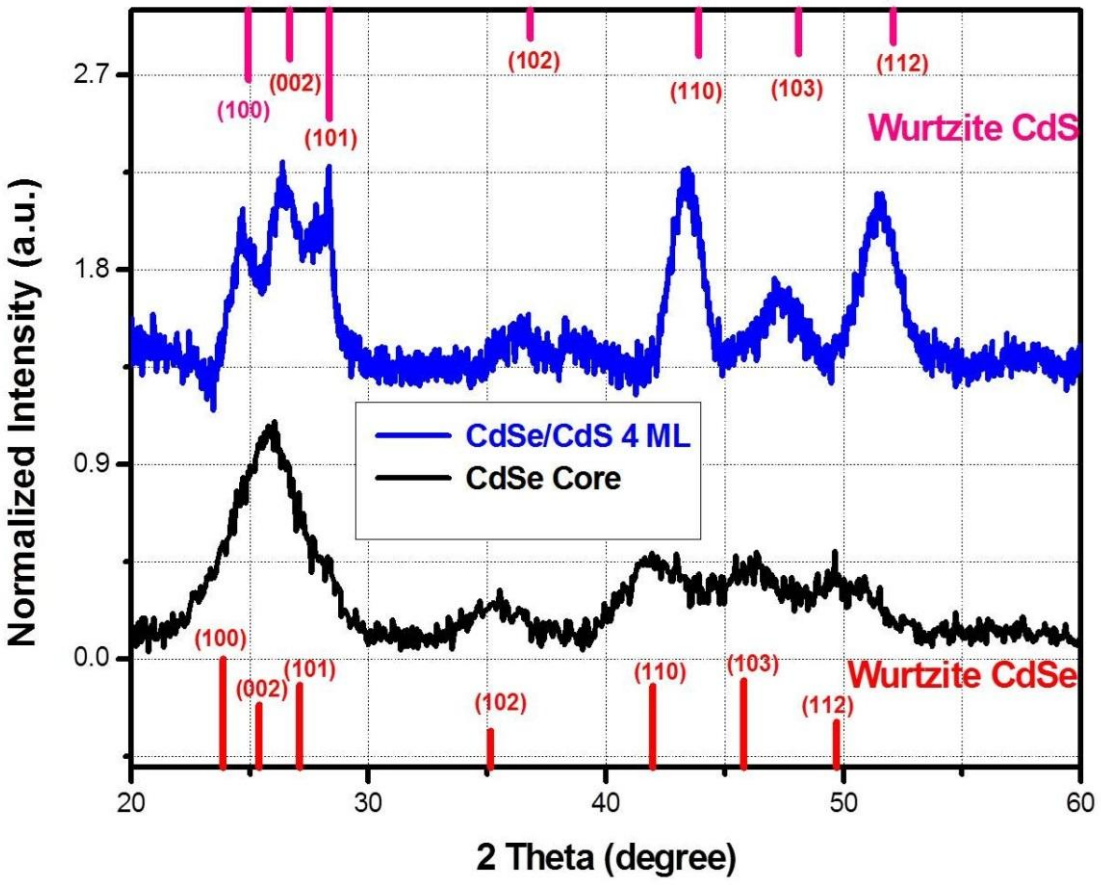

Figure 3.3.2.7 Comparison X-ray diffraction pattern of CdSe core and 4 ML CdSe/CdS core/shell NQDs.

In addition, the crystal structure of NQDs can be determined from the selected area electron diffraction pattern (SAED). Figure 3.3.2.8 shows the SAED images taken from the CdSe/CdS core/shell NQDs having a core size of 3.8 nm and 4 ML CdS shell. In SAED image, each ring represents diffraction from corresponding planes. Moreover, from the SAED image, we calculated the interplanar spacing for different planes by using

$$d_{hkl} = \frac{1}{R_{SAED}} \qquad (11)$$

where d_{hkl} is the interplanar spacing and R_{SAED} is the radius of rings in SAED pattern. Then, we compared them with bulk values of wurtzite CdSe and CdS crystals. The values are between the bulk values of wurtzite CdSe and CdS crystals as we expected and show strong correlation with the X-ray diffraction results (Table 3.3.2.1).

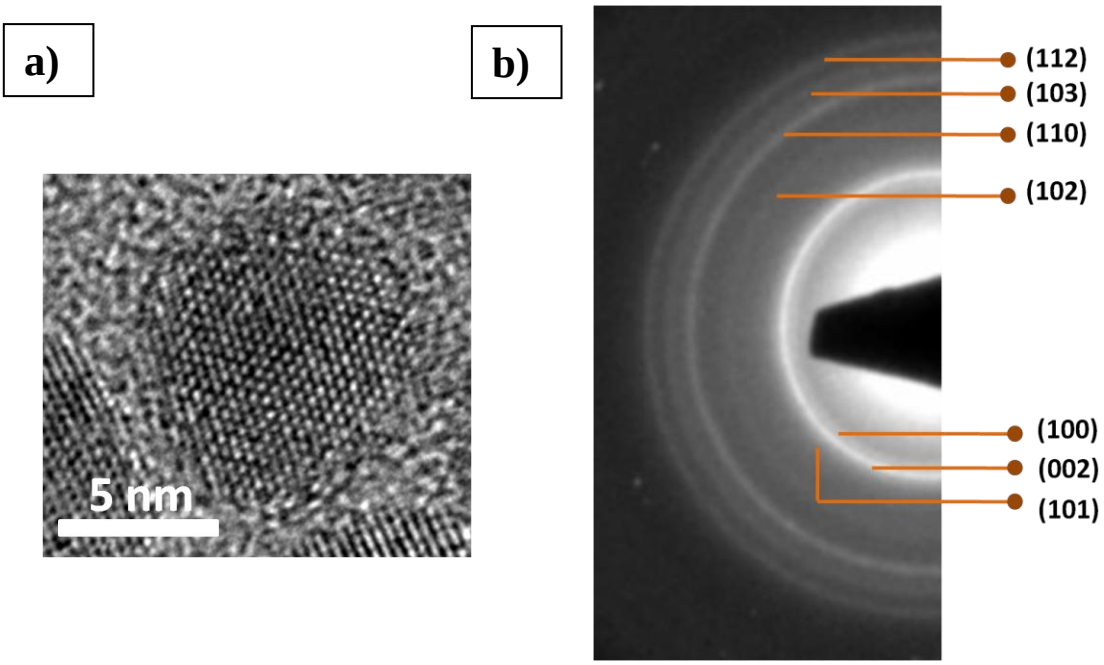

Figure 3.3.2.8 a) High resolution TEM image of 4 ML CdSe/CdS core/shell NQDs and b) selected area diffraction pattern (SAED) images of the same 4 ML CdSe/CdS.

	Interplanar spacing d(Å)		
Planes (hkl)	CdSe Wurtzite	4 ML CdSe/CdS	CdS Wurtzite
1 0 0	3.723	3.618	3.568
0 0 2	3.505	3.411	3.341
1 0 1	3.288	3.182	3.148
1 0 2	2.552	2.458	2.439
1 1 0	2.150	2.074	2.061
1 0 3	1.979	1.905	1.890
1 1 2	1.832	1.763	1.754

Table 3.3.2.1 Interplanar spacing values of different planes for bulk wurtzite CdSe crystal, 4 ML CdSe/CdS core/shell NQDs and bulk wurtzite CdS crystal.

Finally, we performed X-ray photoelectron spectroscopy for the analysis of chemical bonding and shell thickness by spin-coating NQD solution on Si wafer. For the CdSe core NQDs, the position of Cd $3d_{5/2}$ peak is approximately at 405.2 eV and the position of Se 3d peak is at 54.8 eV (Figure 3.3.2.9). For the 3 ML CdSe/CdS core/shell NQDs, the positions of peaks for Cd $3d_{5/2}$ and Se 3d does not change but S $2p_{3/2}$ appears at 161.2 eV. These values are strongly consistent with the observed values for CdSe and CdSe/CdS core/shell NQDs in the literature [49].

.

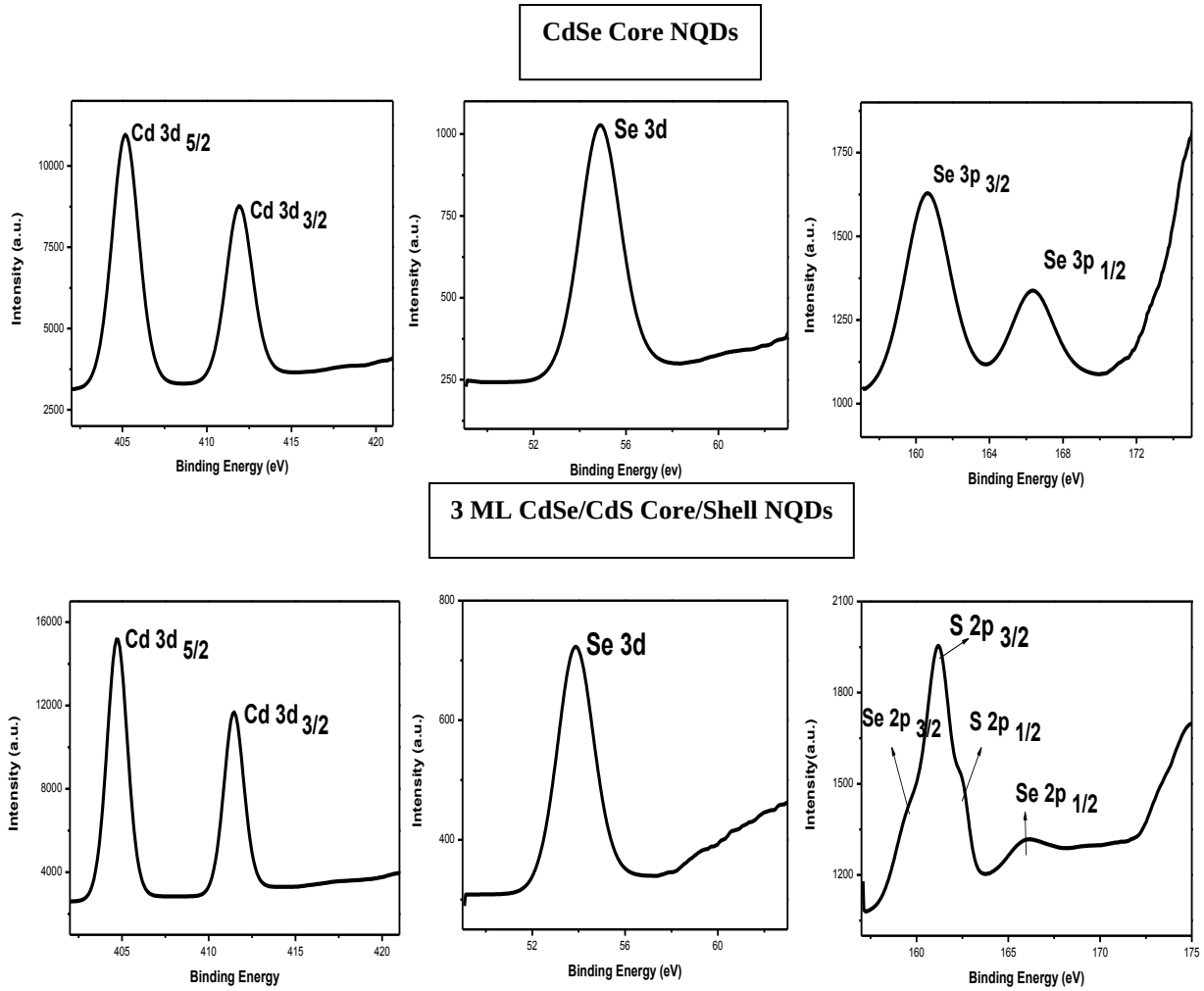

Figure 3.3.2.9 XPS spectra of Cd, Se and S peaks for CdSe core NQDs and 3 ML CdSe/CdS core/shell NQDs.

Next, we performed XPS for the calculation of shell thickness with CdSe/CdS core/shell NQDs having a core diameter of 3 nm. As it can be seen clearly from Figure 3.3.2.10, we observed only Se 2p peaks for the CdSe core NQDs. However, with the formation of 1 ML CdS, S 2p peaks emerge, and the intensity of the S 2p starts to increase upon growing CdS shell. Then, for 3 ML CdSe/CdS core/shell NQDs, S 2p peaks becomes dominating and the intensity of Se 2p peaks decreases. After that, by using the intensity ratio of S 2p peak to Se 3d peak, we calculated the shell thickness with Equation (4) described in Chapter 2.

In addition, by using TEM, we also measured the size of NQDs. Then, we compared the expected radius of NQDs with the radius obtained from XPS and TEM. As it can be seen from Table 3.3.2.2, the values obtained from the XPS give better results when compared to TEM. Although TEM is the most powerful technique for the characterization of NQDs, because of smaller size and lower resolution of NQDs, it is normal to observe such a small difference for the size of NQDs.

	Radius of NQDs (nm)		
	XPS	**TEM**	**Expected Radius**
CdSe Core	1.50	1.50	1.40
1 ML CdSe CdS	1.95	-	1.75
2 ML CdSe CdS	2.23	1.97	2.10
3 ML CdSe CdS	2.56	-	2.45
4 ML CdSe CdS	2.76	2.45	2.80

Table 3.3.2.2 Expected radii of NQDs and measured radii of NQDs using XPS and TEM.

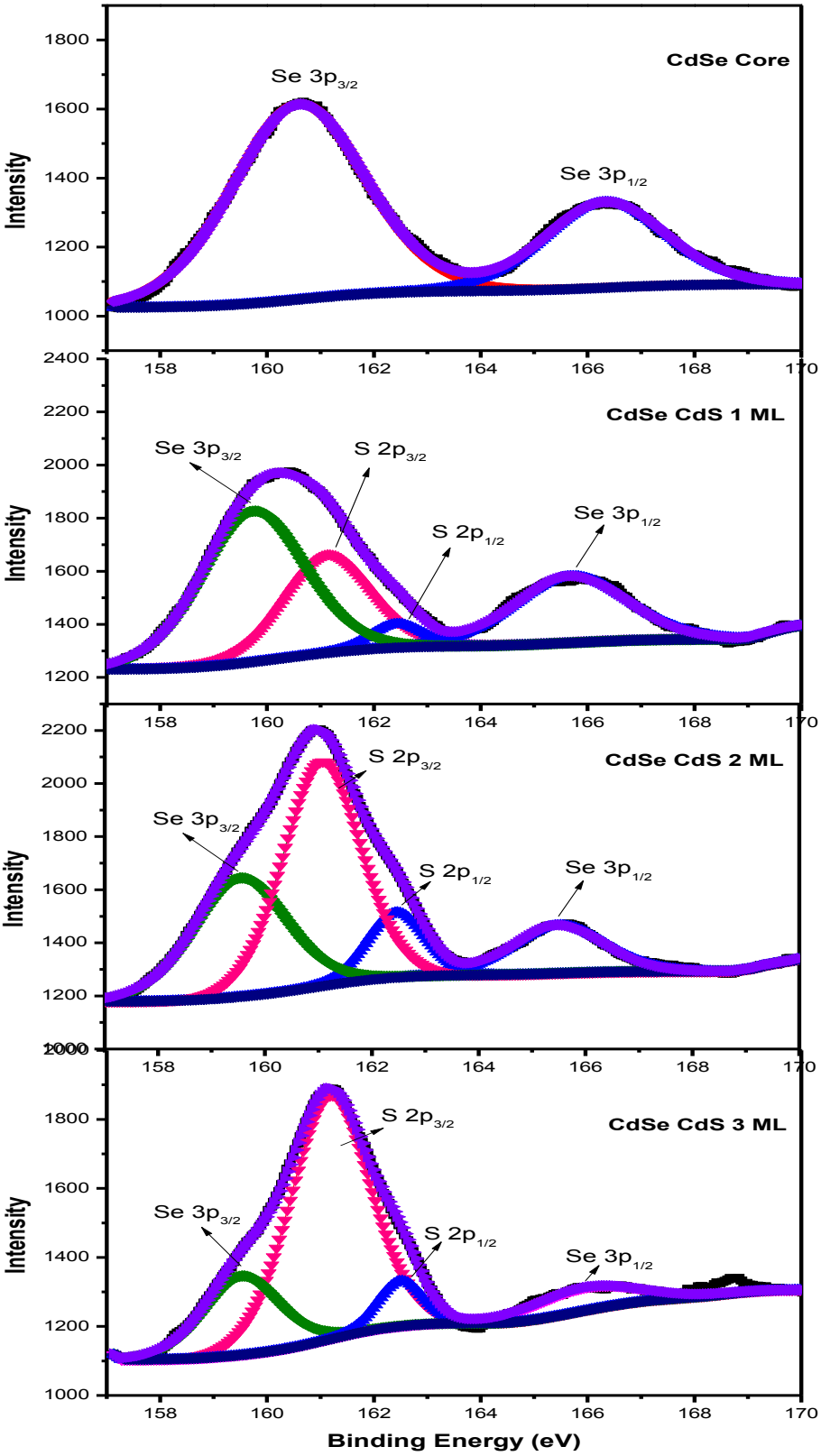

Figure 3.3.2.10 XPS spectra of Se and S peaks for CdSe core NQDs and CdSe/CdS core/shell NQDs having different number of monolayers.

3.4. Application

Today, both electrically and optically pumped semiconductor lasers are the most common type of laser systems for the technologies including telecommunication, information storage, computing and medical diagnostics [67,68]. They have high power output with low lasing thresholds. In addition, they have better stability against temperature change. With the introduction of semiconductor quantum well lasers [69], it is shown that there is still room for the improvement of lasers. With the confinement of electrons and holes in one direction [70], a higher density of electronic states is obtained near the conduction and valence bands for quantum structures. As a result of this, concentration of carriers contributing to the band edge emission increases. Therefore, lower lasing threshold values can be achieved by using quantum structure in semiconductor lasers with better temperature stability and a narrower emission line.

Recently, NQDs also have become attractive materials for lasing applications. When compared to a quantum well structure, NQDs have a better confinement of electrons and holes in all three dimensions [70] and, as a result of the quantum confinement effect, they show atomic like discrete energy levels. Therefore, the lowest lasing threshold value can be expected for the lasers based on NQDs. In addition, owing to greater spacing between atomic-like states in energy levels, NQDs can be considered as more temperature insensitive gain medium. Moreover, with the size tunable emission properties of NQDs, it is possible to obtain lasers having emission spanning from UV to infrared region depending on the size and composition of NQDs.

In theory, NQDs based lasers offer very low lasing threshold, temperature insensitive lasing and multicolor lasing. In addition, like other lasing media, population inversion where the number of electrons in high energy excited state is higher than that in the low energy ground state is required for producing optical gain in NQDs. However, with the formation of more than one electron

hole pair inside NQDs, nonradiative Auger recombination becomes a dominant process which inhibits optical gain for NQDs [10]. Auger recombination is a physical process where the recombination energy of electron and hole pair is not released as a photon and instead transferred to another electron hole pair to re-excite them to higher energy state. Therefore, to obtain population inversion and optical gain from NQDs, Auger recombination must be suppressed. Optical gain with CdSe core NQDs was first shown by Klimov and coworkers with the suppression of Auger recombination by simply increasing the concentration of NQDs solution in order to enhance the rate of stimulated emission [10]. After that, cleverly designed NQDs such as giant CdSe/CdS core/shell NQDs [62] and nanorods [71] were synthesized for the suppression of Auger recombination in order to obtain lower lasing threshold values.

Conventional laser systems are generally working in the infrared region of the spectrum, which are widely used for the telecommunication. However, for other applications, lasers operating in UV and visible region of the spectrum are required. Therefore, specifically designed expensive doubling crystals such as β – barium borate crystals (BBO) or potassium dihydrogen phosphate (KDP) are used for the conversion of infrared source by technique of second harmonic generation. Here we study another way for the up-conversion of infrared source using NQDs with a multi photon absorption mechanism. To exhibit efficient multi-photon absorption mechanism, the materials should have high two-photon absorption cross-section, high photoluminescence quantum yields and high chemical and photo stability [72].

Here, we show that highly efficient CdSe/CdS core/shell NQDs are suitable for optical gain with two-photon infrared pumping owing to their electronic and optical properties. As we discussed earlier, as a result of partial separation of electron and hole wavefunctions, suppression of Auger recombination is observed for CdSe/CdS core/shell NQDs. In addition, having defect-free crystal structure of CdSe/CdS core/shell NQDs is also contributed to the suppression of Auger recombination.

We performed optical gain studies by drop-casting of highly concentrated CdSe/CdS core/shell NQDs solution on glass substrates from the hexane solution. Highly concentrated NQD film is required to obtain population inversion and to increase the rate of stimulated emission. These films were excited with femtosecond laser pulses at 800 nm (1 kHz, 40 fs, Spitfire, Newport Inc.) via focusing lens. Light emission from the NQDs deposited glass substrates was collected with a spectrometer (Ocean Optics Inc). The experimental setup for optical gain is shown in Figure 3.4.1.

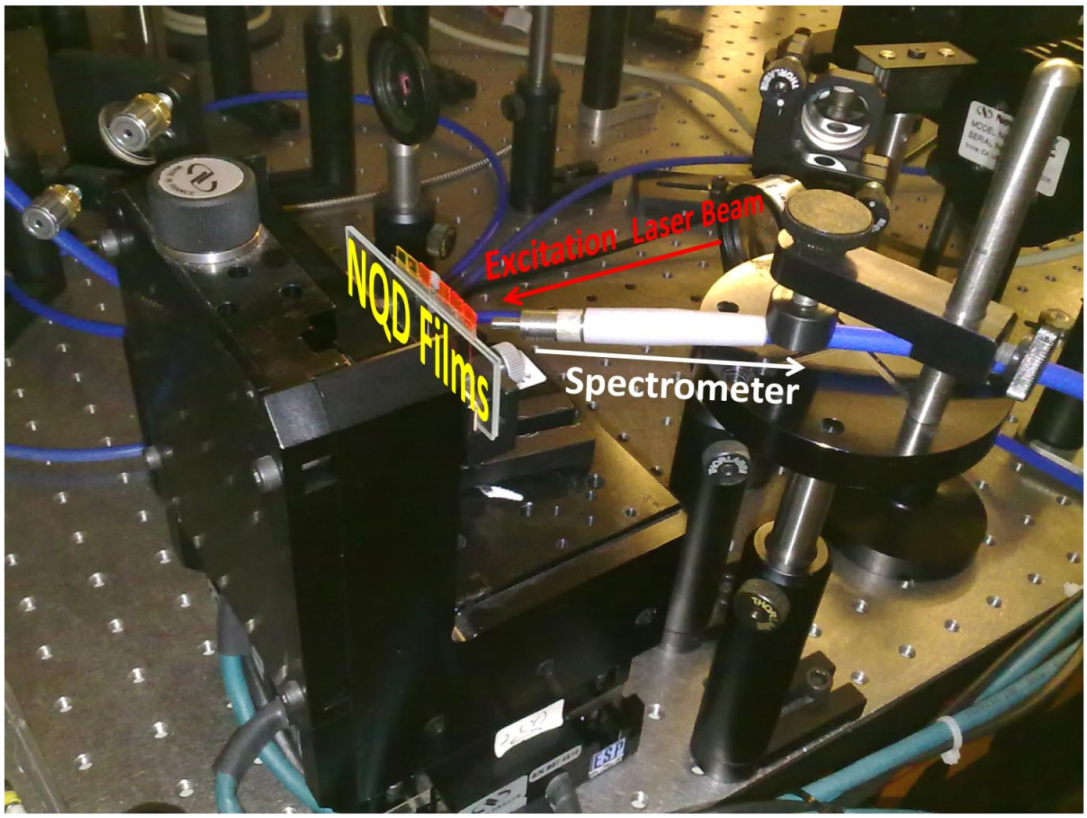

Figure 3.4.1 Experimental setup for optical gain study with NQDs.

Room-temperature amplified spontaneous emission (ASE) was shown with 3.2 ML CdSe/CdS core/shell NQDs in Figure 3.4.2. With the low excitation energy, only spontaneous emission of CdSe/CdS core/shell NQDs was observed having a maximum peak at 602 nm with 26 nm of FWHM. When the excitation energy reached the lasing threshold value of 6 mJ/cm^2 (Figure 3.4.3), ASE was started with a narrower emission behavior having a red shifted emission peak. Then, with increasing the excitation energy, ASE became dominated with a red shifted emission peak at 607 nm and a decreased FWHM value of 8 nm (Figure 3.28, 3.30). Finally, when compared to most widely used CdSe/CdS/ZnS core/shell/shell structures [72,73], a lower lasing threshold value is achieved with such near unity CdSe/CdS core/shell NQDs.

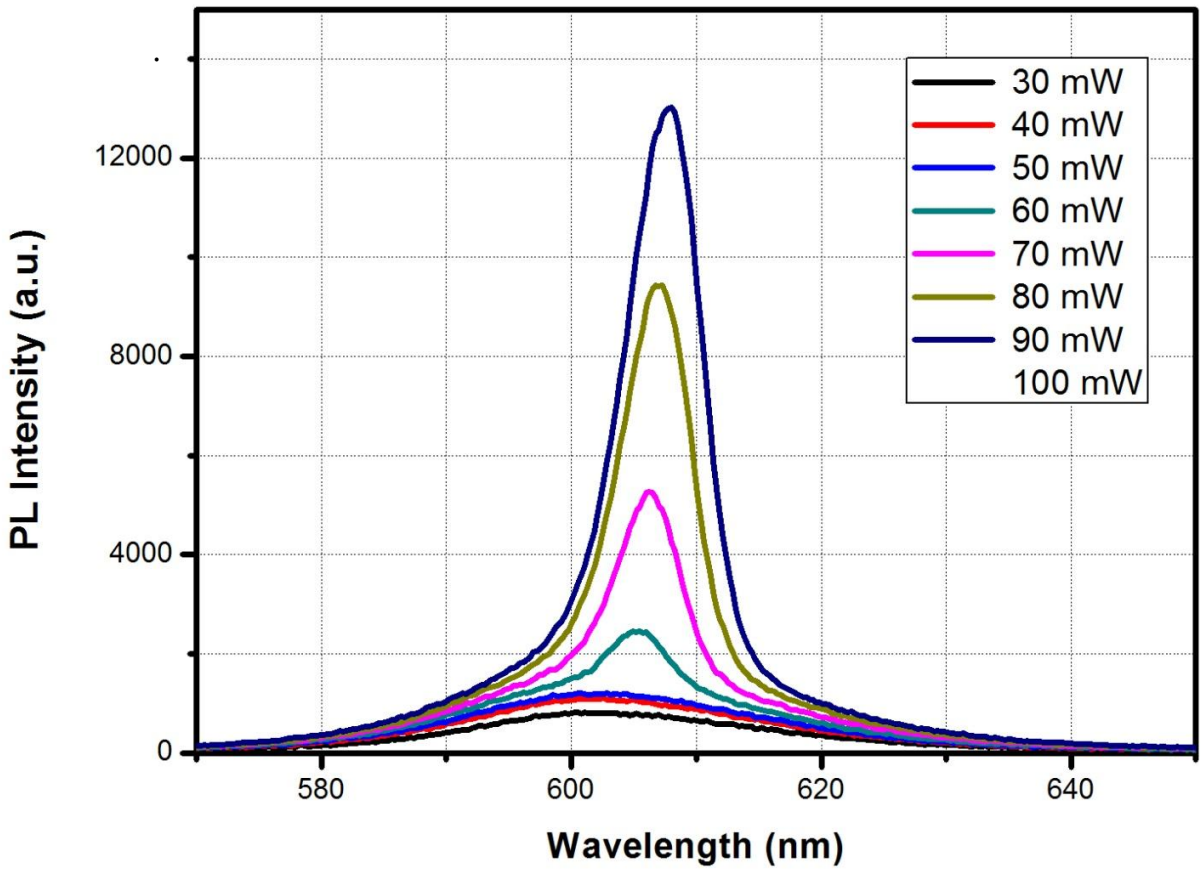

Figure 3.4.2 Photoluminescence spectra of CdSe/CdS core/shell NQDs showing both spontaneous and amplified spontaneous emission (ASE).

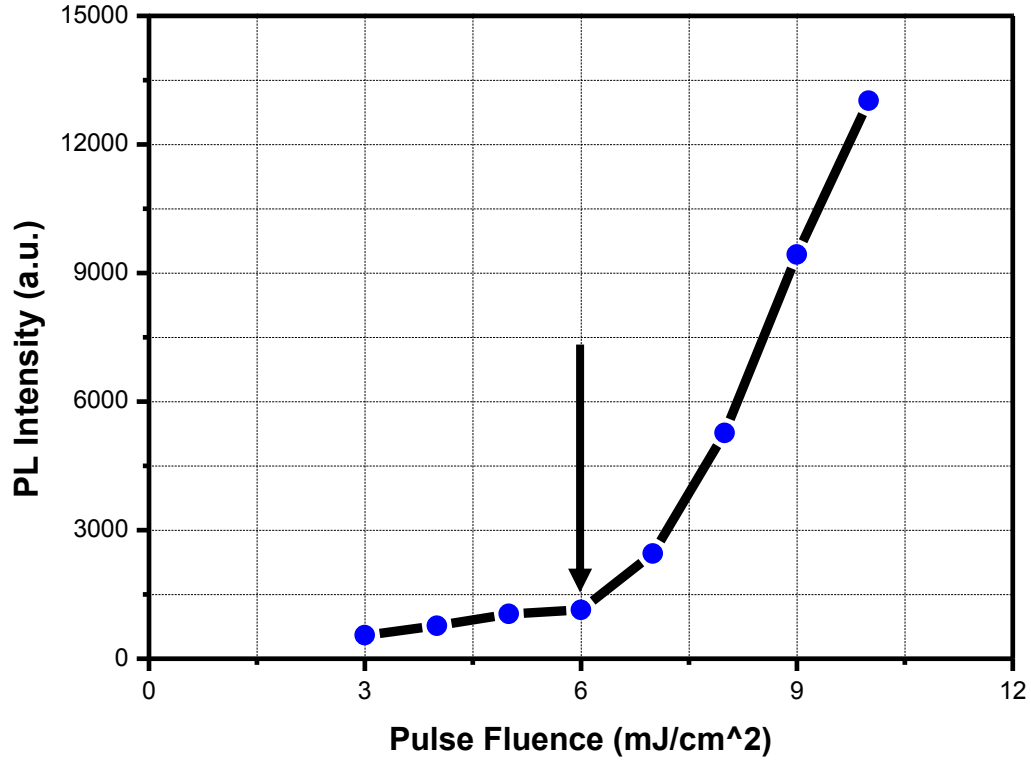

Figure 3.4.3 Change in the photoluminescence intensity with the change in the excitation pulse fluence.

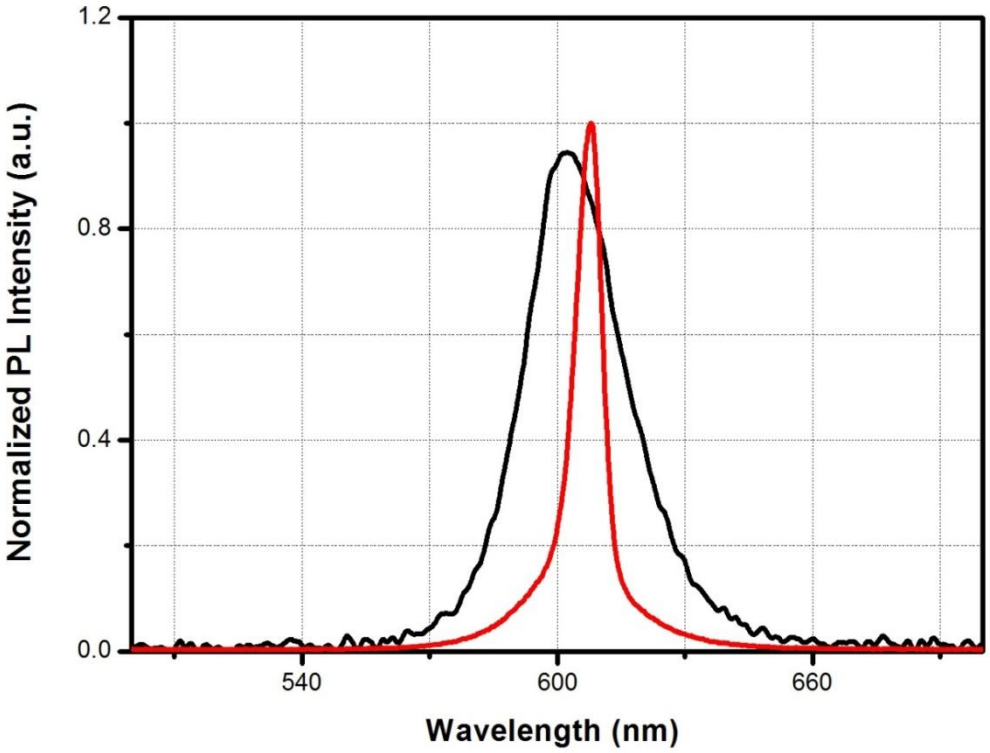

Figure 3.4.4 Normalized photoluminescence spectra of CdSe/CdS core/shell having spontaneous emission (black line) and amplified spontaneous emission (ASE) (red line).

Chapter 4

Conclusion

Nanocrystals quantum dots are tiny particles consisting of a few hundred to thousand of atoms. As a result of decreased particle size of less than exciton Bohr radius, quantum confinement effect is observed in NQDs. Therefore, they have atomic-like discrete energy levels and the energy gap can be modified by changing particle size. Novel size tunable optical properties are consequently observed for NQDs which make them attractive materials for many applications. However, in order to obtain better performance from NQDs and NQD incorporated devices, highly monodisperse, highly stable and highly efficient NQDs are required.

In this thesis, to meet these requirements, we synthesized CdSe/CdS core/shell NQDs with SILAR technique by means of which highly precise shell thickness control and highly uniform shell coating can be achieved. We systematically performed CdSe/CdS core/shell NQD synthesis by using different size of CdSe cores ranging from 2 to 4 nm. It was shown that with the coating of smaller size CdSe cores, near-unity photoluminescence quantum yield was achieved. Since, as a result of the decrease in the interface area between the core and shell material, the probability of strain and defect formation was decreased which decreasing nonradiative recombination channels. In addition, when compared to larger CdSe cores, more red shift in the emission peak was observed for the small CdSe cores by coating with CdS shells owing to strong confinement effect.

Moreover, we performed detailed structural characterization of CdSe/CdS core/shell NQDs using SEM, high resolution TEM, XRD and XPS. By using SEM, we showed the formation of uniform shell by EDAX analysis. Then, with the high resolution TEM images, highly monodisperse CdSe/CdS core/shell NQDs were demonstrated with a homogenous shell coating. Furthermore, wurtzite crystal structure was observed for the both CdSe core and CdSe/CdS core/shell NQDs. In addition, for the first time, highly accurate shell thickness calculation was shown for the core/shell NQDs with the XPS. Finally, owing to suppressed Auger recombination and defect free crystal structure, the lowest lasing threshold value of 6 mJ/cm^2 was observed with two photon infrared pumping of highly concentrated film of CdSe/CdS core/shell NQDs.

BIBLIOGRAPHY

[1] M. G. Bawendi, M. L. Steigerwald, and L. E. Brus, "The quantum mechanics of larger semiconductor clusters ('Quantum Dots')," *Annual Review of Physical Chemistry*, 41, 1, 477-496, 1990.

[2] A. Alivisatos, "Perspectives on the physical chemistry of semiconductor nanocrystals," *Journal of Physical Chemistry*, 3654, 95, 13226-13239, 1996.

[3] C. Murray and D. Norris, "Synthesis and characterization of nearly monodisperse CdE (E= sulfur, selenium, tellurium) semiconductor nanocrystallites," *Journal of the American Chemical Society*, 115, 4, 8706-8715, 1993.

[4] I. Medintz, H. Uyeda, and E. Goldman, "Quantum dot bioconjugates for imaging, labelling and sensing," *Nature Materials*, 435-446, 2005.

[5] C. Leatherdale, W. Woo, and F. Mikulec, "On the absorption cross section of CdSe nanocrystal quantum dots," *Journal of Physical Chemistry B*, 02139, 7619-7622, 2002.

[6] W. Yu, L. Qu, and W. Guo, "Experimental determination of the extinction coefficient of CdTe, CdSe, and CdS nanocrystals," *Chemistry of Materials*, 125, 17, 2854-2860, 2003.

[7] C.-Y. Zhang, H.-C. Yeh, M. T. Kuroki, and T.-H. Wang, "Single-quantum-dot-based DNA nanosensor," *Nature Materials*, 4, 11, 826-831, 2005.

[8] S. Coe and W. Woo, "Electroluminescence from single monolayers of nanocrystals in molecular organic devices," *Nature*, 420, 2002.

[9] W. U. Huynh, J. J. Dittmer, and a P. Alivisatos, “Hybrid nanorod-polymer solar cells.,” *Science*, 295, 5564, 2425-2427, 2002.

[10] V. I. Klimov, “Optical gain and stimulated emission in nanocrystal quantum dots,” *Science*, 290, 5490, 314-317, 2000.

[11] N. Morgan, C. Leatherdale, M. Drndić, M. Jarosz, M. Kastner, and M. Bawendi, “Electronic transport in films of colloidal CdSe nanocrystals,” *Physical Review B*, 66, 7, 1-9, 2002.

[12] C. Leatherdale, C. Kagan, and N. Morgan, “Photoconductivity in CdSe quantum dot solids,” *Physical Review B*, 62, 4, 2000.

[13] L. Carbone et al., “Synthesis and micrometer-scale assembly of colloidal CdSe/CdS nanorods prepared by a seeded growth approach.,” *Nano Letters*, 7, 10, 2942-2950, 2007.

[14] D. V. Talapin, J. H. Nelson, E. V. Shevchenko, S. Aloni, B. Sadtler, and a P. Alivisatos, “Seeded growth of highly luminescent CdSe/CdS nanoheterostructures with rod and tetrapod morphologies.,” *Nano Letters*, 7, 10, 2951-2959, 2007.

[15] J. E. Halpert, V. J. Porter, J. P. Zimmer, and M. G. Bawendi, “Synthesis of CdSe/CdTe nanobarbells,” *Journal of the American Chemical Society*, 128, 39, 12590-12591, 2006.

[16] A. M. Smith, A. M. Mohs, and S. Nie, “Tuning the optical and electronic properties of colloidal nanocrystals by lattice strain,” *Nature Nanotechnology*, 4, 1, 56-63, 2009.

[17] X. Zhong, Y. Feng, Y. Zhang, Z. Gu, and L. Zou, “A facile route to violet- to orange-emitting Cd x Zn 1− x Se alloy nanocrystals via cation exchange reaction,” *Nanotechnology*, 18, 38, 385606, 2007.

[18] A. A. Ekimov, A.I.O., *JETP Letters.*, vol. 34, p. 345, 1981.

[19] P. Frigeri, a Bosacchi, S. Franchi, P. Allegri, and V. Avanzini, "Vertically stacked quantum dots grown by ALMBE and MBE," *Journal of Crystal Growth*, 201–202, 1136-1138, 1999.

[20] E. M. Goldys and T. L. Tansley, "Growth optimization of GaSb/GaAs self-assembled quantum dots grown by MOCVD," *Journal of Crystal Growth*, 236, 4, 621-626, 2002.

[21] W. K. Bae et al., "Multicolored light-emitting diodes based on all-quantum-dot multilayer films using layer-by-layer assembly method," *Nano Letters*, 10, 7, 2368-2373, 2010.

[22] L. Kim, P. O. Anikeeva, S. a Coe-Sullivan, J. S. Steckel, M. G. Bawendi, and V. Bulović, "Contact printing of quantum dot light-emitting devices," *Nano Letters*, 8, 12, 4513-4517, 2008.

[23] M. Panzer, V. Wood, and S. Geyer, "Tunable infrared emission from printed colloidal quantum dot/polymer composite films on flexible substrates," *Journal of Display*, 6, 3, 90-93, 2010.

[24] X. Peng and J. Wickham, "Kinetics of II-VI and III-V colloidal semiconductor nanocrystal growth : ' Focusing ' of size distributions," *Journal of the American Chemical Society*, 7863, 98, 5343-5344, 1998.

[25] W. Yu and X. Peng, "Formation of high-quality CdS and other II-VI semiconductor nanocrystals in noncoordinating solvents: tunable reactivity of monomers," *Angewandte Chemie International Edition*, 13, 2368-2371, 2002.

[26] C.B.Murray, "Synthesis and characterization of monodisperse nanocrystals and close- packed nanocrystal assemblies," *Annual Review of Material Science*, 545-610, 2000.

[27] M. a. Hines and P. Guyot-Sionnest, “Bright UV-Blue luminescent colloidal ZnSe nanocrystals,”*Journal of Physical Chemistry B*, 102, 19, 3655-3657, 1998.

[28] L. Li, N. Pradhan, and Y. Wang, “High quality ZnSe and ZnS nanocrystals formed by activating zinc carboxylate precursors,” *Nano Letters*, 4, 11, 2261-2264, 2004.

[29] M. a. Hines and G. D. Scholes, “Colloidal PbS nanocrystals with size-tunable near-infrared emission: observation of post-synthesis self-narrowing of the particle size distribution,” *Advanced Materials*, 15, 21, 1844-1849, 2003.

[30] D. Battaglia and X. Peng, “Formation of high quality InP and InAs nanocrystals in a noncoordinating solvent,” *Nano Letters*, 2, 9, 1027-1030, 2002.

[31] T. Erdem and S. Nizamoglu, “Computational study of power conversion and luminous efficiency performance for semiconductor quantum dot nanophosphors on light-emitting diodes,” *Optics Express*, 20, 3, 3275-3295, 2012.

[32] R. Xie, U. Kolb, J. Li, T. Basché, and A. Mews, “Synthesis and characterization of highly luminescent CdSe-core CdS/Zn0.5Cd0.5S/ZnS multishell nanocrystals., ”*Journal of the American Chemical Society*, 127, 20, 7480-7488, 2005.

[33] B. Dabbousi and J. Rodriguez-Viejo, “(CdSe) ZnS core-shell quantum dots: synthesis and characterization of a size series of highly luminescent nanocrystallites,” *Journal of Physical Chemistry. B*, 9463, 97, 9463-9475, 1997.

[34] M. Protière and P. Reiss, “Highly luminescent Cd1-xZnxSe/ZnS core/shell nanocrystals emitting in the blue-green spectral range,” *Small*, 3, 3, 399-403, 2007.

[35] A. B. Greytak et al., “Alternating layer addition approach to CdSe/CdS core/shell quantum dots with near-unity quantum yield and high on-time fractions,” *Chemical Science*, 2028-2034, 2012.

[36] F. García-Santamaría et al., “Breakdown of volume scaling in Auger recombination in CdSe/CdS heteronanocrystals: the role of the core-shell interface,” *Nano Letters*, 11, 2, 687-693, 2011.

[37] J. McBride, J. Treadway, L. C. Feldman, S. J. Pennycook, and S. J. Rosenthal, “Structural basis for near unity quantum yield core/shell nanostructures,” *Nano Letters*, 6, 7, 1496-1501, 2006.

[38] A. Striolo, J. Ward, and J. Prausnitz, “Molecular weight, osmotic second virial coefficient, and extinction coefficient of colloidal CdSe nanocrystals,” *Journal of Physical Chemistry B*, 106, 5500-5505, 2002.

[39] J. Jasieniak, L. Smith, J. V. Embden, P. Mulvaney, and M. Califano, “Re-examination of the size-dependent absorption properties of CdSe quantum dots,”*Journal of Physical Chemistry C*, 113, 45, 19468-19474, 2009.

[40] J. S. Kamal et al., “Size-dependent optical properties of zinc blende cadmium telluride quantum dots,”*Journal of Physical Chemistry C*, 116, 8, 5049-5054, 2012.

[41] B. Mahler and N. Lequeux, “Ligand-controlled polytypism of thick-shell CdSe/CdS nanocrystals,” *Journal of the American Chemical Society*, 132, 8, 953-959, 2009.

[42] A. Rogach, “Semiconductor nanocrystal quantum dots: synthesis, assembly, spectroscopy and applications,” 2008.

[43] M. Grabolle, M. Spieles, V. Lesnyak, N. Gaponik, A. Eychmüller, and U. Resch-Genger, "Determination of the fluorescence quantum yield of quantum dots: suitable procedures and achievable uncertainties," *Analytical Chemistry*, 81, 15, 6285-6294, 2009.

[44] U. Resch-Genger, M. Grabolle, and S. Cavaliere-Jaricot, "Quantum dots versus organic dyes as fluorescent labels," *Nature Methods*, 5, 9, 763-775, 2008.

[45] E. Jang, S. Jun, H. Jang, J. Lim, B. Kim, and Y. Kim, "White-light-emitting diodes with quantum dot color converters for display backlights," *Advanced Materials*, 22, 28, 3076-3080, 2010.

[46] K. H. Drexhage, *J. Res. Natl. Bur. Stand.,A,* no. 80A, pp. 421-428, 1976.

[47] J. Huang and M. Kovalenko, "Alkyl chains of surface ligands affect polytypism of CdSe nanocrystals and play an important role in the synthesis of anisotropic nanoheterostructures," *Journal of American Chemical Society*, 132, 15866-15868, 2010.

[48] J. Jasieniak, C. Bullen, and J. V. Embden, "Phosphine-free synthesis of CdSe nanocrystals," *Journal of Physical Chemistry B*, 109, 44, 20665-20668, 2005.

[49] J. Katari and V. Colvin, "X-ray photoelectron spectroscopy of CdSe nanocrystals with applications to studies of the nanocrystal surface," *Journal of Physical Chemistry*, 4109-4117, 1994.

[50] J. J. Li et al., "Large-scale synthesis of nearly monodisperse CdSe/CdS core/shell nanocrystals using air-stable reagents via successive ion layer adsorption and reaction," *Journal of the American Chemical Society*, 125, 41, 12567-12575, 2003.

[51] J. Nanda, B. A. Kuruvilla, and D. D. Sarma, “Photoelectron spectroscopic study of CdS nanocrystallites,” *Physical Review B*, 59, 11, 7473-7479, 1999.

[52] J. Nanda and D. D. Sarma, “Photoemission spectroscopy of size selected zinc sulfide nanocrystallites,” *Journal of Applied Physics*, 90, 5, 2504-2510, 2001.

[53] S. Jun, E. Jang, and J. E. Lim, “Synthesis of multi-shell nanocrystals by a single step coating process,” *Nanotechnology*, 17, 15, 3892-3896, 2006.

[54] J. van Embden, J. Jasieniak, and P. Mulvaney, “Mapping the optical properties of CdSe/CdS heterostructure nanocrystals: the effects of core size and shell thickness,” *Journal of the American Chemical Society*, 131, 40, 14299-309, 2009.

[55] C. J. Murphy, “Optical sensing with quantum dots,” *Analytical. Chemistry*, 520-526, 2002.

[56] B. Dubertret, P. Skourides, D. J. Norris, V. Noireaux, A. H. Brivanlou, and A. Libchaber, “In vivo imaging of quantum dots encapsulated in phospholipid micelles,” *Science*, 298, 5599, 1759-1762, 2002.

[57] X. Peng, M. Schlamp, and A. Kadavanich, “Epitaxial growth of highly luminescent CdSe/CdS core/shell nanocrystals with photostability and electronic accessibility,” *Journal of the American Chemical Society*, 7863, 25, 7019-7029, 1997.

[58] W. Bae, K. Char, and H. Hur, “Single-step synthesis of quantum dots with chemical composition gradients,” *Chemistry of Materials*, 22, 531-539, 2008.

[59] W. Liu et al., “Compact biocompatible quantum dots via RAFT-mediated synthesis of imidazole-based random copolymer ligand,” *Journal of the American Chemical Society*, 132, 2, 472-483, 2010.

[60] D. D. Sarma, A. Nag, P. K. Santra, A. Kumar, S. Sapra, and P. Mahadevan, “Origin of the enhanced photoluminescence from semiconductor CdSeS nanocrystals,” *Journal of Physical Chemistry Letters*, 1, 14, 2149-2153, 2010.

[61] D. V. Talapin et al., “Highly emissive colloidal CdSe / CdS heterostructures of mixed dimensionality,” *Nano Letters*, 3, 12, 1677-1681, 2003.

[62] F. García-Santamaría, Y. Chen, J. Vela, R. D. Schaller, J. a Hollingsworth, and V. I. Klimov, “Suppressed auger recombination in ‘giant’ nanocrystals boosts optical gain performance,” *Nano Letters*, 9, 10, 3482-3488, 2009.

[63] B. N. Pal et al., “‘Giant’ CdSe/CdS core/shell nanocrystal quantum dots as efficient electroluminescent materials: strong influence of shell thickness on light-emitting diode performance,” *Nano Letters*, 2011.

[64] S. Kudera et al., “Sequential growth of magic-size CdSe nanocrystals,” *Advanced Materials*, 19, 4, 548-552, 2007.

[65] D. Underwood and T. Kippeny, “Ultrafast carrier dynamics in CdSe nanocrystals determined by femtosecond fluorescence upconversion spectroscopy,” *Journal of Physical Chemistry B*, 105, 2, 436-443, 2001.

[66] A. Smith, “Semiconductor nanocrystals: structure, properties, and band gap engineering,” *Accounts of Chemical Research*, 43, 2, 190-200, 2009.

[67] K. Itoh and W. Watanabe, “Nonlinear ultrafast focal-point optics for microscopic imaging, manipulation, and machining,” *Proceedings of the IEEE*, 97, 6, 1011-1030, 2009.

[68] R. Byer, “Nonlinear optics and solid-state lasers: 2000,” *Selected Topics in Quantum Electronics, IEEE*, 6, 6, 911-930, 2000.

[69] Y. Arakawa, “Quantum well lasers--Gain, spectra, dynamics,” *IEEE Journal of Quantum Electronics*, QE–22, 9, 1887-1899, 1986.

[70] Y. Arakawa, “Multidimensional quantum well laser and temperature dependence of its threshold current,” *Applied Physics Letters*, 40, 11, 939, 1982.

[71] R. Krahne, M. Zavelani-Rossi, M. G. Lupo, L. Manna, and G. Lanzani, “Amplified spontaneous emission from core and shell transitions in CdSe/CdS nanorods fabricated by seeded growth,” *Applied Physics Letters*, 98, 6, 063105, 2011.

[72] F. Todescato et al., “Soft-lithographed up-converted distributed feedback visible lasers based on CdSe-CdZnS-ZnS quantum dots,” *Advanced Functional Materials*, 22, 2, 337-344, 2012.

[73] J. J. Jasieniak et al., “Highly efficient amplified stimulated emission from CdSe-CdS-ZnS quantum dot doped waveguides with two-photon infrared optical pumping,” *Advanced Materials*, 20, 1, 69-73, 2008.

[74] http://www.photonicmicrodevices.com/XRD.html

[75] http://www.tf.uni-kiel.de/matwis/amat/semitech_en/kap_2/illustr/i2_1_2.html

[76] http://robertdewayneevans.edu.glogster.com/microscopy-5107/